Flow-driven orientation dynamics in two classes of fibre suspensions

Uldis Strautins

Acknowledgements

Abstract

In this dissertation we consider mesoscale based models for flow driven fibre orientation dynamics in suspensions. Models for fibre orientation dynamics are derived for two classes of suspensions. For concentrated suspensions of rigid fibres the Folgar-Tucker model is generalized by incorporating the excluded volume effect. For dilute semi-flexible fibre suspensions a novel moments based description of fibre orientation state is introduced and a model for the flow-driven evolution of the corresponding variables is derived together with several closure approximations.

The equation system describing fibre suspension flows, consisting of the incompressible Navier-Stokes equation with an orientation state dependent non-Newtonian constitutive relation and a linear first order hyperbolic system for the fibre orientation variables, has been analyzed, allowing rather general fibre orientation evolution models and constitutive relations. The existence and uniqueness of a solution has been demonstrated locally in time for sufficiently small data.

The closure relations for the semiflexible fibre suspension model are studied numerically. A finite volume based discretization of the suspension flow is given and the numerical results for several two and three dimensional domains with different parameter values are presented and discussed.

Contents

Chapter 1

Introduction

1.1 Motivation

Transport of suspensions of elongated particles is a feature of various natural and industrial processes. The suspended particles range from rod-like macromolecules, viruses, elongated cells to wood pulp fibres in paper making or chopped glass or carbon fibres used to reinforce a plastic material. The liquid phase of the suspension can be a *Newtonian* fluid, such as water or oil, or a *non-Newtonian* fluid, for instance, a molten polymer. Addition of fibres even in small concentrations results in non-linear dynamics of the suspension, thus, in general, fibre suspensions are non-Newtonian fluids even when the suspending fluid is Newtonian.

As an example, let us consider the injection and compression molding techniques for processing fibre reinforced thermoplastics. These materials are heated up before the pressure driven injection in the mold so that the matrix is liquid during the flow. The suspension flow in the mold is coupled to the fibre orientation in the suspension, namely, the orientation affects the flow and the flow changes the orientation. The fibre alignment persists after the solidification of the matrix. Since the mechanical properties of a fibre reinforced material sensitively depend on the fibre orientation, understanding the phenomena governing the suspension flow is a neccessary prerequisite for modelling and optimization of the production process.

Direct simulations of the solid-fluid interactions taking place in a fibre suspension while it flows in a typically sized domain used in industrial applications require huge data sets and computational efforts that are way out of reach of the modern computing technology. For dilute and semi-dilute rigid fibre suspensions there exist models based on mesoscale, allowing the prediction of both macroscopic flow and the averaged fibre orientation state with reasonable accuracy at relatively low computational costs. However, these models are not valid for all relevant types of fibre suspensions, for instance, for highly concentrated suspensions and for suspensions of long flexible fibres. Deriving mesoscale models valid for these suspension regimes would be an important contribution to the modelling of fibre suspensions.

When the microstructure of the suspension is described in mesoscale, the equations governing the suspension flow form a coupled system of partial differential equa-

tions, consisting of a generalized incompressible Navier-Stokes equation with a non-Newtonian constitutive law and of a hyperbolic first order system for scalar variables describing the fibre orientation dynamics. Mathematical analysis of well-posedness of the system in a unified framework valid for *different* fibre orientation models and constitutive laws is another challenging task.

We start this introductory Chapter with a review of some models proposed in scientifical literature, devoting seperate sections to models for short rigid fibres and for long semiflexible fibres. In the end of this Chapter, the goals of this thesis are presented and an outline of the following chapters is given.

1.2 Review of short fibre suspension theory

Flow of fibre suspensions is usually studied in the context of rheology, the science of flowing complex fluids. A good introduction to the subject are the books of Doi and Edwards [17], Huilgol and Phan-Thien [35] and the review paper [42]. An introduction to theory and applications of short fibre suspension flows can be found in the book [3], in particular Chapter 6, and in the review article [58].

A material consisting of a collection of particles immersed in a liquid is called a *suspension* if a typical length scale l_m resolving the individual particles (microscale) is distinctly seperated from the length scale l_M characterizing the macroscopic flow (macroscale): $l_m \ll l_M$. To describe the suspension at the macroscale, averaged *bulk* material properties can be defined by appropriately averaging the corresponding microscale quantities. A prerequisite for applications of such upscaling techniques is the existence of a representative volume that is small in comparison to the macroscale but contains a sufficient number of fibres for statistical description to make sense. Strictly speaking, this is not always the case for fibre suspensions. The length of a typical fibre ranges from milimeters to several centimeters, and thus can even exceed the thickness of a typical semistructural part, so a representative volume can hardly be called pointlike or *very small*. The application of upscaling techniques is justified by considering bulk flows, where the macroscopic flow properties are uniform over a larger volume containing sufficiently many fibres (see e.g. the discussion in [20]), possibly adopting 2D models for thin shell like domains.

Due to the different length scales, two different values of Reynolds number can be defined. The microscale Reynolds number is typically much smaller than the macroscale Reynolds number. In [35], a typical value $\text{Re}_{\text{micro}} = O(10^{-3})$ is estimated. The flow of an incompressible Newtonian fluid through the microscale defined by the fibres is therefore nearly Stokesian: $\nabla \cdot v = 0$, $\eta \triangle v = \nabla P$. The Stokes equations are linear and exhibit no inertial effects due to the absence of time derivatives, thus the boundary data are transported instantaneously. The dynamics of the microstructure is therefore expected to be instantaneous and linear in driving forces.

The dynamics of a single fibre is described by Jeffery's equation.

1.2.1 Jeffery's equation

In the original paper of 1922 [38], George Barker Jeffery considers the dynamics of a particle of the shape of a prolate ellipsoid immersed in a Newtonian liquid. The orientation of an axissymmetric particle with a head-to-tail symmetry can be described by a unit vector p as shown in Figure 1.1.
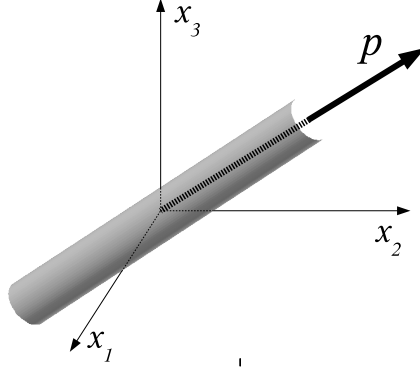
Figure 1.1: The unit vector p describing the orientatation of a fibre

In his model it is assumed that the only forces acting on the fibre are the traction forces, which are transfered from the fluid on the boundary. The momentum transfer from the fibre to the fluid is neglected. Using a first order (linear) expansion of the fluid velocity field around the particle, the following equation for the fibre orientation vector p is obtained (see [41] for a modern exposition of the matter):

$$\frac{dp}{dt} = M \cdot p - (p \otimes p : M)p, \qquad (1.1)$$

where the effective velocity gradient is defined as

$$M = \frac{\lambda + 1}{2}\kappa + \frac{\lambda - 1}{2}\kappa^\top,$$

$\kappa = \nabla v$ is the spatial velocity gradient (Jacobian matrix), and

$$\lambda = \frac{r_a^2 - 1}{r_a^2 + 1}$$

is a fibre geometry parameter with $r_a = l_f/d_f$ denoting fibre aspect ratio.

The solutions of (1.1) satisfy $\left\|\frac{dp}{dt}\right\|^2 = 0$, hence the unit sphere S^{d-1} is an invariant manifold of this equation. This fact can be stressed by writing the equation in the equivalent form $\dot{p} = (I - p \otimes p) \cdot (Mp)$, where the projection operator on the tangential space of the sphere is involved explicitly, or writing the equation in the angular velocity formulation. The angular velocity can be computed from (1.1) as $\omega = p \times \dot{p} = p \times (Mp)$.

The solutions of Jeffery's equations have been studied for stationary flow fields with analytical (cf. [38], [33]) and numerical (cf. [41]) methods. Depending on the Jacobian κ and fibre aspect ratio, the orientation vector p either follows periodic trajectories in the configurational space S^2 (so called *Jeffery's orbits*) or reaches a stationary state.

Bretherton has studied the motion of particles of arbitrary axis-symmetric shape including cylindrical rods ([7]). He has demonstrated that the particle rotation can be described with Jeffery's equation, and finds that the parameter λ depends on the shape of particle.

Jeffery's equation is not valid if the suspending fluid is non-Newtonian. For example, it is well known that in simple shear flows the orientation vector slowly drifts towards the vorticity axis (see [36], [39]), while Jeffery's model predicts periodic orbits. A simple correction to Jeffery's equation accounting for this effect has been proposed in [20], where the expression for the effective velocity gradient is changed to

$$\tilde{M} = \kappa^{\top} - 2\epsilon D - 4c\frac{D \cdot D}{\dot{\gamma}},$$

where $D = \frac{1}{2}\left[\kappa + \kappa^{\top}\right]$ is the rate of strain tensor and $\dot{\gamma} = \sqrt{\frac{1}{2}D : D}$ is the shear rate; c and ϵ are real parameters.

1.2.2 Orientation distribution function

An equation $\dot{p} = (I - p \otimes p)f(p)$, where $p : S^{d-1} \to \mathbb{R}^d$, defines a vector field on the $d-1$-dimensional sphere S^{d-1}. If the associated flow transports some quantity ψ that is defined on the sphere, then the law of conservation of this quantity is given by the Liouville equation $\frac{\partial \psi}{\partial t} = -\nabla_p \cdot (\dot{p}\psi)$, where ∇_p is the gradient operator on the sphere. We are mainly interested in the case $d = 3$, so let us illustrate the calculus of the sphere embedded in $\mathbb{R}^3$. We introduce the spherical coordinates (Figure 1.2).
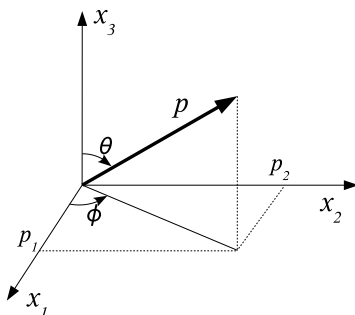
Figure 1.2: Spherical coordinates (ϕ, θ) of a vector $p \in S^2$

The sphere is parametrized by the set of unit vectors

$$S^2 = \{(\cos(\phi)\sin(\theta), \sin(\phi)\sin(\theta), \cos(\theta)) : \ 0 \leq \phi < 2\pi, \ 0 \leq \theta \leq \pi\}.$$

The gradient on S^2 is the angular part of the 3-dimensional gradient,

$$\nabla_p = \begin{pmatrix} \cos(\phi)\cos(\theta) \\ \sin(\phi)\cos(\theta) \\ -\sin(\theta) \end{pmatrix} \frac{\partial}{\partial\theta} + \frac{1}{\sin(\theta)} \begin{pmatrix} -\sin(\phi) \\ \cos(\phi) \\ 0 \end{pmatrix} \frac{\partial}{\partial\phi}.$$

We will frequently make use of an equivalent formulation based on the angular momentum $\omega = p \times \dot{p}$ instead of the velocity $\dot{p}$. A differential operator called the *rotation operator* is very useful in angular velocity formulation. It is defined by $\mathscr{R}_p := p \times \frac{\partial}{\partial p}$ or componentwise by

$$\mathscr{R}_p = \begin{pmatrix} -\cos(\phi)\cos(\theta) \\ -\sin(\phi)\cos(\theta) \\ \sin(\theta) \end{pmatrix} \frac{\partial}{\partial\phi} + \begin{pmatrix} -\sin(\phi) \\ \cos(\phi) \\ 0 \end{pmatrix} \frac{\partial}{\partial\theta}.$$

For $\omega = p \times \dot{p}$ it holds $\mathscr{R}_p \cdot \omega = \nabla_p \cdot \dot{p}$. The integration by parts rule is

$$\int_{S^2} u\mathscr{R}_p v \mathrm{d}\sigma(p) = -\int_{S^2} v\mathscr{R}_p u \mathrm{d}\sigma(p) \tag{1.2}$$

for sufficiently smooth (say, C^1) u and v, see [14] for a proof.

Let us introduce the fibre orientation distribution function $\psi(x, p)$ measuring the probability density for an arbitrarily chosen fibre near $x \in \Omega$ to have the orientation p. More precisely, by assumption, for $x \in \Omega$ there exists a representative volume $V_x \subset \Omega$ containing x and sufficiently many fibres. Let $\Sigma \subset S^{d-1}$ be a (measurable) subset of the orientational space containing no antipodal points (i.e, if $p \in \Sigma$, then $-p \notin \Sigma$), then the probability of finding an arbitrary fibre from V_x having an orientation in Σ is given by the integral $2\int_\Sigma \psi(x, p)\mathrm{d}\sigma(p)$.

Being a probability distribution function, ψ must satisfy three properties:

1. non-negativity: $\psi(x, p) \geq 0$,

2. symmetry: $\psi(x, p) = \psi(x, -p)$ for all $(x, p) \in \Omega \times S^{d-1}$ and

3. normalization: $\int_{S^{d-1}} \psi(x, p)\mathrm{d}\sigma(p) = 1$.

The law of conservation of probability is the Liouville equation:

$$\frac{\partial\psi}{\partial t} = -\nabla_p \cdot (\dot{p}\psi). \tag{1.3}$$

Taking into account the transport of the material in the domain Ω, time derivative should be replaced by the material derivative: $\frac{D\psi}{Dt} = -\nabla_p \cdot (\dot{p}\psi)$.

1.2.3 Fibre-fibre interactions and concentration regimes

The orientation of a fibre is affected by interactions with other fibres. One distinguishes between long range and short range hydrodynamical interactions and mechanical contacts between the fibres; the dominant type of interactions depends on

the *concentration* of the suspension. The most important variables determining the concentration regime are fibre *number density* n_f (the average number of fibres in a unit volume), fibre length l_f and diameter d_f. The fibre volume fraction ϕ_f can be expressed through the fibre number density and the volume of a single fibre; for cylindrical fibres we obtain $\phi_f = \frac{\pi n_f d_f^2 l_f}{4}$. Fibre suspensions are classified in three regimes - dilute, semi-dilute and concentrated (see [17], [58]).

If $n_f l_f^3 < 1$, then the average distance between neighbouring fibres is larger than the fibre length. It is generally assumed that the perturbations caused by a fibre can noticably affect the orientation of other fibres only across a limited distance comparable with fibre length $O(l_f)$, therefore the fibre-fibre interaction are negligible. This is called the *dilute* regime. If the average distance between the fibres is larger than the fibre diameter d_f but shorter than the fibre length l_f, then the suspension is called *semi-dilute*; this regime is characterized by $n_f l_f^3 > 1$ and $n_f l_f^2 d_f < 1$. Here the fibres are close enough for long- and short-range hydrodynamic interactions to play an important role. Finally, if the average distance between the fibres is smaller than the fibre diameter ($n_f l_f^2 d_f > 1$), then the suspension is classified as *concentrated*. Here a change of orientation of a single fibre is impossible without turning the surrounding fibres and mechanical contacts between the fibres are dominating.

Intuitively, long range hydrodynamical interactions can be thought of as small perturbations in velocity field near a test fibre, which cause a smooth and small deviation of orientation. Short range hydrodynamic interactions are rather like collisions, that "kick" the fibre. Direct mechanical contact between fibres leads to a complicated behaviour, featuring formation of fibre bundles, clusters or networks (flocculation), where the dynamics of a fibre is strictly constrained by the neighbours. For a short review of the microscale modelling of these processes see Section 1.2.7. In dilute and semi-dilute cases the fibre-fibre interactions can be modelled in an average sense

The fibre-fibre interactions result in deviations from Jeffery's orbits. By denoting the perturbation of the velocity in the orientation space by F_r, the correction can be added to Jeffery's equation:

$$\dot{p} = (I - p \otimes p) \cdot (Mp + F_r); \tag{1.4}$$

in the angular velocity formulation the perturbed Jeffery's equation is $\omega = p \times (Mp + F_r)$. In the *dilute* and *semi-dilute* regimes the perturbation F_r is usually modelled as a vector valued random process. Assuming that the perturbations have no preferred direction and are not correlated in time, we get vanishing mean value $\mathbb{E}\{F_r(t)\} = 0$ and the autocorrelation function $\mathbb{E}\{F_r(t_1) \cdot F_r(t_2)\} = 2D_r I \delta(t_1 - t_2)$, where D_r is called the *rotary diffusion coefficient*. Thus $F_r(t)$ is a white noise random process,

$$F_r(t)dt = \sqrt{2D_r}dw, \tag{1.5}$$

where $w(t)$ is the vector valued Wiener process. Thus (1.4) is interpreted as a stochastic differential equation on the unit sphere, i.e., a Langevin equation.

This Langevin equation can be used for Brownian dynamics simulation, see [56], [20]. Other approach is to calculate the average probability flux due to the Brownian

term utilizing the fibre orientation distribution function $\psi(x,p)$ and applying Ito's formula ([26], [56]). *If the stochastic differential of p is given $dp = F_r dw(t)$, then for a function $\psi(p)$ Ito's formula gives $d\psi(p) = D_r \nabla_p^2 \psi dt + \sqrt{2D_r} \nabla_p \psi dw(t)$. Calculating the mean value, we obtain a diffusion equation on the sphere: $d\mathbb{E}(\psi(p)) = D_r \nabla_p^2 \mathbb{E}(\psi) dt$. Interpreting the rate of change of ψ as a flux on the sphere, we obtain the mean value of the flux due to the white noise process: $\dot{p} = -\frac{D_r}{\psi} \nabla_p \psi$.* This procedure recovers the equation given in [22]:

$$\dot{p} = Mp - (M : p \otimes p)p - \frac{D_r}{\psi} \nabla_p \psi. \tag{1.6}$$

In the angular velocity formulation $\omega = p \times \dot{p}$ the probability conservation law can be written as ([17])

$$\frac{D\psi}{Dt} = -\mathscr{R}_p(\omega\psi) \tag{1.7}$$

where $\frac{D \cdot}{Dt} = \frac{\partial \cdot}{\partial t} + v \cdot \nabla_x$ is the material derivative.

In [22], Fransisco Folgar and Charles L. Tucker III propose to choose the rotary diffusion coefficient proportional to the shear rate: $D_r = C_i \dot{\gamma}$, where the constant C_i was selected to fit the experimentally observed orientation distribution. It has been suggested that the isotropic rotary diffusion modelled by a scalar C_i might be too restrictive, therefore anisotropic versions have been proposed, see [60], [39], [20]. In these models the equations are modified to accomodate C_i as a symmetric positive definite second rank tensor. However, the scalar model is preferred due to difficulties of parameter estimation for the tensorial model.

It is generally assumed that C_i is a function of concentration. This function is known to increase for low concentrations, to reach a peak at a critical concentration and then to decrease. Petrich et al have studied the fibre orientation diffusion experimentally in [57]. They find that the peak is reached at the concentration $n_f l_f^2 d_f \approx 0.5 \ldots 0.8$, which corresponds to the transition from semi-dilute to concentrated regime. This effect can be incorporated within the Folgar-Tucker mocel by changing C_i appropriately, however, such models do not explain the physical reasons behind this phenomenon. In fact, the decrease of C_i can be explained using the concept of excluded volume, see [57], where a nematic potential is introduced to model this effect. We discuss the related concepts in Section 2.1.

Models including both translational (in Ω) and rotational (in S^{d-1}) diffusion are discussed e.g. in [17] and [14]. We assume the fibre concentration to be constant in Ω and therefore focus exclusively on orientational dynamics.

1.2.4 Folgar-Tucker equation

For a nonnegative integer n we introduce the moment

$$a^{(n)} = \int_{S^{d-1}} p^n \psi(p) d\sigma(p).$$

It is a completely symmetric tensor of rank n. The antipodal symmetry of ψ implies that the odd order moments vanish, i.e., $a^{(2n+1)} = 0$. The equations for the moments are obtained from the Smoluchowski equation (1.7) by multiplying both sides with p^n and integrating over the configurational space S^{d-1}; in particular, we get

$$\dot{a}^{(2)} = -\int_{S^{d-1}} p \otimes p \left[\mathscr{R}_p(\omega\psi) - D_r \mathscr{R}_p^2 \psi \right] d\sigma(p). \tag{1.8}$$

The second order moment was introduced by Advani and Tucker in [1], where the importance of this orientation structure tensor for both suspension rheology and the material properties in the solid phase is stressed. Plugging $\omega = p \times \dot{p}$ with (1.6) into (1.8) and integrating by parts using (1.2) gives

$$\dot{a}^{(2)} = \int_{S^2} \mathscr{R}_p(p \otimes p)(\psi p \times Mp) dp + D_r \int_{S^2} \mathscr{R}_p^2(p \otimes p)\psi dp.$$

The third rank tensor $\mathscr{R}_p(p \otimes p)$ for $d = 3$ has the following components:

Index (i, j)	Component $\mathscr{R}_p(p \otimes p)_{ij}$
$(1, 1)$	$2(p_3 p_1 e_2 - p_1 p_2 e_3)$
$(2, 2)$	$2(p_1 p_2 e_3 - p_2 p_3 e_1)$
$(3, 3)$	$2(p_2 p_3 e_1 - p_3 p_1 e_2)$
$(2, 3)$ or $(3, 2)$	$(p_2^2 - p_3^2)e_1 + p_3 p_1 e_3 - p_1 p_2 e_2$
$(3, 1)$ or $(1, 3)$	$(p_3^2 - p_1^2)e_2 + p_1 p_2 e_1 - p_2 p_3 e_3$
$(1, 2)$ or $(2, 1)$	$(p_1^2 - p_2^2)e_3 + p_2 p_3 e_2 - p_3 p_1 e_1,$

where e_i form the standard basis of $\mathbb{R}^3$. Further, $\mathscr{R}_p^2(p \otimes p) = (2I - 6p \otimes p)$. Using these identities, integrating and recalling the definition of moments yields

$$\dot{a}^{(2)} = M \cdot a^{(2)} + a^{(2)} \cdot M^\top - (M + M^\top) : a^{(4)} + 2D_r(I - 3a^{(2)}), \tag{1.9}$$

which is the most used variant of the Folgar-Tucker model and is often called the *Folgar-Tucker equation* in the open form. Note that the right-hand side of (1.9) depends on the moment $a^{(4)}$.

1.2.5 Closure approximations

The equation (1.9) is not closed in the sense that given only $a^{(2)}$ and M, the term $(M + M^\top) : a^{(4)}$ cannot be calculated. Moreover, as pointed out by Hinch and Leal in [34], the equation for the moment $a^{(2n)}$ always contains the higher order moment $a^{(2n+2)}$. In the modelling part we will show that, in general, higher order moments do not depend on the lower order moments. Hence, the approach of computing the evolution of moments of ψ without knowing ψ itself requires an approximation of an unknown moment tensor.

Closure rules expressing $a^{(6)}$ in terms of lower order moments have been developed (see [37]), however this approach is found to increase the computational costs without providing a higher accuracy, therefore we focus on the classical closure problem, namely, to approximate $a^{(4)}$ in terms of $a^{(2)}$.

We return to the problem of closure approximations in Section 2.2; here we review some of the closure relations, i.e., formulae of the form $a^{(4)} \approx f(a^{(2)})$ that have been proposed in scientific literature.

The most simple closure relation is the **quadratic** closure ([34], [2]):

$$a^{(4)}_{\text{quadratic}} = a^{(2)} \otimes a^{(2)}. \tag{1.10}$$

This closure relation is exact for an uniaxial distribution, i.e., if $a^{(2)} = p_0 \otimes p_0$ for a vector $p_0 \in S^{d-1}$, then the orientation distribution ψ is uniquely determined: $\psi = \frac{1}{2}[\delta_{p_0} + \delta_{-p_0}]$, and it holds $a^{(2n)} = p_0^{2n}$, hence (1.10) is exact. However, in most other cases the quadratic closure is a poor approximation to the exact value of $a^{(4)}$. Nevertheless, this approximation is still often used in simulations (see e.g. [64]) mainly due to the appealing simplicity (resulting in low computational costs) and certain stability considerations. For example, in [53] it is demonstrated that the application of the quadratic closure for computing the stress in suspension is consistent with the second law of thermodynamics and that the suspension flow is energetically stable in the sense that the kinetic energy of the fluid is never increasing in the absence of external forces.

Even older is the **linear** closure proposed in [30]; this approximation (which is discussed further in Section 2.2.3) is given by

$$\left(a^{(4)}_{\text{linear}}\right)_{ijkl} = \frac{1}{7}\left[a^{(2)}_{ij}\delta_{kl} + a^{(2)}_{ik}\delta_{jl} + a^{(2)}_{il}\delta_{jk} + a^{(2)}_{jk}\delta_{il} + a^{(2)}_{jl}\delta_{ik} + a^{(2)}_{kl}\delta_{ij}\right] - \frac{1}{35}\left[\delta_{ij}\delta_{kl} + \delta_{ik}\delta_{jl} + \delta_{il}\delta_{jk}\right],$$

where $\delta_{i_1 i_2}$ is the Kronecker symbol. The linear closure approximation is exact for isotropic orientation state, however, it is known to lead to unphysical results, e.g., violating the non-negativity of ψ, and hence is not used in pure form.

Advani and Tucker have proposed the **hybrid** closure (see [1, 2]) as a convex linear combination of the linear and quadratic closures:

$$a^{(4)}_{\text{hybrid}} = f_h a^{(4)}_{\text{quadratic}} + (1 - f_h)a^{(4)}_{\text{linear}},$$

where $f_h = 1 - d^d \det(a^{(2)})$. In the paper [2] Advani and Tucker analyze several closure approximations available at that time (including the ones proposed by Hinch and Leal in [34]). Their results suggest that the approximations designed to be exact for a certain fibre orientation state or a specific flow tend perform poorly for other data.

A remedy is more general closure approximations containing parameters that can be tuned to fit to the exact data. Verleye and Dupret have proposed the **natural** closure in [80] starting with such a general expression:

$$\left(a^{(4)}_{\text{nat}}\right)_{ijkl} = \beta_1 \mathscr{S}(\delta_{ij}\delta_{kl}) + \beta_2 \mathscr{S}(\delta_{ij}a(2)_{kl}) + \beta_3 \mathscr{S}(a^{(2)}_{ij}a^{(2)}_{kl}) +$$
$$\beta_4 \mathscr{S}(\delta_{ij}a^{(2)}_{ij}a^{(2)}_{kl}) + \beta_5 \mathscr{S}(a^{(2)}_{ij}a^{(2)}_{km}a^{(2)}_{ml}) + \beta_6 \mathscr{S}(a^{(2)}_{im}a^{(2)}_{mj}a^{(2)}_{kn}a^{(2)}_{nl}),$$

where we sum over repeating indices, the symmetrization operator $\mathscr{S}$ is averaging the tensor under all possible permutations of the indices and β_i are real parameters. Since the closure relation should be objective (independent on the choice of coordinate system), the constants β_i may only depend on the invariants of $a^{(2)}$, given by $I_2 = \frac{1}{2}\left[\text{Tr}(a^{(2)})^2 - \text{Tr}(a^{(2)} \cdot a^{(2)})\right]$ and $I_3 = \det(a^{(2)})$. The first invariant, $I_1 = \text{Tr}(a^{(2)})$, is constant and equals 1 by the normalization of ψ. Further constraints (see [19], [28]) reduce the number of independent β_i to three.

For planar flows Verleye and Dupret find analytical expressions for β_i ([80]) basing on the analytical solution of (1.7) with $C_i = 0$ and $\lambda = 1$. For three-dimensional flows they propose to express β_i as polynomials in I_1 and I_2 with coefficients fitted with a least squares algorithm, exploiting the data of $a^{(2)}$ and $a^{(4)}$ obtained from direct simulations of (1.7) for prescribed flow fields.

The very same procedure for liquid crystal flows is carried out in [28].

More recently, Chung and Kwon ([12]) have developed the approach of natural closure, proposing the **IBOF** (Invariant based optimal fitting) closure, which is constructed by fitting the coefficients of certain polynomial expressions $\beta_i(I_2, I_3)$.

A closely related approach using the eigenvalues of $a^{(2)}$ instead of the invariants leads to the family of orthotropic fitted closures (**ORF**) proposed by Cintra and Tucker in [13]. The tensor $a^{(4)}_{\text{ORF}}$ is assumed to be orthotropic and to have the same principal axes as $a^{(2)}$.

Several variants of ORF closures have been published in the literature, differing in details of the fitting process and choice of parameters for (1.7), cf. Verveyst ([81]), Chung and Kwon ([11]). The main drawback of the ORF closure family is the need to compute the eigenvalues and eigenvectors of $a^{(2)}$, thus slowing down the computation of the closure.

A review comparing some of the fitted closure approximations can be found e.g. in [11].

As a general remark, there is always a trade-off between the computational costs and quality of the approximation. When the fibre orientation must be computed with high accuracy, a fitted closure such as IBOF should be preferred. In the framework of this thesis, however, we are interested in the behaviour of certain fibre orientation models rather than the effect of closure approximations. For the numerical experiments a prototype closure relation is needed, and we prefer a simple and well understood closure over a highly accurate one. For this reason we have chosen the quadratic closure (1.10). Nevertheless, the scope of our theoretical analysis extends to a broad class of different closures including the aforementioned ones.

1.2.6 Rheology of fibre suspensions

At the microscale the fluid field variables such as stress T, velocity v and pressure P fluctuate rapidly due to the inhomogeneities introduced by the fibres. The macroscopic field variables are obtained by applying a homogenization technique (see [35] and references therein). For a suspension in Newtonian fluid the homogenized stress can be shown to be linear in the strain rate so that the constitutive relation has the

form
$$T = \eta : D,$$
where η is a fourth-rank tensor with the symmetries $\eta_{ijkl} = \eta_{klij} = \eta_{jikl}$. In praxis, determining the viscosity tensor requires solving a micromechanical problem for a representative volume for various configurations and boundary conditions; this is a major task of rheology. Again it is found that the dominating mechanisms increasing the stress in suspension depend on the concentration. For dilute suspensions the dominating extra forces are originating from fluid-fibre interactions, for semi-dilute suspensions hydrodynamic fibre-fibre interactions have a larger contribution, while for concentrated suspensions the effects from mechanical contacts between the fibres dwarf the other contributions to the stress ([44]).

A lot of theoretical work has been devoted to studies of dilute and semi-dilute suspensions in a Newtonian liquid. Usually the stress in the suspension is decomposed in a matrix part and fibre part:
$$T = -PI + 2\eta_s D + S,$$
where P is hydrostatic pressure, $D = \frac{1}{2} \left[\kappa + \kappa^\top \right]$, $\kappa = \nabla v$, v is the average fluid velocity in the suspension and η_s is the viscosity of the matrix. S is the extra stress term due to the presence of the fibres.

Suspended fibres transfer force to the surrounding liquid through surface traction, thus contributing to the stress in the suspension. Estimating the averaged hydrodynamic stress is a difficult task since the perturbations introduced by the fibres propagate over large distances. Batchelor (see e.g. [5]) has studied the stress in semi-dilute suspension of aligned slender rods. He introduced the concept of an isolated cell, assuming that the perturbations caused by fibres outside the cell are screened by the fibres in the cell and thus do not influence the suspension in the cell. For the extra stress he found the following expression:
$$S = \eta_f \left[a^{(4)} - \frac{1}{3} I \otimes a^{(2)} \right] : D.$$

Dinh and Armstrong ([15]) have generalized this approach for arbitrary fibre orientation. Shahfeq and Fredrickson ([68]) dismiss the concept of cell and compute the stress, accounting for the effects from all mutually interacting fibres in the infinite suspension.

The result of such modelling work is a constitutive relation of the general form given in [2]:
$$S_{ij} = c\eta_s \left[A\kappa_{kl} a^{(4)}_{ijkl} + B(\kappa_{ik} a^{(2)}_{kj} + a^{(2)}_{ik} \kappa_{kj}) + C\kappa_{ij} + 2F a^{(2)}_{ij} D_r \right],$$
where c, A, B, C and F are material constants. The exact expressions for these constants are reviewed in the literature, cf. [48], [2] and [58]. For non-Brownian fibre suspensions the constitutive relation can be rewritten in a convenient form (see [2])
$$T = PI + \eta \left[\kappa + N_p \kappa : a^{(4)} + N_s(a^{(2)} \cdot \kappa + \kappa \cdot a^{(2)}) \right], \tag{1.11}$$

where η is the effective suspension viscosity, representing the isotropic components of viscosity from both the matrix and the fibres, and N_s and N_p are parameters called the shear number and the particle number (see [2]).

The model by Dinh and Armstrong ([15]) predicts the following results.

$$N_s = 0, \qquad N_p = \frac{\phi r_a^2}{3\ln(2h_f/d)},$$

where h_f is a typical distance between two neighbouring fibres, which depends on the volume fraction and type of orientation:

$$h_f = \frac{d_f}{2}\sqrt{\frac{\pi}{\phi}}$$

for aligned fibres (uniaxial orientation distribution) and

$$h_f = \frac{\pi d_f}{4\phi r_a}$$

for isotropic orientation distribution.

For fibres with finite aspect ratio r_a the shear number N_s has a nonzero value, however, already for moderate aspect ratios $r_a > 10$, N_s is negligibly small in comparison with N_p (see [2]). Thus using the slender body approximation $N_s = 0$ is justified.

At concentration levels where the direct mechanical contacts between the fibres become important, the theories based on hydrodynamical fibre interactions fail (see [5], [49], [57], [44]). In fact, the stress can be showed to be proportional to the number of fibre contacts per unit volume ([18]). For flat 2D geometries Le Corre et al ([43], [44]) neglect the suspending liquid, considering the whole suspension as a net of rigid rods linked by viscous point interactions of power law type. They show that, depending on the relation of local translation and rotational viscosities, the suspension is an effective Cauchy or Cosserat medium.

1.2.7 Simulation techniques

Simulations of fibre suspension flow can be performed at different resolutions. The most detailed are fibre level simulations, where each fibre is resolved individually, and the positions and forces acting on each fibre are computed directly. High accuracy is reached at the price of high computational costs. In multiscale aproaches the evolution of microstructure is computed directly in certain small cells distributed over Ω. The microstructure is used to compute the orientation tensors, which are then used to calculate the macroscopic stress. An example the multiscale aproach is the CONNFFESSIT method. To decrease the computational costs further, the suspension can be considered in the mesoscale only. The microstructure is described by orientation tensor field, which evolves according to Folgar-Tucker model. The advantages and disadvantages of each aproach are discussed in [61].

Microscale simulations. Simulations resolving the dynamics of individual fibres are useful for testing suspension models as well as to study the processes in suspensions that are not accessible by means of physical experiments. For example, [85] use a direct simulation method by including the short-range hydrodynamic interactions using the lubrication approximation and ignoring the long-range hydrodynamic interactions. In [49] the fibres are approximated as slender bodies, but all types of hydrodynamical interactions are included and simulations are done for concentrations varying from dilute to semi-dilute. Frictionless mechanichal fibre contacts have been included in [74]. See also [10], [51], [20].

Multiscale simulations. A compromise between the expensive fibre level simulations and the coarse grained (and suffering from closure approximations) mesoscale simulations is the CONNFFESSIT method (Calculation of Non-Newtonian Flow: Finite Element and Stochastic Simulation Technique, see [56]). Here the flow equations are solved by a finite element method, but Brownian dynamics simulation is applied in selected cells for calculating the fibre orientation.

Mesoscale simulations. This computationally cheapest method solves the non-Newtonian flow equations coupled to the fibre orientation equations. Several methods have been proposed to solve non-Newtonian flow problems, for instance, finite difference, finite volume, finite element, boundary element and spectral methods, see [35] for a review.

Different techniques have been proposed to implement the coupling of the flow to the fibre orientation field. Lipscomb et al. ([48]) use the full alignment assumption, namely, the fibres are oriented along the tangents to the respective streamlines, to compute the flow in a planar contraction domain using a finite element method for the flow equations. Rosenberg et al. ([65]) seek a steady-state solution, using a FEM approach to discretize the flow equations and integrating the hyperbolic Folgar-Tucker system along the streamlines. This procedure is iterated until convergence is reached. Reddy and Mitchell ([63]) analyze a finite element method for the coupled problem, using a standard Galerkin method for the momentum equation and a discontinuous Galerkin method for the Folgar-Tucker equation. The orientation field from the previous time-step is used to compute the stress tensor. Apart from theoretical studies, there exists a range of commercial software, see [59].

1.3 Review of long fibre suspension theory

As we have seen, several models for rigid fibre suspension flows have been proposed and are used for simulations. Obviously, the microstructure of semiflexible and flexible fibre suspensions is more complicated than the one for rigid fibres, due to the additional degrees of freedom needed to describe the dynamics of a deformable body. Since the effects of flexibility scale with fibre length, semiflexible fibres are typically longer than rigid ones. Hence non-local effects play a more important role. Due to these and other complications, the most of the proposed models of long semiflexible fibre suspensions are based at the microscale, i.e., fibre level models, and are therefore

computationally expensive. Only a few ansatzes for mesoscale models exist.

The first part of this short survey describes some qualitative properties of dilute long fibre suspensions in low Reynolds number flows as observed experimentally. In the next part we briefly touch some microscale based approaches used for fibre level simulations. Finally we review some work that has been done towards modelling semiflexible fibre suspensions in mesoscale.

1.3.1 Experimental results

The cruical difference distinguishing flexible fibres from rigid ones is the ability to bend under applied forces. In dilute suspensions the forces arise from fluid-solid interactions. A lot of experimental work has been devoted to studies of the deformations of a single flexible fibre undergoing a rotation in a shear flow. Forgacs and Mason ([23]) have classified the observed fibre orbits in several orbit classes. A scalar parameter - *flexibility* - is found to determine the type of orbit (see also [70]). The concept of flexibility is discussed in Section 2.3.1.

At low flexibility the fibres rotate as rigid rods, obeying Jeffery's model (class I). With increasing flexibility, the fibre describes a class II orbit (*springy rotation* or *C-turn*), where the fibre is deformed in the shape of an arc in the fastest part of the orbit. The next is the class IIIa orbit - *loop turn* or *S-turn* and the IIIb orbit - *snake turn*. A feature of all of these orbits is that the fibre straightens out in the phase of minimal acting forces, i.e., when the fibre is oriented closely to the flow direction. At higher value of flexibility the fibres perform a snake turn like orbit, never straightening out completely. This characterizes a class IV orbit, *complex rotation*. The periods of the orbits are increasing with increasing flexibility. Thus, the results of Forgacs et al. show that the dynamics of a single suspended fibre depend on the flexibility, which itself depends on the shear rate, bending stiffness and fibre length.

Already at low volume fractions the mutual interactions of flexible fibres play an important role. Even rare collisions among the fibres may easily lead to mutual entanglement, thus forming small isolated regions with high fibre concentration called *flocs*.

It is well known that the shape of fibres has a significant influence on the bulk viscosity of the suspension, cf. [7]. For example, it has been observed that slightly curved fibres bent in the shape of a circular arc with the normal vecors to the centerline at both endpoints forming an angle of 176 degrees increase the viscosity as much as by 13% over that for a suspension of straight fibres, other parameters being equal (see [39] and references therein).

1.3.2 Microscale models

Various models for a single flexible fibre have been proposed and used in simulations. Stockie ([71], [70]) describes the surface of a 3D fibre as an interwoven net of one dimensional elements using the *immersed boundary method*. Tornberg and Shelley ([77]) approximate the fibre (filament) with an inextensible slender body. In models

of this type the fibre acts on the surrounding fluid through a force defined along the centerline. Another important class of fibre models are the *bead* models, where the fibre is modelled as a string of spherical, ellipsoidal or cylindrical segments connected by rigid connectors. The fibre interacts with the fluid at points associated with the beads, which experience external hydrodynamic forces (Stokes drag and lubrication forces) and internal forces (modelling bending stiffness).

Yamamoto and Matsuoka ([83], [84]) simulate the dynamics of bead chains suspended in a shear flow. Here a fibre consists of spheres connected with springs with additional potentials to mimic resistance to bending and twisting. Ross and Klingenberg ([66]) employ a chain of rigid prolate spheroids connected through ball and socket joints. Joung et al. ([39]) consider connectors that can bend and twist to a limited amount. A similar model has been implemented by Tang and Advani ([75]).

The microscale models cannot be used for direct simulations of industrial suspension flows due to the high computational costs. However, the microscale models can be used as ingredients for CONNFESSIT like multiscale simulations.

1.3.3   Mesoscale models

The progress towards developing mesoscale based models of flexible fibre suspensions is slow due to the complexity of the problem. Hinch has given one of the first theoretical works studying the motion of a single inextensible flexible thread in a Newtonian fluid, cf. [32]. The stress generated by macroscopic strain applied to a semidilute long fibre suspension has been studied by Doi and Kuzuu in [16]. However, in most of the recent works the stress in a long fibre suspension is computed under the assumption that the fibres remain nearly straight at all times, thus the stress is computed from the fibre orientation tensor from the relations derived for short fibre suspensions (see [39]). The simulation is multiscale in the sense that the evolution of fibre orientation is computed in a fibre level simulation, using hundreds or thousands of fibres per element and making appropriate averages.

Recently Rajabian et al have developed a mesoscale model of semiflexible fibre suspensions in polymeric fluids, taking into account fibre-fibre interactions, fibre-polymer interactions and the semiflexible nature of the fibres ([61]). The fibre orientation is described by the moment tensor $a^{(2)}$, a similar tensor field is introduced to describe the orientation of the rodlike polymer molecules. In this model, the tensor field $a^{(2)}$ evolves according to a Folgar-Tucker like equation with an additional dissipation potential, which incorporates both fibre-fibre and fibre-polymer interactions and the fibre flexibility through the Khokhlov-Semenov potential.

1.4   Objectives and structure of the thesis

This thesis is concerning with modelling, analysis and implementation of mesoscale models of fibre suspensions. The main objectives of the thesis are:

- *for modelling part*: developing mesoscale models for fibre orientation dynamics

in suspensions, incorporating the excluded volume effect for concentrated short fibre suspensions and semiflexibility for dilute long fibre suspensions.

- *for analysis part*: analyzing well-posedness of the coupled system of mass and momentum conservation laws and fibre orientation dynamics equations with a non-Newtonian constitutive relation in a general formulation.

- *for implementation part*: a finite volume based implementation capable of accomodating various mesoscale based fibre suspension flow models, based on an existing implementation for complex rheology problems.

The thesis is organized as follows.

In **Chapter 2** we consider the derivation of mathematical models. The first part is concerned with modelling of flow driven orientational dynamics in concentrated short fibre suspensions. The local orientation state is described in terms of moments of orientational distribution function, the orientational dynamics of a fibre is assumed to be a superposition of dynamics governed by Jeffery's equation and perturbations due to fibre-fibre interactions. The interaction part is modelled as a combination of a diffusive part familiar from the Folgar-Tucker theory and a part arising from geometrical constraints to the rotation of an elongated rigid body in a complex geometry characteristic for a concentrated suspension. The geometrical constraints are described in an averaged sense by using the *excluded volume* concept. A generalization of the Folgar-Tucker model is derived. In the second part we study the problem of closure approximation, which is an integral part of moment based models. A general procedure for deriving the familiar linear and quadratic closures is proposed. In the third part we consider the suspensions of semiflexible fibres, i.e., fibres capable of slight bending into a C-shaped form. The orientation of a fibre is described by a set of two unit vectors, leading to a local orientational distribution function depending on two orientational variables. The moments of such functions are linear combinations of the coefficients of the bispherical harmonics expansion. In the moments description, local orientational state of a semiflexible fibre suspension is described by a first order moment and two second-order moments. The closure problem arising in the moments formulation is investigated in the fourth part of this Chapter. We derive three variants of linear closure, a polynomial closure and a hybrid closure.

Chapter 3 is devoted to the analysis of well-posedness (existence, uniqueness and continuous dependence on the data) of the system consisting of a model developed in Chapter 2 and macroscopic flow equations described by an incompressible Navier-Stokes equation, which is coupled to the orientation equations through a non-Newtonian constitutive relation. We prove the existence and uniqueness of a weak solution locally in time for sufficiently small data. Some of the fibre orientation models need to be regularized, e.g., the definition of the shear rate $\dot{\gamma}$ near the origin for Folgar-Tucker like equations and the velocity curvature field μ for the semiflexible fibre models need to be smoothed (mollified). In order to prove the existence of a solution, the system is formulated as a fixed-point problem for a mapping consisting of a solution operator to a Stokes equation and a solution operator to a linearized

transport equation, and the existence is proved by Schauder's principle. The continuous dependence of the solution on the data is demonstrated near the trivial solution for vanishing data.

Numerics and computational experiments are presented in **Chapter 4**. We start with comparing the closure approximations for the semiflexible fibres model in two-dimensional case and find that the polynomial closure is the most robust choice, and is therefore recommended for implementations. In the second part we present a finite volume discretization for complex rheology problems, which is implemented in the CoRheoS (Complex Rheology Solver) software, and describe an upstream discretization of the transport equations modelling the fibre orientation dynamics. The third part summarizes the simulation results obtained by using the model developed in Chapter 2.1 in two and three dimensional domains, and validates the results for the Folgar-Tucker limit against experimental results and simulations published in scientific literature.

The work is summarized and conclusions are drawn in **Chapter 5**.

Chapter 2

Modelling

This chapter is concerning with mesoscale modelling of fibre orientation dynamics described by fibre orientation tensors. In the first part a nematic potential is incorporated in the framework of Folgar-Tucker model, aiming to study the effects of excluded volume in concentrated short fibre suspensions. In the second part a method for constructing simple closure approximations is presented and the familiar linear and quadratic closures are reconstructed. The third part is concerning with semiflexible fibre suspensions. A semiflexible fibre is modelled as a system consisting of three connected beads, and from the dynamics of a single fibre evolution equations for low order statistical moments of orientation distribution function are derived. The last section is dealing with the closure problem that origins from the semiflexible fibre model. We use the techniques developed in Section 2.2 to construct closures.

2.1 Concentrated short fibre suspensions

As discussed in [57], a decrease of effective rotary diffusivity as a function of concentration has been observed at fibre concentration $n_f l_f^2 d_f > 0.5$. In most models the effective rotary diffusion is expressed through the Folgar-Tucker coefficient C_i determined in an empirical way. However, the physical reasons behind rotary diffusivity are quasi-random fibre-fibre interactions, and there is no reason to believe that the frequency of interactions would decrease with increasing concentration. A physical explanation of this phenomenon can be achieved by using the concept of the *excluded volume.*

Let us consider a *test* fibre in a concentrated suspension. The test fibre has several geometrically close neighbours, which impose geometrical constraints for the position and rigid body motion of the test fibre.

Let us denote the fibre length by l_f and the diameter by d_f. Let the orientation of a background fibre be denoted by $p_1 \in S^2$, and consider a test fibre with orientation $p \in S^2$ located near the background fibre. The domains occupied by the test fibre and the background fibre partially overlap if the geometric center of the test fibre is located in a certain parallelepiped shaped region around the geometric center of the background fibre as illustrated in Figure 2.1.
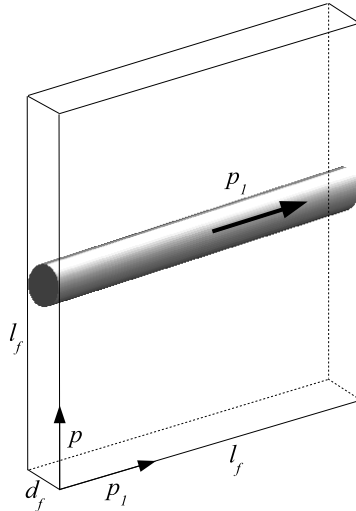
Figure 2.1: Illustration of the excluded volume concept. A background fibre with orientation p_1 does not leave space for a test fibre with orientation p within the sketched volume.

The volume of this region is approximately $V_{\text{ex}}(p, p_1) = r_f l_f^2 |p \times p_1|$ and is called the excluded volume.

In a mesoscale description we think of the test fibre as located in a background mean field enforced by the surrounding fibres. The excluded volume effect can be modelled as an additional potential acting on the test fibres, thus Jeffery's equation (1.6) is modified:

$$\omega = p \times (Mp) - \frac{D_r}{\psi} \mathscr{R}_p \psi - \mathscr{R}_p U(p, \psi). \tag{2.1}$$

The potential U can be derived by using entropic considerations (cf. [45]). Fibre structures with locally aligned orientation state occupy less volume than disordered structures, hence at a fixed concentration an ensemble of locally aligned fibres has more degrees of freedom and thus larger entropy than a disordered ensemble. This observation gives a qualitative explanation of the fact that at high concentrations the fibres show a collective orientational behaviour like the molecules of a liquid crystal in the nematic phase.

L. Onsager proposed the following expression for the potential:

$$U_{\text{Onsager}}(p, \psi) = \int_{S^2} V_{\text{ex}}(p, p_1)\psi(p_1)\mathrm{d}\sigma(p_1) = r_f l_f^2 \int_{S^2} |p \times p_1|\psi(p_1)\mathrm{d}\sigma(p_1),$$

see [55], [17], [14]. The lack of smoothness of the kernel $|p \times p_1|$ causes difficulties to work with this potential. A commonly used approximation of the Onsager potential has been proposed by Maier and Saupe (see [50] or [14] for a modern exposition)

$$U_{\text{MS}}(p, \psi) = r_f l_f^2 \int_{S^2} |p \times p_1|^2 \psi(p_1)\mathrm{d}\sigma(p_1).$$

Using the Lagrange identity $|p \times p_1|^2 = |p|^2|p_1|^2 - (p \cdot p_1)^2$, the integral can be evaluated:

$$U_{MS}(p) = r_f l_f^2 (1 - a^{(2)} : p \otimes p).$$

The potential reaches its minimum at the points where $a^{(2)} : p \otimes p$ is maximal, i.e, when p is an eigenvector of the matrix $a^{(2)}$ with the largest eigenvalue. Thus, the force due to the Maier-Saupe potential drives the test fibre towards the average mean field orientation, resisting thereby the rotary diffusion and explaining the observed decrease in effective rotary diffusivity. We use a potential proportional to Maier-Saupe potential, namely,

$$U(p, \psi) = N_0(1 - a^{(2)} : p \otimes p). \tag{2.2}$$

In general, the constant N_0 may depend on the parameters of the suspension.

The function ψ satisfies the Smoluchowski equation (1.7) with $\omega = p \times \dot{p}$ and (2.1) - (2.2). The equation for second order moment $a^{(2)}$ can be obtained by multiplying both sides of (1.7) with $p \otimes p$ and integrating over the unit sphere. For the right hand side we obtain terms that are familiar from the Folgar-Tucker model and an extra term

$$-\int_{S^2} p \otimes p \mathscr{R}_p \left[\psi \mathscr{R}_p [N_0(a^{(2)} : (p \otimes p) - 1)] \right] = 4N_0 \left(a^{(2)} \cdot a^{(2)} - a^{(4)} : a^{(2)} \right).$$

By setting N_0 proportional to the shear rate: $4N_0 = U_0 \dot{\gamma}$, we obtain a *generalized Folgar-Tucker equation for concentrated suspensions* in the following form:

$$\begin{aligned} \tfrac{D}{Dt} a^{(2)} &= a^{(2)} \cdot M + M^\top \cdot a^{(2)} - (M + M^\top) : a^{(4)} \\ &+ \dot{\gamma} \left\{ C_i(I - 3a^{(2)}) + U_0(a^{(2)} \cdot a^{(2)} - a^{(2)} : a^{(4)}) \right\}. \end{aligned} \tag{2.3}$$

This model contains two scalar parameters: the Folgar-Tucker rotary diffusivity constant C_i and the Maier-Saupe coefficient U_0. The physical interpretation of these parameters is similar as for the Doi-Edwards equation describing the orientational dynamics of macromolecules, cf. [14], namely, the term proportional to C_i drives the suspension to the isotropic state, while the term with U_0 drives it to an aligned (nematic) state.

In applications of the model, the parameter values should be estimated, e.g., by using a formula for calculating C_i from the parameters of the suspension and identify the corresponding value of U_0 by experimentally measuring the fibre alignment degree in a shear flow, see Section 4.1. Note also that by setting $U_0 = 0$ in (2.3), the Folgar-Tucker equation is obtained.

2.2 On closure approximations

As described in Section 1.2.5, various closures have been proposed for the Folgar-Tucker equation. Some of the proposed approximations have been taylored for the specific application (such as the natural closure and the fitted closures), others can be applied for various similar problems that arise in the field of statistical mechanics.

This section aims to provide an unified treatment of the closure problem, explaining and formalizing the ideas behind some of the most simple closure relations - the linear and quadratic closures. A formal procedure for constructing analogous closures for more general situations is formulated; in Section 2.4 it is applied to a new closure problem.

We start with considering the parent model of the moment equations, namely, the Smoluchowski equation. In the formulation (1.7) it is expressed in Eulerian coordinates, where it is a *degenerate* parabolic equation for $\psi(t, x, p)$ on $[T_0, T] \times \Omega \times S^{d-1}$, since the diffusive term is acting only in the p space and not in the x space. In Lagrangian coordinates formulation the convective partial derivatives in x direction are eliminated, leaving a parabolic equation on the sphere:

$$\dot{\psi} = \mathscr{R}_p \left[D_r \mathscr{R}_p \psi - p \times q_j(p) \psi + \psi \mathscr{R}_p U_{MS}(p, \psi) \right], \qquad (2.4)$$

where $q_j(p)$ is the right-hand side of Jeffery's equation. Observe that all components of $p \times q_j(p) = p \times (Mp)$ as well as U_{MS} are second order polynomials in the components of p. Observe further that the operator $\mathscr{R}_p = p \times \nabla_p$ maps polynomials to polynomials, and leaves the polynomial degree invariant.

By multiplying (2.4) with p^n and integrating by parts, we obtain an equation with respect to the moment $a^{(n)}$ with source term components given by the integral of ψP_{n+2}, where P_n denotes a polynomial of degree n. Hence the equation for the n-th order moment can be written as $\dot{a}^{(n)} = f_n(a^{(n+2)})$. Since the odd order moments vanish due to the symmetry of ψ, it suffices to consider the moments of even order $n = 2, 4, \ldots$ In fact, the Smoluchowski equation is equivalent to the infinite system of ordinary differential equations

$$\dot{a}^{(n)} = f_n(a^{(n+2)}), \quad n = 2, 4, \ldots$$

Clearly, this expansion is equivalent to the expansion of ψ in orthogonal polynomials on the sphere, i.e., spherical harmonics for $d = 3$ and Fourier series for $d = 2$.

Numerical simulations cannot directly handle equation systems with infinite number of components, therefore a reduction to finite dimension is required. Let a finite subset of the equations be chosen, and let the maximal order of a component be $2n_l$, then the evolution of this component depends on components of $a^{(2n_l+2)}$, which are unknown by the assumption. To ensure the uniqueness of solution for the resulting underdetermined system of equations, it must be supplemented with additional constraints of the form $a^{(2n_l+2)} = f(a^{(2)}, \ldots, a^{(2n_l)})$ called *closure approximations*.

Let us provide a way of constructing the additional constraints so that the classical linear and quadratic closure approximations are reconstructed for $n_l = 2$. These construction tools are used later in Section 2.4 for constructing analogous closures for other problems.

2.2.1 Abstract formulation of the closure problem

By definition, the moments are linear operators on ψ, hence the closure problem can be formulated as approximating an operator using a given set of other operators.

Let H be a Hilbert space, and let H' be its dual space of continuous functionals $m : H \to \mathbb{R}$. By Riesz theorem, H and H' are isomorphic, therefore the elements of H' can be identified with the pendants in H. With this identification, the dual pairing operator $\langle \cdot, \cdot \rangle_{H',H} : H' \times H \to \mathbb{R}$ defined as $\langle m, \psi \rangle_{H',H} = m(\psi) = m\psi$ equals the inner product $(m, \psi)_H$, with the short-hand notation $m\psi = \psi m$.

Let $\mathscr{M} \subset H$ be a countable set of functionals $\mathscr{M} = \{m_i : i \in \mathbb{N}\}$. For every $i \in \mathbb{N}$ m_i is said to generate a moment $m_i : (\psi \in H) \mapsto m_i\psi \in \mathbb{R}$.

Let a subset $\mathscr{I} \subset \mathscr{M}$ be given, we call the elements of $\mathscr{I}$ the accessible moments and write $\mathscr{I} = \{m_i : i \in \mathcal{I}_0\}$, where $\mathcal{I}_0 \subset \mathbb{N}$. The linear hull of the set $\mathscr{I}$ is denoted by $G_{\mathscr{I}} \subset H$. The orthogonal projector from H to the subspace $G_{\mathscr{I}}$ is denoted by $\Pi_{\mathscr{I}}$. Projectors are self-adjoint operators, in particular, for every $m_i \in \mathscr{M}$ and every $\psi \in H$ it holds

$$(\Pi_{\mathscr{I}} m_i)\psi = (\Pi_{\mathscr{I}}\psi)m_i.$$

The closure problem can be formulated as follows. Suppose that for an unknown $\psi \in H$ the real values of $m_i\psi$ for $i \in \mathscr{I}_0$ are given. Let $m \in \mathscr{M}\setminus\mathscr{I}$. Estimate $m\psi$.

Example. For $\psi \in H = L^2(S^2)$, consider the set of all components of the moments $a^{(n)}$, thus $\mathscr{M} = \{p^i : i \in \mathbb{N}_0^d\}$ using multi-index notation. In the classical setting the moments of order up to 2 are accessible: $\mathscr{I} = \{p^i : |i| \leq 2\}$, and the closure problem is formulated for each component of $m \in \{p^i : |i| = 4\}$ separately.

Due to the linearity of the moment operators, the values of the accessible moments $m_i\psi$ uniquely determine the projection $\Pi_{\mathscr{I}}\psi$ and vice versa.

The sought moment can be splitted as

$$m\psi = m(\Pi_{\mathscr{I}}\psi) + m(\Pi_{\mathscr{I}}^{\perp}\psi), \qquad (2.5)$$

but the available information does not suffice for determining the last summand unless $m(\Pi_{\mathscr{I}}^{\perp}\psi) = 0$.

The set $\mathscr{I}$ is not necessarily orthonormal or even linearly independent in H. For example, for the "classical" closure problem the linear relation $p_1^2 + p_2^2 + p_3^2 - 1 = 0$ holds. For technical reasons we prefer to work using an orthonormal basis. Let $\{\chi_i : i \in \mathscr{I}_1\}$ be an orthonormal basis of $G_{\mathscr{I}}$, then $\chi_i\psi$ can be computed as linear combinations of $m_i\psi$, and

$$\Pi_{\mathscr{I}}\psi = \Sigma_{i \in \mathscr{I}_1}(\chi_i\psi_i)\chi_i.$$

In the special case $H = L^2(S^{d-1})$, m_i polynomial and $\mathscr{I}$ containing polynomials up to a certain degree, a suitable choice of the orthogonal basis for G is the Fourier basis functions $(d = 2)$ and the spherical harmonics $(d = 3)$, see e.g. Appendix A in [27].

2.2.2 Linear closure

The essence of the closure problem is to invert a projection operator. Indeed, given $m(\Pi_{\mathscr{I}}\psi) = (\Pi_{\mathscr{I}}m)\psi$, then formally

$$m\psi = m(\Pi_{\mathscr{I}}^{-1}\Pi_{\mathscr{I}}\psi).$$

Of course, the projector $\Pi_{\mathscr{I}}$ is singular unless it is identity, hence the closure problem is ill-posed. We use a regularization technique, where the ill-posed problem is approximated by a family of well-posed problems. In this case, the singular operator $\Pi_{\mathscr{I}}$ is approximated by a family of regular operators $(\Pi_{\mathscr{I}} + \alpha I)$, where $\alpha > 0$ is a regularization parameter and I is the identity operator. The inverse is given by

$$(\Pi_{\mathscr{I}} + \alpha I)^{-1} = (1 + \alpha)^{-1} \Pi_{\mathscr{I}} + \alpha^{-1} \Pi_{\mathscr{I}}^{\perp}.$$

Thus the regularized closure problem can be solved as

$$m\psi = m \left[(1 + \alpha)^{-1} \Pi_{\mathscr{I}} + \alpha^{-1} \Pi_{\mathscr{I}}^{\perp} \right] \Pi_{\mathscr{I}} \psi = (1 + \alpha)^{-1} (\Pi_{\mathscr{I}} m) \psi.$$

The limit $\alpha \to 0$ is regular, and the last expression can be calculated from accessible moments, thus we have found a unique solution to the regularized problem, which we call the linear closure approximation, given by

$$(m\psi)_{lin} = (\Pi_{\mathscr{I}} m) \psi. \tag{2.6}$$

The decomposition (2.5) gives the following interpretation of the linear closure. *Of all the possible choices of ψ with a given projection choose the one with the least norm in H.* In other words, the unknown part is assumed to vanish: $\Pi_{\mathscr{I}}^{\perp} \psi = 0$. The linear closure is a linear combination of the accessible moments $\{m_i \psi : i \in \mathscr{I}_0\}$, motivating the name.

Examples. Let us consider the closure problem for the Folgar-Tucker model, where the task is to reconstruct $a^{(4)}$ from $a^{(2)}$. Since the components of a moment $a^{(n)}$ are generated by the monomials p^i of order $|i| = n$, the accessible space $G_{\mathscr{I}} \subset L^2(S^{d-1})$ can be identified with the subspace of the polynomials of (even) order not greater than n. Let the orthogonal projection onto the subspace of polynomials of order *not greater than n* be denoted by $\Pi_{(n)}$ and the projection onto the subspace of *homogeneous* polynomials of order n be denoted by Π_n.

Of course, in the relation (2.6) the projector $\Pi_{\mathscr{I}}$ can be substituted by another operator Π' as long as $\Pi' m = \Pi_{\mathscr{I}} m$. In this case we observe that for a homogeneous polynomial m of even order $k \leq (n + 2)$ the identity $\Pi_{(n)} m = \Pi_{n+2}^{\perp} m$ holds. This reformulation allows to easily obtain necessary and sufficient conditions for ψ, under which the linear closure is exact.

2D case. To compute the linear closure, we evaluate (2.6) with $\Pi_{\mathscr{I}} = \Pi_4^{\perp}$ and $m = p^i$ for all i with $|i| = 4$. Here $p = (p_1, p_2) \in S^1$. We compute

$$
\begin{aligned}
\Pi_4^{\perp} p_1^4 &= \tfrac{3}{8} + \tfrac{1}{2}(p_1^2 - p_2^2), \\
\Pi_4^{\perp} p_1^3 p_2 &= \tfrac{1}{2} p_1 p_2, \\
\Pi_4^{\perp} p_1^2 p_2^2 &= \tfrac{1}{8}, \\
\Pi_4^{\perp} p_1 p_2^3 &= \tfrac{1}{2} p_1 p_2, \\
\Pi_4^{\perp} p_1^4 &= \tfrac{3}{8} - \tfrac{1}{2}(p_1^2 - p_2^2).
\end{aligned}
$$

This gives relations for all the components of $\Pi_4^{\perp} p^4$. The right-hand sides can be expressed as linear combinations of the components of p^i, $|i| = 2$ and p^0, thus giving

the linear closures. For a matrix $M \in \mathbb{R}^{2 \times 2}$ we compute the contraction

$$
\begin{aligned}
\langle p^4 \rangle_{lin,\,4} : M \;=\; & \tfrac{1}{8}\mathrm{Tr}(M)I - \tfrac{1}{8}(M + M^\top) + \\
& \tfrac{1}{4}\left[a^{(2)} \cdot (M + M^\top) + (M + M^\top) \cdot a^{(2)} \right].
\end{aligned} \tag{2.7}
$$

From the derivation it is obvious that *the linear closure is exact if and only if* $\Pi_4 \psi = 0$.

3D case. 1. Let us first assume that the only accessible moment is $a^{(0)}$, and compute the linear closure for $a^{(4)}$. In this case, the projector $\Pi = \Pi_2^\perp \circ \Pi_4^\perp$ can be used instead of $\Pi_{(0)}$. Obviously, this closure is exact if and only if $\Pi_2 \psi = \Pi_4 \psi = 0$. We have: $\Pi p_i^4 = \tfrac{1}{5}$ and $\Pi p_i^2 p_j^2 = \tfrac{1}{15}$; the projection of all other fourth-order monomials vanishes. Thus, the "constant" closure is

$$
\left(a_{lin,0}^{(4)} \right)_{ijkl} = \frac{1}{15}(\delta_{ij}\delta_{kl} + \delta_{ik}\delta_{jl} + \delta_{il}\delta_{jk}).
$$

2. Let the moments $a^{(0)}$ and $a^{(2)}$ be accessible, then the linear closure for $a^{(4)}$ can be computed by using the projector $\Pi = \Pi_4^\perp$. Evaluating (2.6), we find the familiar linear closure approximation formula:

$$
\begin{aligned}
\left(a_{lin,2}^{(4)} \right)_{ijkl} = & -\tfrac{1}{35}(\delta_{ij}\delta_{kl} + \delta_{ik}\delta_{jl} + \delta_{il}\delta_{jk}) + \\
\tfrac{1}{7}\Big(\delta_{ij}a_{kl}^{(2)} + \delta_{kl}a_{ij}^{(2)} & + \delta_{ik}a_{jl}^{(2)} + \delta_{jl}a_{ik}^{(2)} + \delta_{il}a_{jk}^{(2)} + \delta_{jk}a_{il}^{(2)} \Big).
\end{aligned}
$$

The contraction with a matrix $M \in \mathbb{R}^{3 \times 3}$ is given by

$$
\begin{aligned}
M : a_{lin,2}^{(4)} \;=\; & -\tfrac{1}{35}\left[\mathrm{Tr}(M)I + M + M^\top \right] + \tfrac{1}{7}\Big[\mathrm{Tr}(M)a^{(2)} + (M : a^{(2)})I + \\
& a^{(2)} \cdot (M + M^\top) + (M + M^\top) \cdot a^{(2)} \Big].
\end{aligned}
$$

Note the difference between the linear closure in two and three-dimensional cases with the same set of accessible moments. We have developed a general procedure for constructing linear closure approximations. Next we consider a generalization of the quadratic closure approximation.

2.2.3 Quadratic closure

In this section we assume that ψ is a generalized function (distribution), i.e., an element of the topological dual space to $C(S^{d-1})$. Let $m_i \in C(S^{d-1})$. In the special case when ψ is a delta-distribution $\psi = \delta_{p_0}$, where $p_0 \in S^{d-1}$, the moment generated by the product of two generators factors as $(m_1 m_2)\psi = (m_1 \psi)(m_2 \psi)$.

Of course, this identity holds only for few particular cases, and not for an arbitrary distribution ψ. However, let us consider the following special case, when ψ is the sum of two delta distributions: $\psi = \tfrac{1}{2}\left[\delta_{p_1} + \delta_{p_2}\right]$. Moreover, we assume that $p_1 = -p_2 = p_0$. Such a distribution is the asymptotic solution of the Smoluchowski equation with $C_i = 0$ under certain stationary flow fields, and thus is of interest for our application.

Again we are interested in the case when the moment generators m_i are homogeneous polynomials, in the tensorial notation given by $m_1(p) = p^n$, $m_2(p) = p^m$. An easy explicit calculation of two expressions yields

$$(m_1 m_2)\psi = \frac{1}{2} \left[(-1)^{n+m} + 1 \right] p_0^{n+m}$$

and

$$(m_1 \psi)(m_2 \psi) = \frac{1}{4} \left[1 + (-1)^{n+m} + (-1)^n + (-1)^m \right] p_0^{n+m}.$$

The right-hand sides of both identities are equal unless n and m are odd simultaneously. Thus, for this particular class of ψ the identity

$$a^{(n)} = a^{(n_1)} \otimes a^{(n_2)}$$

holds whenever $n_1 + n_2 = n$ and the product $n_1 \cdot n_2$ is even.

By setting $n_1 = n_2 = 2$, the classical quadratic approximation is reconstructed.

2.2.4 Summary and open questions

The description of local fibre orientation state in terms of low order statistical moments is efficient due to the low dimension of the configurational space and powerful since it allows to predict both the rheological properties of the suspension and the mechanical properties of the fibre reinforced material after solidification of the matrix. However, the models based on this description require closure approximations. In Section 1.2.5 we have reviewed closures for the Folgar-Tucker model.

Of course, the closure problem for related models such as (2.3) may require different approximations. In this section we have shown that the expressions for linear and quadratic closures depend only on the set of available moments and the polynomial degree of the source terms in the Smoluchowski equation. Thus we have justified the application of linear and quadratic closures for the modified fibre orientation dynamics model (2.3).

The applicability of other closures taylored for Folgar-Tucker model remains an open question. In particular, the family of fitted closures is derived using the exact dynamics of the underlying model. It can be expected that using a modified fibre orientation model, e.g., (2.3) would lead to a different set of optimal fitting parameters. The question, whether the resulting corrections are significant, should be investigated further.

A further interesting question is at which degree $2n$ the closure approximation $a^{(2n+2)} = f(a^{(2n)})$ can be introduced in an optimal way. For the linear closure this question is closely related with the spherical harmonics expansion method for solving the Smoluchowski equation. It can be expected that the optimal value of n depends on the polynomial degree needed to approximate the stationary values of $\psi(p)$, which in turn depend on the shear rate $\dot{\gamma}$ and the constants C_i and U_0.

2.3   3-beads model for semiflexible fibres

In this section we derive a mesoscale based model for dilute suspensions of semiflexible fibres (as published in [72]). The concept of semiflexibility is discussed in the first part. Next, a model of single fibre dynamics is derived, where the fibre is modelled as a system consisting of three spherical beads, connected by rigid connectors. Fibre bending is assumed to be driven by the curvature of the surrounding fluid velocity field. In the third part we derive the Smoluchowski equation describing the dynamics of ensembles of fibres, introduce suitable low-order statistical moments and derive the equations for these moments. Construction of the closure approximations is described in the next Section 2.4.

2.3.1   Semiflexibility

The surrounding fluid exerts traction forces on an immersed fibre, causing a deformation. Let us quantify the degree of fibre bending and find a rough estimate for a typical degree of bending of a fibre in a suspension.

Following [71], we introduce the concept of fibre deflection δ_f as illustrated in Figure 2.2. This concept can be defined conveniently for a fibre under stationary planar load at equilibrium. Let us fix one end of the fibre and define δ_f as the maximal magnitude of deformation. For the set of the fibres in a suspension parameter
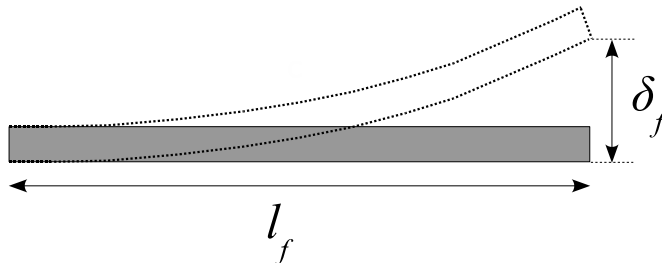
Figure 2.2: Deflection of a semiflexible fibre.

characterizing a *typical* deflection δ_f can be introduced. The fibre *flexibility* in that particular suspension is then defined by the dimensionless quantity

$$\chi = \frac{\delta_f}{l_f}.$$

Let us assume that the fibres are immersed in a viscous fluid. Let the mass of the fibres be negligible, so the elastic response is quasi-static, i.e., the fibre shape is instantaneously adjusted to any changes in the forces. Thus, the surface forces are always balanced by the elastic forces. We also assume that the suspension is dilute, so each fibre can rotate freely. Thus the translational and angular velocity of the fibre is always such that the net linear momentum and net torque due to the surface

forces vanish. Finally, we assume that the presence of the fibres does not significantly disturb the fluid velocity field.

Let us roughly estimate the flexibility χ for a straight cylindrical fibre for a given fluid velocity field.

At low Reynolds numbers (creeping flow) in the three-dimensional case Stockie ([71]) considers fibres with fixed orientation. For this case he derives the following estimate:

$$\chi \propto \frac{\eta \dot{\gamma} d_f l_f^3}{EI},$$

where η is viscosity of the liquid, $\dot{\gamma}$ is velocity shear rate and EI is the bending stiffness (E is Young's modulus of the fibre material and I is area momentum of inertia of a cross-section of the fibre in the bending plane). In our model the shear rate $\dot{\gamma}$ may induce rotation of the fibre, but does not bend it. We assume that the bending of the fibre is caused by the *variation* of the velocity gradient along the fibre. This can be expressed through the curvature of fluid veloctiy field μ, which we define as the tensor $\mu_{jk}^i = \frac{\partial^2 v_i}{\partial x_j \partial x_k}$. The variation of κ is given by Taylor's formula $\kappa(x_0 + \Delta x) - \kappa(x_0) \approx \mu \cdot \Delta x$. Using the distance $|\Delta x| = l_f$, we obtain the estimate

$$\chi \propto \frac{\eta |\mu| d_f l_f^4}{EI},$$

where $|\mu|$ measures the magnitude of the tensor μ.

This estimate is only of qualitative nature; it demonstrates that the flexibility depends on the shape and material constants of the fibre and the velocity field and viscosity of the fluid.

In Section 1.3.1 the classification of fibre orbits has been mentioned. Both experimental evidence (see e.g. [23]) and simulations ([71]) suggest that the dominating fibre orbit class depends on the flexibility. At small values of χ most fibres rotate in the *springy* or C-shaped turn mode. In the framework of this thesis we say that a flowing fibre suspension is a *semiflexible* fibre suspension if the dominating fibre rotation mode is the springy rotation.

In the rest of this section we are concerning with deriving a mesoscale model for semi-flexible fibre suspensions.

2.3.2   3-beads system

The main parameter describing the shape of a semi-flexible fibre in springy rotation mode is the averaged curvature of the center-line. The curvature can be captured by specifying the positions of the end-points and a point in the middle of the fibre, as shown in Figure 2.3.

We introduce the three-beads model for a semiflexible fibre. A 3-beads system consists of three spherical beads connected by two rigid rods. The interaction with the flow takes place only at the beads. The connecting rods are inextensible and do not interact with the fluid.
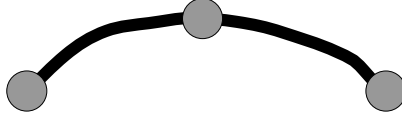
Figure 2.3: Describing the shape of a semi-flexible fibre by positions of three points.
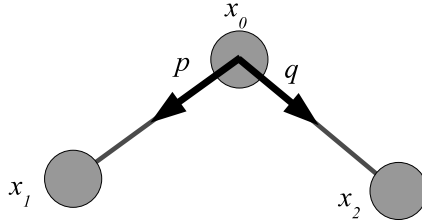

Figure 2.4: 3-beads system.

Let the position of the central bead be x_0, and the positions of the lateral beads be x_1 and x_2, obeying the constraints $\|x_1 - x_0\| = \|x_2 - x_0\| = l_B$. The segment length l_B is one half of the fibre length $l_f/2$.

We introduce the unit *orientation* vectors $p = (x_1 - x_0)/l_B$ and $q = (x_2 - x_0)/l_B$, which are pointing from the central bead located at x_0 to the two other beads as shown in Figure 2.4. Thus, the position and orientation of a 3-beads system is uniquely determined by specifying the coordinates of the central bead x_0 and the set of orientation vectors $\{p, q\}$. The lateral beads are assumed to be indistinguishable, hence the order of the set $\{p, q\} \subset S^2$ does not matter.

The surrounding fluid exerts forces on the 3-beads system through interactions with the beads.

We introduce an elastic potential $U(p, q)$ mimicking the bending rigidity of the fibres. Since the elastic forces are invariant with respect to rotations, U depends only on the angle between p and q or, equivalently, on the scalar product $p \cdot q$. The potential reaches the minimum if the 3-beads systems are straight ($p \cdot q = -1$). The potential is used to calculate the torque acting on the lateral beads. Let the 3-beads system have the orientation $\{p_0, q_0\}$, where p_0 shows the direction from the central bead to a lateral bead B, then the torque acting on B is computed by evaluating $\mathscr{R}_p U(p, q) = \left(p \times \frac{\partial}{\partial p}\right) U(p, q)$ at $(p, q) = (p_0, q_0)$. We neglect the elastic forces acting against torsional motions of the rods.

A typical choice for the potential is the power law

$$U(p, q) = \tilde{k}(p \cdot q + 1)^{\hat{m}}, \tag{2.8}$$

where the coefficient $\tilde{k}$ and the exponent $\hat{m}$ are free parameters that can be used to fit the model.

2.3.3 Dynamics of 3-beads system

Let us consider the dynamics of a single 3-beads system with a fixed rod length l_B, position of the central bead x_0 and the unit orientation vectors $\{p, q\}$. The velocity of the central bead is denoted by V, the velocity of the lateral beads is expressed through the angular velocity of the connectors with respect to the central bead ω_1 and ω_2, where the index 1 refers to the lateral bead in the direction p and index 2 refers to the one in direction q, see Figure 2.5. The linear velocities of the lateral beads can be expressed as $V + l_B\omega_1 \times p$ and $V + l_B\omega_2 \times q$. This description of bead velocities ensures the inextensibility of the connectors since the radial component of the relative veloctity of the lateral beads with respect to the central is zero.
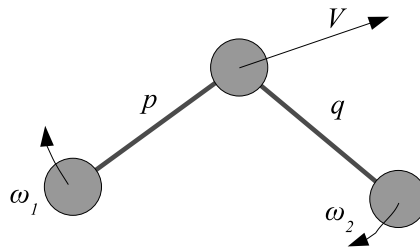

Figure 2.5: Velocity of the 3-beads system.

We make the following assumptions.

1. The beads and the connectors are massless, hence the inertial effects can be ignored.

2. The presence of the fibre does not affect the surrounding fluid, hence the fluid velocity is decoupled from the dynamics of the 3-beads system.

3. The force transfer from the fluid to the fibre occurs through the beads only. The connectors do not interact with the fluid. The beads are assumed to be pointlike with a given drag coefficient ζ.

We assume that the fibre is immersed in a fluid, which occupies a sufficiently large domain Ω so that the 3-beads system can travel through it without hitting any obstacles. One can think of an unbounded domain, e.g., $\Omega = \mathbb{R}^d$. Let the flow velocity $v(x, t)$ be given for all $x \in \Omega$ and time points t under consideration; we assume v to be twice continuously differentiable with respect to x.

The drag force acting on the beads depends on the the relative velocity of the fluid with respect to the beads. We assume that the relative velocity is sufficiently small, so that the drag F_D is proportional to the relative velocity δv:

$$F_D = \zeta \delta v.$$

For spherical beads ζ is given by the Stokes drag coefficient, see [17].

Since the fibre is assumed to be massless, the linear and angular momentum equations are quasi-static: the sum of all acting forces as well as the sum of all torques vanish. The linear momentum conservation law can be expressed in the form

$$\zeta \left[3V + l_B\omega_1 \times p + l_B\omega_2 \times q - v(x_0) - v(x_1) - v(x_2)\right] = -\nabla_x U. \tag{2.9}$$

In this relation the sum of drag forces acting on the three beads is balanced by the totality of forces represented by the conservative potential $U = U(p, q, x)$, which accounts both for external forces (such as gravity) and internal forces (elastic forces due to displacement from the equilibrium state $p + q = 0$). Assuming that the beads are neutrally buoyant and in the absence of other external forces (an example of such potential is (2.8)), we have $\nabla_x U = 0$.

The angular momentum conservation law states that the total torque acting on each of the rigid rods vanishes:

$$\zeta l_B p \times \left[V + l_B\omega_1 \times p - v(x_1)\right] = -\mathscr{R}_p U, \tag{2.10}$$

$$\zeta l_B q \times \left[V + l_B\omega_2 \times q - v(x_2)\right] = -\mathscr{R}_q U. \tag{2.11}$$

From the equations (2.9-2.11) we can express the velocity of the central bead:

$$\begin{aligned}
V &= (I + p \otimes p + q \otimes q)^{-1} \cdot \\
&\quad \left[v(x_0) + (p \cdot v(x_1))p + (q \cdot v(x_2))q + \right. \\
&\quad \left. \frac{1}{\zeta l_B}\mathscr{R}_p U \times p + \frac{1}{\zeta l_B}\mathscr{R}_q U \times q\right].
\end{aligned} \tag{2.12}$$

This expression can be simplified further by using the zeroth order approximation $v(x_1) \approx v(x_2) \approx v(x_0)$:

$$v = v(x_0) + (I + p \otimes p + q \otimes q)^{-1} \cdot \left[\frac{1}{\zeta l_B}\mathscr{R}_p U \times p + \frac{1}{\zeta l_B}\mathscr{R}_q U \times q\right]. \tag{2.13}$$

Let us consider the spectral properties of the matrix

$$A = (I + p \otimes p + q \otimes q)^{-1},$$

assuming that $p \times q \neq 0$. The eigenvectors of A are $w_1 = \frac{p+q}{\|p+q\|}$, $w_2 = \frac{p-q}{\|p-q\|}$ and $w_3 = \frac{p \times q}{\|p \times q\|}$, where the eigenvalues λ_i satisfying $A \cdot w_i = \lambda_i w_i$ are $\lambda_1 = \frac{1}{2(1+p \cdot q)}$, $\lambda_2 = \frac{1}{2(1-p \cdot q)}$ and $\lambda_3 = 1$. Since A is symmetric, we have the decomposition $A = \lambda_i w_i \otimes w_i$ (with summation over i).

The vectors $\mathscr{R}_p U \times p$ and $\mathscr{R}_q \times q$ are orthogonal to p and q respectively. Assuming the fibre deflection to be small, we have $p \approx -q$, and hence these vectors lie in a "narrow" cone around the direction of w_3. Thus, the left multiplication of these vectors by A can be approximated with multiplication by $\lambda_3 = 1$, and we arrive at the approximation

$$V \approx v(x_0) + \frac{1}{\zeta l_B}\left[\mathscr{R}_p U \times p + \mathscr{R}_q U \times q\right]. \tag{2.14}$$

Assuming that $v(x)$ is twice continuously differentiable in a neighbourhood of x_0 (this can be guaranteed, e.g., for a solution of Stokes problem in nice domains), we apply the Taylor expansion

$$v(x_0 + \delta x) = v(x_0) + \kappa \cdot \delta x + \frac{1}{2}\mu^i_{jk}(\delta x \otimes \delta x)_{jk} + \mathcal{O}(|\delta x|^3), \tag{2.15}$$

where $\kappa_{ij} = \frac{\partial v_i}{\partial x_j}$ and $\mu^i_{jk} = \frac{\partial^2 v_i}{\partial x_j \partial x_k}$, both evaluated at x_0. By inserting (2.14) into (2.10-2.11) and by using the expansion (2.15), we get

$$\omega_1 = p \times \left[\kappa \cdot p + \frac{l_B}{2}\mu : (p \otimes p)\right] - \frac{1}{\zeta l_B^2} p \times \left[\frac{\partial U}{\partial p} + \frac{\partial U}{\partial q}\right], \tag{2.16}$$

$$\omega_2 = q \times \left[\kappa \cdot q + \frac{l_B}{2}\mu : (q \otimes q)\right] - \frac{1}{\zeta l_B^2} q \times \left[\frac{\partial U}{\partial p} + \frac{\partial U}{\partial q}\right]. \tag{2.17}$$

The equations (2.14-2.17) are valid for arbitrary potenital U. Let us derive the equations for a particular case of the potential (2.8) with $\hat{m} = 1$, i.e.,

$$U_1(p, q) = \tilde{k}(p \cdot q + 1).$$

In this case, the application of the angular momentum operator on the potential can be approximated:

$$p \times \left[\frac{\partial U_1}{\partial p} + \frac{\partial U_1}{\partial q}\right] = \tilde{k}p \times q(1 - p \cdot q) \approx 2\tilde{k}p \times q. \tag{2.18}$$

Plugging this approximation in (2.16-2.17), we get equations for the rotational dynamics for a 3-beads system in a closed form:

$$\omega_1 = p \times \left[\kappa \cdot p + \frac{l_B}{2}\mu : (p \otimes p)\right] - kp \times q, \tag{2.19}$$

$$\omega_2 = q \times \left[\kappa \cdot q + \frac{l_B}{2}\mu : (q \otimes q)\right] - kq \times p, \tag{2.20}$$

where $k = \frac{2\tilde{k}}{\zeta l_B^2}$.

2.3.4 Smoluchowski equation

We have derived equations for a singe 3-beads system. Next we consider an ensemble of independent 3-beads systems located in a representative volume (RV) near a point $x \in \Omega \subset \mathbb{R}^d$, where $d = 2$ or 3 is the dimension of the physical domain.

Let us introduce the fibre orientation distribution function $\psi(p, q, x) : S^{d-1} \times S^{d-1} \times \Omega \to [0, \infty)$, measuring the probability density to find a fibre in a RV arond x with orientation (p, q). Since the 3-beads system is invariant with respect to a permutation of the lateral beads, the physically relevant quantity is the probability density to find a fibre with orientation $\{p, q\}$; it is given by $\psi(p, q, x) + \psi(q, p, x)$. Hence ψ has the following properties:

- Normalization: $\int_{S^{d-1}} \mathrm{d}\sigma(p) \int_{S^{d-1}} \psi(p,q,x)\mathrm{d}\sigma(q) = 1$,

- Symmetry: $\psi(p,q,x) = \psi(q,p,x)$,

- Nonnegativity: $\psi(p,q,x) \geq 0$ on $S^{d-1} \times S^{d-1} \times \Omega$.

The Smoluchowski equation represents the conservation law of probability density in the state space, which is a generalization of the mass conservation law $\frac{\partial \rho}{\partial t} + \mathrm{div}(\rho v) = 0$, where ρ is the density of a quantity and v is the transport velocity. In our case the velocity in S^{d-1} is described as angular velocity, therefore the divergence is replaced by the angular momentum operator:

$$\frac{\partial \psi}{\partial t} = -\nabla_x(V\psi) - \mathscr{R}_p(\omega_1 \psi) - \mathscr{R}_q(\omega_2 \psi).$$

A term describing orientational diffusion, analogous to the one in Folgar-Tucker model, proportional to $\left(\mathscr{R}_p^2 + \mathscr{R}_q^2\right)\psi$, can easily be included in this model, however, we do not consider mutual interactions of semi-flexible fibres within this thesis.

Assuming that the central bead is travelling with the velocity of the surrounding fluid, i.e., $V \approx v(x_0)$, and given the incompressibility of the fluid $\mathrm{div}\,v = 0$, we can collect two terms appearing in (2.21) in the convective derivative: $\frac{\partial \psi}{\partial t} + \nabla_x(v\psi) = \frac{D\psi}{Dt}$, where $\frac{D}{Dt} = \frac{\partial}{\partial t} + v \cdot \nabla_x$:

$$\frac{D\psi}{Dt} + \mathscr{R}_p(\omega_1 \psi) + \mathscr{R}_q(\omega_2 \psi) = 0. \tag{2.21}$$

By inserting the expressions (2.19 - 2.20) we obtain the Smoluchowski equation in closed form.

2.3.5 Equations for moments

For nonnegative integers m and n we define the (n,m)-th order moment of $\psi(p,q,x)$ as the $(m+n)$-th rank tensor field

$$a^{(m,n)}(x) = \int_{S^2} \int_{S^2} p^m q^n \psi(p,q,x)\mathrm{d}\sigma(p)\mathrm{d}\sigma(q),$$

where $p^m q^n = p^{\otimes m} \otimes q^{\otimes n}$ is an $(m+n)$-th rank tensor. Let $i \in \{1,\dots,d\}^m$ and $j \in \{1,\dots,d\}^n$ be multi-indices, then the (i,j)-th component of $p^m q^n$ is defined as $p^i q^j$.

From the properties of ψ we can deduce certain *symmetries* of the moments. From $\psi(p,q,x) = \psi(q,p,x)$ it follows that $a_{i,j}^{(m,n)} = a_{j,i}^{(n,m)}$, where i and j are multi-indices as above. Thus, the moments $a^{(m,n)}$ and $a^{(n,m)}$ consist of the same elements. Let us assume that $m \geq n$. The moment $a^{(m,n)}$ is invariant with respect to the following permutations of indices.

1. Any permutations of the index set $\{i_1,\dots,i_m\}$.

2. Any permutations of the index set $\{i_{m+1}, \ldots, i_{m+n}\}$.

This is evident from the definition: $a^{(m,n)}$ preserves all the symmetries of $p^m q^n$.

The evolution equations for the moments are obtained directly from the Smoluchowski equation (2.21) by multiplying both sides by $p^m q^n$ and integrating by parts.

For particles with the head-to-tail symmetry such as axis-symmetric rigid fibres ψ can be defined to satisfy $\psi(p) = \psi(-p)$, hence the odd order moments vanish. The 3-beads systems do *not* exhibit this symmetry since a system with orientation $\{p, q\}$ is not equivalent with the system $\{-p, -q\}$ unless $p = -q$, therefore the odd moments can be different from zero, in particular, this holds for the first order moments $a^{(1,0)} = a^{(0,1)}$.

For this reason, the moments description for the 3-beads model is more complicated than for the rigid fibres, for example, a single equation for the second-order moment $a^{(2,0)}$ leads to severe difficulties in constructing closure approximations. In order to construct meaningful closures, we need the equations for the moments $a^{(2,0)}$, $a^{(1,1)}$ and $a^{(1,0)}$, which are derived below.

1. The moment $a^{(2,0)}$ is the direct generalization of the Advani-Tucker tensor $a^{(2)}$ in the sense that, interpreting each 3-beads system as a pair of rigid rods, the computed second order moment satisfies $a^{(2)} = a^{(2,0)}$. The equation is obtained in a similar way as for Folgar-Tucker equation: the Smoluchowski equation is multiplied with $p \otimes p$ and integrated over the variables p and q:

$$\frac{Da^{(2,0)}}{Dt} = -\int_{S^{d-1}} \mathrm{d}\sigma(p) \int_{S^{d-1}} p \otimes p \left[\mathscr{R}_p(\omega_1 \psi) + \mathscr{R}_q(\omega_2 \psi)\right] \mathrm{d}\sigma(q)$$

Integrating the right-hand side by parts and using $\mathscr{R}_q(p \otimes p) = 0$ gives

$$-\int_{S^{d-1}} \mathrm{d}\sigma(p) \int_{S^{d-1}} \mathscr{R}_p(p \otimes p)\psi \left[p \times \left[\kappa \cdot p + \frac{l_B}{2}\mu : (p \otimes p)\right] - kp \times q\right] \mathrm{d}\sigma(q).$$

This expression is the sum of three parts. The part containing κ is familiar from the rigid fibre models, the part containing μ models the bending forces acting on the fibre due to the velocity curvature. The last part, which is proportional to k, stands for elastic forces. Denoting $\mu(p)_i := \mu^i_{jk} p_j p_k$,

$$\mathscr{R}_p(p \otimes p) \cdot (p \times \mu(p)) = p \otimes \mu(p) + \mu(p) \otimes p - 2(\mu(p) \cdot p)p \otimes p;$$

$$\mathscr{R}_p(p \otimes p) \cdot (p \times q) = p \otimes q + q \otimes p - 2(p \cdot q)p \otimes p.$$

Calculating the integrals and using the definition of the moments, we obtain an equation for $a^{(2,0)}$:

$$
\begin{aligned}
\frac{Da^{(2,0)}}{Dt} &= a^{(2,0)} \cdot \kappa^\top + \kappa \cdot a^{(2,0)} - (\kappa + \kappa^\top)_{kl} a^{(4,0)}_{klij} + \\
&\quad \frac{l_B}{2}\left[\mu_{jkl} a^{(3,0)}_{ikl} + \mu_{ikl} a^{(3,0)}_{jkl} - 2\mu_{klm} a^{(5,0)}_{klmij}\right] - \\
&\quad 2k\left[a^{(1,1)} - a^{(3,1)}_{ijkk}\right].
\end{aligned}
\tag{2.22}
$$

2. The moment $a^{(1,1)}$ is defined as the averaged value of $p \otimes q$. The trace $\mathrm{Tr}[a^{(1,1)}] = \int \mathrm{d}\sigma(p) \int p \cdot q \psi \mathrm{d}\sigma(q)$, can be interpreted as the averaged cosine of the angle between the rods connecting the beads, thus $\mathrm{Tr}[a^{(1,1)}]$ can be used as a scalar measure of the local degree of fibre bending. The corresponding equation is obtained from the Smoluchowski equation

$$\frac{Da^{(1,1)}}{Dt} = -\int_{S^{d-1}} \mathrm{d}\sigma(p) \int_{S^{d-1}} p \otimes q \left[\mathscr{R}_p(\omega_1\psi) + \mathscr{R}_q(\omega_2\psi)\right] \mathrm{d}\sigma(q).$$

Integrating by parts, we obtain expressions of the type $(\mathscr{R}_p(p \otimes q))_{ij} = (\mathscr{R}_p(p))_i q_j$, which we calculate explicitly:

$$(\mathscr{R}_p(p))_1 = p_3 e_2 - p_2 e_3;$$
$$(\mathscr{R}_p(p))_2 = p_1 e_3 - p_3 e_1;$$
$$(\mathscr{R}_p(p))_3 = p_2 e_1 - p_1 e_2.$$

Plugging in the relations (2.19-2.20), we find that the integral splits in three summands, again representing Jeffery's dynamics, bending and spring force parts of the model. The integrands can be computed directly:

$$\mathscr{R}_p(p \otimes q) \cdot (p \times \kappa p) = \kappa \cdot p \otimes q - (p \otimes q)(p \otimes p : \kappa),$$

$$\mathscr{R}_q(p \otimes q) \cdot (q \times \kappa q) = p \otimes \kappa \cdot q - (p \otimes q)(q \otimes q : \kappa),$$

$$\mathscr{R}_p(p \otimes q) \cdot (p \times \mu(p)) = \mu(p) \otimes q - p \otimes q(\mu(p) \cdot p),$$

$$\mathscr{R}_q(p \otimes q) \cdot (q \times \mu(q)) = p \otimes \mu(q) - p \otimes q(\mu(q) \cdot q),$$

$$\mathscr{R}_p(p \otimes q) \cdot (p \times q) = q \otimes q - p \otimes q(p \cdot q),$$

$$\mathscr{R}_q(p \otimes q) \cdot (q \times p) = p \otimes p - p \otimes q(p \cdot q).$$

Integrating these components and using the definitions of the moments, we obtain

$$\frac{Da^{(1,1)}}{Dt} = a^{(1,1)} \cdot \kappa^\top + \kappa \cdot a^{(1,1)} - \kappa_{kl}(a^{(3,1)}_{klij} + a^{(3,1)}_{klji}) +$$
$$\frac{l_B}{2}\left[\mu_{jkl}a^{(2,1)}_{kli} + \mu_{ikl}a^{(2,1)}_{klj} - \mu_{klm}a^{(4,1)}_{klmij} - \mu_{klm}a^{(4,1)}_{klmji}\right] -$$
$$2k\left[a^{(2,0)} - a^{(2,2)}_{ikkj}\right]. \tag{2.23}$$

3. The moment $a^{(1,0)}$ is the ensemble average of $p + q$. The equation is

$$\frac{Da^{(1,0)}}{Dt} = -\int_{S^{d-1}} \mathrm{d}\sigma(p) \int_{S^{d-1}} p \left[\mathscr{R}_p(\omega_1\psi) + \mathscr{R}_q(\omega_2\psi)\right] \mathrm{d}\sigma(q).$$

Integrating by parts and using $\mathscr{R}_q p = 0$, we arrive at the integral of

$$(\mathscr{R}_p p) \cdot \left[p \times \left[\kappa \cdot p + \mu : (p \cdot p^\top)\right] + p \times q\right] =$$
$$\kappa \cdot p - p(p \otimes p : \kappa) + \mu(p) - p(\mu(p) \cdot p) + q - p(p \cdot q).$$

After integration, we get

$$
\begin{aligned}
\frac{Da^{(1,0)}}{Dt} \;=\;& \kappa \cdot a^{(1,0)} - \kappa_{jk} a^{(3,0)}_{jki} + \\
& \frac{l_B}{2} \left[\mu_{ijk} a^{(2,0)}_{jk} - \mu_{jkl} a^{(4,0)}_{jkli} \right] - k \left[a^{(1,0)} - a^{(2,1)}_{ijj} \right].
\end{aligned}
\tag{2.24}
$$

The equations (2.22-2.24) are not closed. In general, the evolution equation for $a^{(m,n)}$ depends on the moments $a^{(m+2,n)}$, $a^{(m+1,n+1)}$ and $a^{(m+3,n)}$, as indicated by the polynomial degree of the right-hand sides of the relations (2.19) and (2.20). To obtain a model in closed form, we introduce suitable closure approximations. This is the goal of the next section.

2.4   Closure approximations for mixed moments

The closure problem for the 3-beads model is more difficult than the corresponding problem for rigid fibre models, as the evolution of a moment depends on *three* higher order moments rather than a single one.

The objective of this section is to follow the approach used for constructing the hybrid closure approximation, which is a convex combination of linear and polynomial closures. This section is organized as follows. We start with computing the linear closure approximation from (2.6). Upon the observation that this closure performs poorly for the important case of nearly straight fibres ($p \approx \pm q$), we derive a modified version of linear closure, assuming the absence of the restoring elastic force. These two relations are called *type 1* and *type 2* linear closures respectively. For the states characterized by an intermediate fibre bending degree we construct a closure interpolating between type 1 and type 2 linear closures, using a scalar measure of fibre bending degree. Next we define a family of *homogeneous order preserving polynomial closures*, generalizing the concept of quadratic closure, and motivate the choice of a particular representative from this class. Finally, a *hybrid* closure approximation is defined as a convex combination of the hybrid linear closure and the homogeneous polynomial closure. We restrict the constructions to the two-dimensional case, leaving the three-dimensional case for future work. The discussion of the performance of the closures is postponed to Section 4.1.

The formula (2.6) contains a projection operator on the space $L^2(C \times C)$, where C is a configurational space. In the two-dimensional case C is the circle S^1, while in the three-dimensional case it is the sphere S^2. The projection of the elements of $L^2(C \times C)$ can be expressed in terms of projections of $L^2(C)$; this fact allows to simplify the computations of closure relations. Let us recapitulate the relevant concepts from functional analysis.

Let H_1 and H_2 be two Hilbert spaces with orthonormal bases $\{w^1_i : i \in I_1\}$ and $\{w^2_i : i \in I_2\}$. The tensor product of H_1 and H_2 is the Hilbert space $H_1 \otimes H_2$ defined by the following steps. First, construct the linear vector space with the basis $\{w_{ij} : i \in I_1, j \in I_2\}$, where we formally define $w_{ij} := w^1_i w^2_j$. Secondly, endow the

vector space with the unique inner product satisfying $\langle w_{ij}, w_{kl} \rangle_H = \delta_{ik}\delta_{jl}$. Finally, form the closure with respect to the inner product norm.

Let X and Y be measurable spaces with measures μ_X and μ_Y. Further let the space of square measurable functionals over the product space $X \times Y$ with the measure $\mu_X \times \mu_Y$ be denoted $L^2(X \times Y)$. Then the space $L^2(X \times Y)$ is isomorphic to the Hilbert space $L^2(X) \otimes L^2(Y)$. It follows that if $f \in L^2(X \times Y)$ is a.e. equal to a continuous function, then it can be expanded as

$$f(p,q) = \sum_{i,j} \left\langle f(\cdot, q), w_i^X \right\rangle_{L^2(X)} \left\langle f(p, \cdot), w_j^Y \right\rangle_{L^2(Y)} w_i^X(p) w_j^Y(q).$$

If f can be expressed as $f(p,q) = P(p)Q(q)$ (*separation of variables*), then

$$f(p,q) = \left(\sum_i \left\langle P, w_i^X \right\rangle_{L^2(X)} w_i^X(p) \right) \cdot \left(\sum_i \left\langle Q, w_i^Y \right\rangle_{L^2(Y)} w_i^Y(q) \right).$$

In this case, the coefficients $\langle f, w_{ij} \rangle$ for all $i \leq n_1$, $j \leq n_2$ can be computed in the following efficient way: first compute $a_i = \left\langle P, w_i^X \right\rangle_{L^2(X)}$ for $i \leq n_1$ and $b_j = \left\langle Q, w_j^Y \right\rangle_{L^2(Y)}$ for $j \leq n_2$, and then use $\langle f, w_{ij} \rangle = a_i b_j$.

Remark: Let $X = Y = S^2$ and the basis functions w_i be the spherical harmonics, then the basis functions $w_{ij}(p,q) = w_i(p)w_j(q)$ are called the *bispherical harmonics*.

2.4.1   Linear closure

Let us formulate the closure problem for the two-dimensional version of the equations (2.22-2.24) using the notation introduced in Section 2.2. We are working in the space $H = L^2(S^1 \times S^1)$. The set of moments is given by $\mathcal{M} = \{p^i q^j : i, j \in \mathbb{N}_0^2\}$. The accessible moments are the components of the moments, for which the equations (2.22-2.24) are solved, namely, $\mathcal{I} = \{p^i q^j : i, j \in \mathbb{N}_0^2, (|i|, |j|) \in \{(1,0), (1,1), (2,0)\}$. The closure problem is formulated for each component of the inaccessible moments appearing in the equations (2.22-2.24), namely, for $m_{ij} = p^i q^j$, where $(|i|, |j|) \in \{(2,1), (2,2), (3,0), (3,1), (4,0), (4,1), (5,0)\}$.

Because of the symmetry $a^{(2,0)} = a^{(0,2)}$ and $a^{(1,0)} = a^{(0,1)}$, the accessible subspace $G_{\mathcal{I}}$ is spanned by the components of p, $p \otimes p$, $p \otimes q$, q, $q \otimes p$ and $q \otimes q$. The normalization condition $\mathrm{Tr}(p \otimes p) = 1$ implies that G contains the constant functions. Throughout this section, let Π be the orthogonal projector $\Pi : H \to G_{\mathcal{I}}$.

Next we cumpute the linear closure by (2.6); this means evaluating Πm for all components of inaccessible moments m.

Note that each component of $p^m q^n$ can be expressed as $p_1^{m_1} p_2^{m_2} q_1^{n_1} q_2^{n_2}$, where $m_1 + m_2 = m$ and $n_1 + n_2 = n$, thus we can exploit the symmetries of $a^{(m,n)}$ and compute only the projections of the different monomials. The results are summarized below, using the following notation. For each inaccessible component of $m(p,q) = p^n q^m$ we write the indices (n, m), followed by the projections of the monomials $p_1^{m_1} p_2^{m_2} q_1^{n_1} q_2^{n_2}$ for all choices with $m_1 + m_2 = m$ and $n_1 + n_2 = n$.

- $(2,1)$: $\Pi p_i p_j q_k = \frac{1}{2}\delta_{ij}q_k$.

- $(2,2)$:
  $\Pi p_1^2 q_1^2 = \frac{1}{2}(p_1^2 + q_1^2) - \frac{1}{4}$, $\Pi p_1^2 q_1 q_2 = \frac{1}{2}q_1 q_2$, $\Pi p_1^2 q_2^2 = \frac{1}{2}(p_1^2 + q_2^2) - \frac{1}{4}$,
  $\Pi p_1 p_2 q_1^2 = \frac{1}{2}p_1 p_2$, $\Pi p_1 p_2 q_1 q_2 = 0$, $\Pi p_1 p_2 q_2^2 = \frac{1}{2}p_1 p_2$,
  $\Pi p_2^2 q_1^2 = \frac{1}{2}(p_2^2 + q_1^2) - \frac{1}{4}$, $\Pi p_2^2 q_1 q_2 = \frac{1}{2}q_1 q_2$, $\Pi p_2^2 q_2^2 = \frac{1}{2}(p_2^2 + q_2^2) - \frac{1}{4}$.

- $(3,0)$: $\Pi p_1^3 = \frac{3}{4}p_1$, $\Pi p_1^2 p_2 = \frac{1}{4}p_2$, $\Pi p_1 p_2^2 = \frac{1}{4}p_1$, $\Pi p_2^3 = \frac{3}{4}p_2$.

- $(3,1)$: Since $q \in G_{\mathscr{I}}$ and $q \perp p^i$ in H, all components can be computed by $\Pi p^i q_j = q_j \Pi p^i$ for any multiindex $|i| = 3$.

- $(4,0)$: $\Pi p_1^4 = \frac{3}{8} + \frac{1}{2}(p_1^2 - p_2^2)$, $\Pi p_1^3 p_2 = \frac{1}{2}p_1 p_2$ $\Pi p_1^2 p_2^2 = \frac{1}{8}$, $\Pi p_1 p_2^3 = \frac{1}{2}p_1 p_2$, $\Pi p_1^4 = \frac{3}{8} - \frac{1}{2}(p_1^2 - p_2^2)$.

- $(4,1)$: $\Pi p_1^4 q_j = \Pi p_2^4 q_j = \frac{3}{8}q_j$, $\Pi p_1^2 p_2^2 q_j = \frac{1}{8}q_j$, all other components vanish.

- $(5,0)$: $\Pi p_1^5 = \frac{5}{8}p_1$, $\Pi p_1^4 p_2 = \frac{1}{8}p_2$, $\Pi p_1^3 p_2^2 = \frac{1}{8}p_1$, $\Pi p_1^2 p_2^3 = \frac{1}{8}p_2$,
  $\Pi p_1 p_2^4 = \frac{1}{8}p_1$, $\Pi p_2^5 = \frac{5}{8}p_2$.

Thus we have derived linear closure approximations for all unknown terms of (2.22-2.24). Let us write out the resulting equations in a convenient way for implementation and analysis.

Equations with Type 1 linear closure. In order to distinguish the solutions of equations (2.22-2.24) with closure approximations from the *exact* moments, we denote the approximation of $a^{(2,0)}$ by a, that of $a^{(1,1)}$ by b and that for $a^{(1,0)}$ by c. Where possible, we simplify the equations by using the incompressibility condition $\mathrm{Tr}(\kappa) = 0$. We denote the components of μ as follows:

$$\mu_{..}^1 = \begin{pmatrix} \mu_1^1 & \mu_3^1 \\ \mu_3^1 & \mu_2^1 \end{pmatrix}, \mu_{..}^2 = \begin{pmatrix} \mu_1^2 & \mu_3^2 \\ \mu_3^2 & \mu_2^2 \end{pmatrix}.$$

The equation (2.22) with linear closure can be written as

$$\frac{Da}{Dt} = \mathcal{A}_{FT} + \frac{l_B}{2}\mathcal{A}_\mu - 2k\mathcal{A}_k, \tag{2.25}$$

where the first component is

$$\mathcal{A}_{FT} = a \cdot \kappa^\top + \kappa \cdot a + \frac{1}{4}(\kappa + \kappa^\top) - \frac{1}{2}\left[a \cdot (\kappa + \kappa^\top) + (\kappa + \kappa^\top) \cdot a\right],$$

$\mathcal{A}_\mu$ is symmetric and has the components

$$
\begin{array}{ll}
(1,1) & \frac{1}{4}\left[(\mu_1^1 + \mu_2^1 - 2\mu_3^2)c_1 + (2\mu_3^1 - \mu_1^2 - \mu_2^2)c_2\right], \\
(2,2) & \frac{1}{4}\left[(2\mu_3^2 - \mu_1^1 - \mu_2^1)c_1 + (\mu_1^2 + \mu_2^2 - 2\mu_3^1)c_2\right], \\
(1,2) & \frac{1}{4}\left[(3\mu_1^2 + \mu_2^2 + 2\mu_3^1)c_1 + (\mu_1^1 + 3\mu_2^1 + 2\mu_3^2)c_2\right],
\end{array}
$$

$$\mathcal{A}_k = \frac{1}{4} \begin{bmatrix} b_{22} - b_{11} & -2b_{12} \\ -2b_{21} & b_{11} - b_{22} \end{bmatrix}.$$

The equation (2.23) with linear closure is

$$\frac{Db}{Dt} = \mathcal{B}_{FT} + \frac{l_B}{2}\mathcal{B}_\mu - 2k\mathcal{B}_k, \tag{2.26}$$

where

$$\mathcal{B}_{FT} = b \cdot \kappa^\top + \kappa \cdot b - B_1,$$

B_1 is a symmetric matrix with the components

$$\begin{aligned} (1,1) \quad & \kappa_{11}b_{11} + \tfrac{1}{2}(\kappa_{12} + \kappa_{21})b_{12}, \\ (2,2) \quad & \kappa_{22}b_{22} + \tfrac{1}{2}(\kappa_{12} + \kappa_{21})b_{12}, \\ (1,2) \quad & \tfrac{1}{4}(\kappa_{12} + \kappa_{21})(b_{11} + b_{22}), \end{aligned}$$

and the term $\mathcal{B}_\mu$ has the components

$$\begin{aligned} (1,1) \quad & -4(\mu_1^1 + \mu_3^2)c_1, \\ (2,2) \quad & -4(\mu_2^2 + \mu_3^1)c_2, \\ (1,2) \quad & -2\left[(\mu_2^2 + \mu_3^1)c_1 + (\mu_1^1 + \mu_3^2)c_2\right]. \end{aligned}$$

Surprisingly, we find that the term modelling the bending rigidity of the fibres is constant:

$$\mathcal{B}_k = \frac{1}{4}I.$$

Finally, (2.24) with linear closure approximation is given by

$$\frac{Dc}{Dt} = \mathcal{C}_{FT} + \frac{l_B}{2}\mathcal{C}_\mu - k\mathcal{C}_k, \tag{2.27}$$

where the summands stand for the following matrices:

$$\mathcal{C}_{FT} = \kappa \cdot c - \frac{1}{4}\begin{bmatrix} 2\kappa_{11}c_1 + (\kappa_{12} + \kappa_{21})c_2 \\ 2\kappa_{22}c_2 + (\kappa_{12} + \kappa_{21})c_1 \end{bmatrix},$$

$$\mathcal{C}_\mu = \mu_{jk}^i : a_{jk} - \begin{bmatrix} \nu_{11}^1 + \nu_{12}^2 \\ \nu_{12}^1 + \nu_{22}^2 \end{bmatrix},$$

where $\nu_{jk}^i := \mu_{lm}^i (a_{cl}^{(4,0)})_{jklm}$, and

$$\mathcal{C}_k = \frac{1}{2}c.$$

The equations (2.25-2.27) form a closed system of equations, which we call the moment equations for dilute semi-flexible fibre suspensions with *type 1 linear closure.*

Discussion. From (2.5) we can find a necessary and sufficient condition for the type 1 linear closure to be exact. The closure is exact if and only if in the bispherical harmonics expansion of ψ all coefficients of order $(2,1)$, $(2,2)$, $(3,0)$, $(3,1)$, $(4,0)$, $(4,1)$

and $(5,0)$ vanish. Unfortunately, there are physically relevant orientation states, for which this closure yields meaningless results.

For instance, let us consider the case of flow with vanishing spatial derivatives $\kappa = 0$ and $\mu = 0$. Let at the initial time the fibres be straight, with isotropic orientation distribution: $b = -\frac{1}{3}I$. In this case, (2.26) reduces to

$$\dot{b} = -\frac{k}{2}I,$$

and the solution is $b(t) = -(\frac{1}{3} + \frac{k}{2}t)I$. For any $k > 0$ and $t > 0$, we have $\mathrm{Tr}(b(t)) < -1$, contradicting the normalization of ψ, which would imply the inequality

$$\left|\mathrm{Tr}[a^{(1,1)}]\right| \leq 1.$$

Thus, type 1 linear closure may fail if the fibres are nearly straight. For such orientational states $\psi(p, q)$ shows a sharp peak in regions near $p = -q$, thus the bispherical harmonics expansion of ψ converges slowly, and the linear closure approximation is indeed likely to fail. An explanation based on the model behaviour can be given as follows. In the modelling we assume no correlation between the orientation vectors p and q of a single fibre, hence the *average* fibre is expected to be bent. Due to the bending rigidity, the fibre exhibits a tendency to straighten out. Since the model fails to recognize the moment when the fibres are straight and the spring forces stop acting, the solution leaves the physically admissible subset of the state space in finite time. Next we present a modification of the linear closure preventing the scenario of this instability.

Type 2 linear closure. Let us construct a linear closure approximation for the case $p \approx -q$. The first naive approach to derive the closure using the identity $p = -q$ implies that $a^{(n,m)} = (-1)^m a^{(n+m,0)}$ and $a^{(2n+1,0)} = 0$, what actually defines rigid fibres. For this reason, we use the identity $p \approx -q$ only to turn off the spring forces.

In terms of closure approximations this can be achieved by using one set of closure approximations for the parts of equations (2.22-2.24) proportional to k and another, namely, type 1 linear closure for the other terms. Using $p = -q$ for the terms proportional to k, by the definition of the moments we compute $a^{(3,1)}_{ijkk} = a^{(2,0)}_{ij}$, $a^{(2,2)}_{ikkj} = a^{(1,1)}_{ij}$ and $a^{(2,1)}_{ijj} = a^{(1,0)}_{i}$. This leads to vanishing of the parts proportional to k. Thus, an equivalent description of the equations with *type 2 linear closure* is using type 1 linear closure with

$$k = 0.$$

The resulting system of equations is identical to (2.25-2.27), with the terms $\mathcal{A}_k$, $\mathcal{B}_k$ and $\mathcal{C}_k$ set to zero.

Discussion. This closure can be used for nearly straight fibres with nearly isotropic orientation distribution. A drawback of this model is that the fibre bending rigidity is neglected, therefore its application is limited to states with low fibre bending degree. An advanage is that the equations are very similar to the ones with type 1 linear closure, therefore a convex combination of type 1 and type 2 linear closures can be implemented efficiently. In next part we construct such a hybrid linear closure, where

the fibre bending degree is used as a interpolation parameter between the two linear closures.

Linear hybrid closure. As for the rigid fibre models, linear closure approximations show the best performance in nearly isotropic fibre orientation states. In the 3-beads model there is another important parameter - the fibre bending degree. We introduce the following parameter measuring the average angle between the segments of the fibre:

$$f_\alpha := \langle p \cdot q \rangle = \mathrm{Tr}(a^{(1,1)}) \approx \mathrm{Tr}(b).$$

If the fibre bending distribution is isotropic, i.e., if the pairs of orientation vectors $\{p, q\}$ are uncorrelated, then $f_\alpha = 0$, while for straight fibres with $p \cdot q = -1$ the value is $f_\alpha = -1$.

Of course, the value of f_α does not contain enough information to identify the bending state uniquely, for example, the value $f_\alpha = 0$ characterizes both bending state, when fibres are bent in a right angle and the bending state, where half of the fibres satisfy $p \cdot q = 1$ and the other half $p \cdot q = -1$. However, $p \cdot q > 0$ indicates a very high flexibility χ, so that the assumptions of the 3-beads model do not hold.

We assume that $f_\alpha \in [-1, 0]$, where $f_\alpha = 0$ indicates an isotropic bending distribution, where type 1 linear closure is exact, and $f_\alpha = -1$ indicates straight fibres, where type 2 linear closure applies. For intermediate values of f_α we propose to use a convex linear combination of the two linear closures. This is equivalent to rescaling the bending rigidity constant

$$k \to k' := (1 + f_\alpha)k. \tag{2.28}$$

In the case of overbent fibres $f_\alpha > 0$ we set $k' = k$.

So the equations with linear hybrid closure are given by the equations (2.25-2.27), where k is replaced by k' as given in (2.28).

Discussion. First we note, that the hybrid linear closure is actually *not* linear in the lower moments, since f_α depends on b. This closure performs well for isotropic orientation states with $a \approx \frac{1}{d}I$, for all degrees of fibre bending. However, the closure may lead to physically impossible results in planar or uniaxial orientation states, when the determinant $\det(a)$ reaches zero. The reason for this is that there is no mechanism to prevent some eigenvalues of the solution a to become negative.

For such nearly uniaxial distributions we construct the homogeneous polynomial closures.

2.4.2 Homogeneous polynomial closure

The homogeneous polynomial closure is constructed as a generalization of the quadratic closure for rigid fibre models. In the two-dimensional case the condition $\det(a) = 0$ is equivalent to saying that the fibre orientation state is uniaxial. It follows that all fibres are straight.

In this case, the probability distribution function is the sum of two δ-distributions $\psi = \frac{1}{2}\left[\delta_{(p_0,-p_0)} + \delta_{(-p_0,p_0)}\right]$. The moments can be computed:

$$a^{(m,n)} = \frac{1}{2}p_0^{m+n}\left[(-1)^m + (-1)^n\right].$$

Let the indices be partitioned as $m = m_1 + m_2$, $n = n_1 + n_2$, then

$$a^{(m_1,n_1)} \otimes a^{(m_2,n_2)} = \frac{1}{4}p_0^{m+n}\left[(-1)^m + (-1)^n + (-1)^{m_1+n_2} + (-1)^{n_1+m_2}\right].$$

Evidently, the right hand sides are equal if and only if $(-1)^m + (-1)^n = (-1)^{m_1+n_2} + (-1)^{m_2+n_1}$. This identity holds if and only if at least one of the congruences hold: $m_1 \equiv n_1 (\mathrm{mod}2)$ *or* $m_2 \equiv n_2 (\mathrm{mod}2)$. An equivalent formlulation: *for an uniaxial FO distribution, the formula*

$$a^{(m,n)} = a^{(m_1,n_1)} \otimes a^{(m_2,n_2)} \tag{2.29}$$

is exact iff $(m_1 + n_1) \cdot (m_2 + n_2)$ *is even.* (We call this the *parity condition.*)

Clearly, the equation (2.29) can be applied recurrently to the multiplicands in the right-hand side, provided that the parity condition holds in each step. In this way, closure relations with more than two multiplicands in the right-hand side can be obtained.

Examples: the formula for splitting the moment $a^{(3,1)} = a^{(2,0)} \otimes a^{(1,1)}$ satisfies the parity condition, while the formula $a^{(3,1)} = a^{(3,0)} \otimes a^{(0,1)}$ does not since $(3+0)\cdot(0+1)$ is odd. From the formulas $a^{(4,1)} = a^{(4,0)} \otimes a^{(0,1)}$ and $a^{(4,0)} = a^{(2,0)} \otimes a^{(2,0)}$ we can "recursively" construct $a^{(4,1)} = a^{(2,0)} \otimes a^{(2,0)} \otimes a^{(0,1)}$.

Since the tensor products of moments for an uniaxial orientation distribution are commutative, this class of closure approximations reminds of spliting a monomial into a product of several monomials of lower order, hence we call these formulas *monomial closures*.

One and the same moment can be expressed in various ways, for example, $a^{(2,2)} = a^{(2,0)} \otimes a^{(0,2)} = a^{(1,1)} \otimes a^{(1,1)}$. Moreover, any covex combination of a set of monomial closures yields a formula which is exact for the uniaxial orientation distribution. We propose the name *(homogeneous) polynomial closures* for this class of closures.

Of course, these relations are not identities for arbitrary fibre orientation states. Even in the case $\psi = \frac{1}{2}\left[\delta_{(p_0,q_0)} + \delta_{(q_0,p_0)}\right]$ for $|p_0 \cdot q_0| \neq 1$ the commutativity of tensor products of the moments is lost, therefore application of the homogeneous polynomial closures in such cases introduces an approximation error.

We have seen that for a moment of given order, a whole family of homogeneous polynomial closures can be constructed. To apply this approach for closing the equation system (2.22-2.24), a *single* closure approximation has to be selected. The problem of choosing the closure in an optimal way is non-trivial. For the purposes of this thesis we have chosen the closure by considerations described below, but the question of optimality remains open.

We use approach of splitting the moment according to (2.29) in building blocks as suggested by the Smoluchowski equation. For example, the moment $a^{(5,0)}$ in (2.22)

is used in the contraction $\mu_{klm}a^{(5,0)}_{klmij}$, which arises from integrating the expression $p \otimes p\mu(p) \cdot p$. We interpret it as the product of the moment $a^{(2,0)}$ and a vector: $\langle p \otimes p\mu(p) \cdot p \rangle \approx \langle p \otimes p \rangle \langle \mu(p) \cdot p \rangle$. In the second step we decompose the vector as a matrix-vector product, to arrive at $\mu_{klm}a^{(5,0)}_{klmij} \approx a^{(2,0)}_{ij} \left[(\mu : a^{(2,0)}) \cdot a^{(1,0)} \right]$. Following this somewhat arbitrary method of decomposition of the inaccessible moments, we obtain (2.22-2.24) with the monomial closure approximation

$$\frac{Da}{Dt} = a \cdot \kappa^\top + \kappa \cdot a - (\kappa + \kappa^\top) : aa +$$

$$\frac{l_B}{2} \left[(\mu : a) \otimes c + c \otimes (\mu : a) - 2(\mu : a) \cdot ca \right] - 2k \left[b - a\mathrm{Tr}(b) \right], \tag{2.30}$$

where $(\mu : a)_i = \mu^i_{jk}a_{jk}$,

$$\frac{Db}{Dt} = b \cdot \kappa^\top + \kappa \cdot b - 2(\kappa : a)b +$$

$$\frac{l_B}{2} \left[(\mu : a) \otimes c + c \otimes (\mu : a) - 2(\mu : a) \cdot cb \right] - 2k \left[a - b\mathrm{Tr}(b) \right], \tag{2.31}$$

$$\frac{Dc}{Dt} = \kappa \cdot c - \kappa : ac +$$

$$\frac{l_B}{2} \left[\mu : a - a \cdot (\mu : a) \right] - k \left[1 - \mathrm{Tr}(b) \right] c. \tag{2.32}$$

Discussion. Since the homogeneous polynomial closure is exact for uniaxial fibre orientation states, the solution of the equations (2.30-2.32) never violates the condition of positive semi-definiteness of a, provided that the initial condition is physically admissible. However, the approximation error is expected to increase for biaxial (or triaxial for the three-dimensional case) fibre orientation states. To bundle the advantages of linear and polynomial closures in a single formula, a hybrid closure approximation is constructed in the next section.

2.4.3 Hybrid closure

The hybrid closure is a generalization of the hybrid closure for the Folgar-Tucker model as proposed by Advani and Tucker in [1]. For the rigid fibre models the hybrid closure is a convex combination of the linear and quadratic closures. For the 3-beads model we construct the hybrid closure as a convex combination of the hybrid linear closure (derived in Section 2.4.1) and the homogeneous polynomial closure (derived in Section 2.4.2).

Following [1], we introduce a scalar parameter

$$f_s := 1 - d^d\det(a),$$

measuring the distance of the fibre orientation state from the isotropic state. For the isotropic orientation state we have $f_s = 0$, while for an uniaxial state $f_s = 1$. Let the

hybrid linear closure for the moment $a^{(m,n)}$ be denoted by $a_{lh}^{(m,n)}$ and the homogeneous polynomial closure - by $a_{hp}^{(n,m)}$, then the hybrid closure is defined as

$$a_{hyb}^{(m,n)} = f_s a_{hp}^{(n,m)} + (1 - f_s) a_{lh}^{(m,n)}.$$

With the scalar parameter $f_\alpha = -\text{Tr}(b)$ we can express the hybrid linear closure as a convex combination of type 1 linear closure $a_{lin1}^{(n,m)}$ and type 2 linear closure $a_{lin2}^{(n,m)}$. Then the hybrid closure is

$$a_{hyb}^{(m,n)} = f_s a_{hp}^{(m,n)} + (1 - f_s) \left[f_\alpha a_{lin2}^{(m,n)} + (1 - f_\alpha) a_{lin1}^{(m,n)} \right].$$

Discussion. The hybrid closure is a convex combination of three closures, constructed to be exact whenever any of the three closures is exact. The closure is further discussed in Section 4.1.

2.4.4 Summary and open questions

For the selected set of accessible fibre orientation moments $a^{(1,0)}$, $a^{(1,1)}$ and $a^{(2,0)}$ we have developed three versions of linear closure, a family of polynomial closures and a hybrid closure.

There are different criteria for measuring the quality of a closure approximation. A local measure (depending on the actual fibre orientation state ψ) is given by the approximation error, however, this measure cannot be evaluated during a moments based simulation since the values of the accessible moments do not suffice to determine the exact fibre orientation state. Therefore, the global properties of the solutions of the moment equations such as the invariance of the physically admissible subset of the state space (as discussed in Section 4.1) are more important to ensure the stability of the model.

The linear closures perform well in terms of local approximation error for suitable fibre orientation states. For example, type 1 linear closure is exact for the isotropic fibre orientation state with isotropic bending distribution $\psi(p,q) = \frac{1}{4\pi^2}$. Type 2 linear closure is exact for isotropic orientation state with straight fibres $\psi(p,q) = \frac{1}{2\pi}\delta(p+q)$ (the support of this distribution is the $(d-1)$ dimensional submanifold characterized by $p + q = 0$), and the hybrid linear closure is exact for both cases. However, the linear closures do not satisfy the global stability criteria.

Hence, the only suitable candidates for applications in fibre orientation simulations are the polynomial and hybrid closures. The performance of the two approximations is discussed in Section 4.1. We next formulate some open questions.

What is an optimal choice of the set of accessible moments? In this thesis we use a minimal set of moments that contains the generalization of the Advani-Tucker tensor $a^{(2,0)}$ and allows constructing meaningful polynomial closures. The other moments used in this model also have physical interpretations. The moment $a^{(1,0)}$ is the average deviation from the axially symmetric state of the bent fibres, and $a^{(1,1)}$ contains information about averaged bending angle and distribution of the bending directions. However, the question of optimality of this choice remains open.

Linear closures and Smoluchowski equation. The linear closure is closely related to orthogonal series expansion of the Smoluchowski equation on the torus $S^1 \times S^1$ or bispherical harmonics expansion on $S^2 \times S^2$. Hence the lowest degree of the moment, at which the linear closure is a sufficiently good approximation, depends on the convergence of orthogonal series expansion of ψ.

Construction of fitted closures. One can follow the strategy used for computing the orthotropic fitted closures for the Folgar-Tucker model. The procedure starts with the construction of a family of closure relations parametrized by a small number of scalars. Next a set of relevant velocity fields is selected, and the Smoluchowski equation is numerically solved for these flow fields (for numerical techniques see e.g. [31]). The accessible and inaccessible moments as functions of time are computed from this numerical solution. Finally, a fitting procedure is used to determine the values of parameters, for which the closure approximation describes the numerical data best.

Three-dimensional case. All closures mentioned here can be naturally generalized for the three-dimensional case. The challenge is to find closures with a reasonably good performance for arbitrary orientational states. In particular, the resulting equations should leave the physically admissible state space invariant.

Chapter 3

Some well-posedness results

Now that we have presented several models for fibre orientation dynamics in suspensions, which further depend on the choice of closure approximations, let us introduce a unified notation for the equations. We assume that the fibre orientation is described by a system of transport equations for a vector function $s : (x, t) \mapsto \mathbb{R}^{d_2}$,

$$\frac{Ds}{Dt} = \mathcal{F},$$

where $\mathcal{F}$ is a function of s and the spatial derivatives of an external velocity field $v(x)$, which we leave unspecified for the moment. Hence, the fibre orientation dynamics equations form a linear first order hyperbolic system with the principal part $\partial_t + v \cdot \nabla_x$.

One can formulate a mixed problem for this hyperbolic system assuming the velocity $v(x)$ to be decoupled from $s(x)$. For this, the input data such as the velocity field v, initial and boundary conditions should be specified so that the resulting mixed problem admits a unique solution. Let us consider the problem on $\Omega \times [t_0, T]$, where $\Omega \subset \mathbb{R}^d$ is an open set. Assume that the data needed to comupte $\mathcal{F}$ are specified, in particular, let a sufficiently smooth time continuous vector field $v(x, t) : \bar{\Omega} \times [t_0, T] \to \mathbb{R}^d$ be given. We specify a suitable initial condition $s(x, t_0) = s_0(x)$ for $x \in \Omega$.

The solution of the transport problem can be constructed by using the method of characteristics, which are curves in $\Omega \times [t_0, T]$ tangent to the vector field $(v(\cdot, t), 1)$. Informally speaking, a solution for $(x, t) \in (t_0, T] \times \Omega$ can be constructed if the characteristic going through the point (x, t) can be traced back in time to a point, where the initial or boundary condition is specified. Hence it is obvious that the uniqueness of solution can be ensured by specifying a Dirichlet boundary condition on the *inflow* part of the boundary, which is defined by the subset $(x, t) \in \partial\Omega \times (t_0, T]$, for which

$$v(x, t) \cdot n(x) < 0,$$

where, for $x \in \partial\Omega$, $n(x)$ denotes the unit outer normal to $\partial\Omega$. Thus, the mixed problem is supplemented with the Dirichlet boundary condition

$$s(x, t) = s_b(x, t), \quad x \in \partial\Omega, \quad v(x, t) \cdot n(x) < 0$$

or, to ensure the continuity of the solution, the homogeneous Neumann boundary condition on the inflow boundary.

The velocity field $v(x, t)$ obeys an incompressible Navier-Stokes like equation

$$Re\frac{Dv}{Dt} = \mathrm{div}T + \rho b, \; \mathrm{div}v = 0,$$

where T is the stress tensor, depending on pressure, ∇v and s. A mixed problem for this system can be formulated by prescribing initial and boundary conditions

$$v(x, t_0) = v_0(x), \quad x \in \Omega,$$
$$v(x, t) = v_b(x, t), \quad x \in \partial\Omega \times (0, T].$$

To the knowledge of author, the well-posedness of suspension flow equations and, indeed, for non-Newtonian flow equations with more general boundary conditions than the non-slip condition has not been studied in literature. Thus, the known well-posedness results are valid for homogeneous Dirichlet boundary condition $v(x) = 0$ on $x \in \partial\Omega$ only. In this case the inflow boundary is empty, hence no boundary conditions are required for s.

Well-posedness of complex fluids models with no-slip boundary conditions has been studied in several works, see e.g. the review article [46] and references therein. For viscoelastic fluids with Oldroyd type constitutive law the pioneering work [29] gives proofs of local in time existence and uniqueness results for arbitrary data and global results for small enough data. In [47], global in time existence results are proven for a simplified Oldroyd-B model. Related results in Banach spaces as well as analysis of finite element approximations have been considered in [6]. An existence result for a multiscale model of general dumbbell suspension models in simple Couette flows has been published in [40]. Upon a smoothing of the convective velocity field and in some cases also the extra stress tensor field, the existence result for a coupled system of flow and Fokker-Planck equations has been shown in [4].

As for fibre suspension flow models, the Folgar-Tucker equations have been analyzed in [25], where a local existence for small data is shown for quadratic closure, and in [52], where for a constant orientational diffusivity and linear and quadratic closures the existence of a unique classical solution is shown locally in time and globally in time for sufficiently small data.

The goal of this section is to extend the results from [25] to a wide class of fibre orientation models and for a wide class of constitutive laws. More precisely, we assume the source term of the transport equation and the constitutive relations to be polynomial in s and at most linear in flow variables. Furthermore, we assume that the fibre orientation state characterized by $|s| = 0$ is stationary for quiescent suspensions $v = 0$ and causes no extra forces in the suspension. These assumptions are formalized in the statement of Problem $\mathscr{P}$ in Section 3.2. In order to apply these theoretical results to actual models for rigid fibre and 3-beads models, the equations must be formulated so that the isotropic orientation state corresponds to $|s| = 0$. This is discussed in Section 3.1.2. The results proven in this Chapter do not apply for the 3-beads model with type 1 linear closure since the rest state $|s| = 0$ fails to be

stationary for $v = 0$. The main results of this Chapter is the existence and uniqueness of a solution locally in time for sufficiently small data s_0, v_0 and external forces.

3.1 Preliminaries

We introduce notation used in the rest of this Chapter and formulate some useful results. In particular, we study the solutions to two auxiliary problems.

3.1.1 Notation and function spaces

Let $\Omega \subset \mathbb{R}^d$, $d = 2$ or 3, be a bounded Lipschitz domain with the boundary $\partial \Omega$. Let us introduce the notation for some standard function spaces with Ω as domain. **Spaces of continuous functions.** The space of continuous real-valued functions on Ω is denoted by $C(\Omega)$, the space of uniformly continuous functions - by $C(\overline{\Omega})$. This space can be equipped with the norm $\|v\|_{C(\overline{\Omega})} := \sup\{v(x) : x \in \Omega\}$, making it a Banach space. For natural m, we introduce the space of m-times continuously differentiable functions $C^m(\overline{\Omega}) = \{v \in C(\overline{\Omega}) : D^\alpha v \in C(\overline{\Omega})$ for $|\alpha| \leq m\}$, where α is d-dimensional multi-index and $D^\alpha = D_1^{\alpha_1} \ldots D_d^{\alpha_d} = \left(\frac{\partial}{\partial x_1}\right)^{\alpha_1} \ldots \left(\frac{\partial}{\partial x_d}\right)^{\alpha_d}$. $C^m(\overline{\Omega})$ is a Banach space, equipped with the norm

$$\|v\|_{C^m(\overline{\Omega})} := \sum_{|\alpha| \leq m} \|D^\alpha v\|_{C(\overline{\Omega})}.$$

Further, let $C^\infty(\overline{\Omega}) = \{v \in C(\overline{\Omega}) : v \in C^m(\overline{\Omega}) \ \forall m \in \mathbb{N}\}$ be the space of smooth functions. The subspace of smooth functions with compact support is denoted by $\mathscr{D}(\Omega) = C_0^\infty(\Omega)$, this is often called the space of *test functions*. The space of vector valued test functions with vanishing divergence is denoted by $\mathscr{V}(\Omega) = C_{0,\sigma}^\infty(\Omega) = \{v \in C_0^\infty(\Omega)^d : \mathrm{div}v = 0\}$.

Lebesgue spaces. For $p \geq 1$, we introduce the Lebesgue space $L^p(\Omega)$. Consider the class of functions $v : \Omega \to \mathbb{R}$, for which $|v|^p$ is Lebesgue integrable, with the seminorm

$$\|v\|_{L^p} = \|v\|_p := \left(\int_\Omega |v(x)|^p \mathrm{d}x\right)^{1/p}.$$

The Lebesgue space $L^p(\Omega)$ is the space of equivalence classes of functions under the equivalence relation $v \sim_p w$ *if and only if* $\|v - w\|_p = 0$. This is a Banach space. Finally, $L^\infty(\Omega)$ is the space of essentially bounded functions with the norm $\|v\|_{L^\infty(\Omega)} := \mathrm{ess–sup}\{v(x) : x \in \Omega\}$.

The space $L^2(\Omega)$ is a Hilbert space with the inner product

$$\langle v; w \rangle_{L^2} = \int_\Omega v(x)w(x)\mathrm{d}x.$$

Sobolev spaces. Let $v \in L^1(\Omega)$ and α be a multi-index. A function $D^\alpha v$ is called the *weak derivative of order α* of v if and only if for all $\phi \in \mathscr{D}(\Omega)$ it holds

$$\int_\Omega \phi D^\alpha v \mathrm{d}x = (-1)^{|\alpha|} \int_\Omega v D^\alpha \phi \mathrm{d}x.$$

The Sobolev space $W^{k,p}$ is defined as

$$W^{k,p}(\Omega) = \{v \in L^p(\Omega) : D^\alpha v \in L^p(\Omega), \ \ \forall \, |\alpha| \leq k\}.$$

This is a Banach space, equipped with the norm

$$\|v\|_{W^{k,p}} = \|v\|_{k,p} = \left[\sum_{|\alpha| \leq k} \|D^\alpha v\|_{L^p}^p \right]^{1/p}.$$

The space $W^{k,2}(\Omega) = H^k$ is a Hilbert space with the inner product

$$\langle v; w \rangle_{H^k} = \sum_{|\alpha| \leq k} \int_\Omega D^\alpha v D^\alpha w \mathrm{d}x.$$

From the Sobolev embedding theorem we deduce the following result.

Proposition 3.1. *(Corollary from Sobolev embedding theorem.)* *Let $\Omega \subset \mathbb{R}^d$ be a bounded Lipschitz domain.*

1. *If $d \leq 3$, then $H^2(\Omega)$ embeds continuously in $L^\infty(\Omega)$, i.e., there exists a constant $c = c(\Omega)$ such that for every $v \in H^2(\Omega)$ it holds*

$$\mathrm{ess\text{--}sup}_{x \in \Omega} |v(x)| \leq c\|v\|_{H^2}. \tag{3.1}$$

2. *If $d \leq 4$, then $H^1(\Omega)$ embeds continuously in $L^4(\Omega)$ and there exists a constant $c = c(\Omega)$ such that for every $v \in H^1(\Omega)$ it holds*

$$\|v\|_{L^4} \leq c\|v\|_{H^1}.$$

Of course, the statements are not sharp. For instance, if $d = 3$, then H^1 continuously embeds in L^6, and if $d = 2$, then H^1 embeds in L^p for every $1 \leq p < \infty$. We will also use the following extension result due to Calderón ([8]).

Proposition 3.2. *If $\Omega \subset \mathbb{R}^d$ has Lipschitz boundary, then it is a $W^{1,p}$ - extension domain for all $1 < p < \infty$. That is, there exists a bounded linear extension operator $E : W^{1,p}(\Omega) \to W^{1,p}(\mathbb{R}^d)$ with $(Eu)|_\Omega = u$ for all $u \in W^{1,p}(\Omega)$.*

The subspaces of functions, whose derivatives up to the order $k-1$ vanish on $\partial\Omega$ in the sense of traces, are defined as:

$$H_0^k(\Omega) = \overline{\mathscr{D}(\Omega)}^{\|\cdot\|_{k,2}}.$$

To study the solutions to Stokes equation, we define the subspaces

$$V := H^1_{0,\sigma}(\Omega) = \overline{\mathscr{V}(\Omega)}^{\|\cdot\|_{1,2}},$$
$$H := \overline{\mathscr{V}(\Omega)}^{\|\cdot\|_2}.$$

The spaces H and V are Banach spaces, endowed with the corresponding norms ($\|\cdot\|_{1,2}$ for V and $\|\cdot\|_2$ for H). These spaces can be characterised as follows (see [76] for details):

$$H = \{v \in L^2(\Omega)^d : \ \mathrm{div}v = 0 \text{ in } \Omega, \ v \cdot n = 0 \text{ on } \partial\Omega\},$$

$$V = \{v \in H^1_0(\Omega) : \ \mathrm{div}v = 0 \text{ in } \Omega\}.$$

The condition $v \cdot n = 0$ is understood in the sense of traces, i.e., there exists a trace operator γ mapping $v \in H$ to $\gamma v \cdot n \in H^{-1/2}(\partial\Omega)$ (see [76]).

We use the standard notation for topological dual spaces.

Bochner spaces. The solution to a non-stationary problem is often sought in a certain Bochner space. For a Banach space X and a real number $p \geq 1$, the Bochner space $L^p(0,T;X)$ consists of all Bochner-measurable functions $v : (0,T) \to X$ with finite value of the integral $\int_0^T \|v(t)\|_X^p \mathrm{d}t < \infty$. This space, endowed with the norm

$$\|v\|_{L^p(0,T;X)} = \|v\|_{X,p;T} := \left[\int_0^T \|v(t)\|_X^p \mathrm{d}t\right]^{1/p}$$

is itself a Banach space. In situations, when the value of T is clear from the context, we use the shorthand notation $\|v\|_{L^p(X)}$. A function $u' \in L^p(0,T;X)$ is called the *weak derivative* of $u \in L^p(0,T;X)$ if and only if for every $\phi \in C_0^\infty(0,T)$ the following identity holds in X:

$$\int_0^T u'\phi \mathrm{d}t = -\int_0^T \phi' u \mathrm{d}t.$$

Mollification is a technique for approximating a locally integrable function with a smooth function. Let $\phi \in \mathscr{D}(\mathbb{R}^d)$ be chosen such that $\phi(x) \geq 0 \ \forall x$ and $\int_{\mathbb{R}^d} \phi(x)\mathrm{d}x = 1$. Let $\mathrm{supp}(\phi) \subset B_r(0)$. For $v \in L^1_{\mathrm{loc}}(\mathbb{R}^d)$ we define the mollification of v as the convolution

$$\mathcal{M}_\phi v(x) = (v \star \phi)(x) = \int_{\mathbb{R}^d} v(x-y)\phi(y)\mathrm{d}y = \int_{\mathbb{R}^d} \phi(x-y)v(y)\mathrm{d}y.$$

The mollification is smooth: $\mathcal{M}_\phi v \in C^\infty$, since

$$D^\alpha \mathcal{M}_\phi v(x) = (-1)^{|\alpha|} \int_{\mathbb{R}^d} v(y) D^\alpha_x \phi(x-y)\mathrm{d}y$$

is well-defined and bounded in all bounded domains $\Omega \subset \mathbb{R}^d$ as can be seen by Hölder's inequality

$$|D^\alpha \mathcal{M}_\phi v(x)| \leq \int_{\tilde{\Omega}} |v(y) D^\alpha_x \phi(x-y)|\mathrm{d}y \leq \|D^\alpha \phi\|_{L^\infty(\tilde{\Omega})} \|v\|_{L^1(\tilde{\Omega})}.$$

51

Here $\tilde{\Omega}$ denotes the r-neighbourhood of Ω.

Let $v \in H^1(\Omega)$ for a bounded Lipschitz domain, and $\tilde{\Omega}$ be the r-neighbourhood of Ω. Let $E : H^1(\Omega) \to H^1(\tilde{\Omega})$ be a continuous extension operator, e.g., the restriction of the operator that exists due to Prop. 3.2, then we define the mollification operator $\mathcal{M}_\phi : H^1(\Omega) \to C^\infty(\Omega)$, mapping v to $\mathcal{M}_\phi v$:

$$\mathcal{M}_\phi v(x) = (v \star \phi)(x) = \int_{\tilde{\Omega}} \phi(x - y) Ev(y) \mathrm{d}y.$$

3.1.2 Formulations

We start with rewriting the equations in **dimensionless form**. Let L_0 represent a typical length scale and V_0 - typical velocity. From this, we compute the typical time scale $T_0 = \frac{L_0}{V_0}$. Further, a typical pressure value is $P_0 = \frac{\eta V_0}{L_0}$ and typical value of force density per unit mass is $B_0 = \frac{\eta V_0}{\rho L_0^2}$. We also introduce the Reynolds number $Re = \frac{\rho V_0 L_0}{\eta}$.

The dimensionless form is obtained by replacing x with $\hat{x} = x/L_0$, t with $\hat{t} = t/T_0$, v with $\hat{v} = v/V_0$, P with $\hat{P} = P/P_0$ and b with $\hat{b} = b/B_0$. We use dimensionless variables in the rest of this Chapter, but we surpress the hats in notation.

We introduce the deformation rate and vorticity tensors $D = \frac{1}{2}(\nabla v + \nabla^\top v)$, $W = \frac{1}{2}(\nabla v - \nabla^\top v)$.

Fluid dynamics equations. The conservation of the linear momentum is given by

$$Re\frac{Dv}{Dt} - \mathrm{div}T = \rho b, \tag{3.2}$$

where b is body force per unit mass and the stress tensor is given by

$$T = -PI + 2\eta D + S, \tag{3.3}$$

$$S = 2\eta[N_p a^{(4)} : D + N_s(D \cdot a^{(2)} + a^{(2)} \cdot D)]. \tag{3.4}$$

N_p and N_s are material constants (particle number and shear number; see [25] and Section 4.3), and η is a dimensionless viscosity. We add the mass conservation law for incompressible fluids:

$$\mathrm{div}v = 0.$$

We introduce the traceless part of $a^{(2)}$ via $s = a^{(2)} - \frac{1}{d}I$. In order to calculate the extra stress tensor, a closure for $a^{(4)}$ is required. For the time being, we formulate the equations using the quadratic closure, however, the well-posedness results extend to arbitrary closure that can be expressed as a polynomial in the components of $a^{(2)}$. With the quadratic closure, (3.4) becomes

$$S = 2\eta[N_p(s : D)(s + \frac{1}{d}I) + N_s(Ds + sD + \frac{2}{d}I)].$$

Concentrated suspensions model. The equation (2.3) with quadratic closure can be written as

$$\begin{aligned} &\tfrac{Ds}{Dt} + (sW - Ws) - \lambda\left[Ds - sD + \tfrac{2}{d}D - 2(s : D)(s + \tfrac{1}{d}I)\right] \\ &+ U_0|D|\left[ss + \omega s - (s : s)(s + \tfrac{1}{d}I)\right] = 0, \end{aligned} \tag{3.5}$$

where $\omega = \frac{c_i d}{U_0} + \frac{1}{d}$ is a constant. The function $|D| = \sqrt{D:D}$ is not differentiable in the point $D = 0$ corresponding to the rest state $\kappa = 0$. Since later we require the source term of the transport equation to be differentiable with respect to D, we introduce an approximation

$$\dot{\gamma}_\epsilon := (D:D + \epsilon^2)^{1/2} - \epsilon,$$

where $\epsilon > 0$ is a constant. $\dot{\gamma}_\epsilon$ is a smooth function of D, moreover, the derivatives $\frac{\partial^{|\alpha|}\dot{\gamma}_\epsilon}{\partial D^\alpha}$ are bounded. As $|D| \to \infty$, the approximation error $\dot{\gamma}_\epsilon(D) - |D| \to 0$.

Observe that all the summands of the source term in (3.5) are either linear in $\kappa = \nabla u$ or grow linearly with $|\kappa|$. By dimension analysis one can verify that this property is not accidental.

General formulation. Assuming the fibre orientation dynamics are described by a system of transport equations with a special kind of source term, we write the equation in general form:

$$\frac{Ds}{Dt} = \mathcal{F}(s, \nabla v), \tag{3.6}$$

where $\mathcal{F}$ is continuously differentiable with respect to the totality of its arguments (this is why a mollification of the diffusive constant in the Folgar-Tucker model is needed). Furthermore, we assume that there exists a polynomial $\mathcal{P}$ with $|\mathcal{F}_i(s, \kappa)| \leq \mathcal{P}(|s|)|\kappa|$ and $|\frac{\partial^j \mathcal{F}_i(s,\kappa)}{\partial \kappa^j}| \leq \mathcal{P}(|s|)$ for $1 \leq j \leq 2$.

3 beads model. The equations (2.22 - 2.24) can be transformed to dimensionless form by introducing $\widehat{l}_B = \frac{l_B}{L_0}$, $\hat{\mu} = L_0 T_0 \mu$, $\hat{k} = T_0 k$. Henceforth we assume that the equations are in dimensionless form and surpress the hats in the notation. Let a set of closure approximations be given as polynomial functions of components of $a^{(2,0)}$, $a^{(1,1)}$ and $a^{(1,0)}$. We introduce a vector s consisting of the independent components of the tensors $a^{(2,0)} - \frac{1}{d}I$, $a^{(1,1)} + \frac{1}{d}I$ and $a^{(1,0)}$. The variables are chosen so that the natural equilibrium state at rest ($\kappa = 0$, $\mu = 0$), characterized by straight fibres with isotropic orientation distribution, corresponds to $|s| = 0$. Due to the symmetry of $a^{(2,0)}$ and $a^{(1,1)}$, the dimension is $s \in \mathbb{R}^{d^2+2d}$. In two dimensions $s \in \mathbb{R}^8$, in three dimensions $s \in \mathbb{R}^{15}$. The equations (2.22 - 2.24) can be written in the general form

$$\frac{Ds}{Dt} + \mathcal{F}_1(s, \kappa) + \mathcal{F}_2(s, \mu),$$

where $\mathcal{F}_1$ is linear in κ and $\mathcal{F}_2$ is linear in μ, furthermore, there exists a polynomial $\mathcal{P}$ such, that $|\mathcal{F}_1(s, \kappa)| \leq \mathcal{P}(|s|)|\kappa|$ and $|\mathcal{F}_2(s, \mu)| \leq \mathcal{P}(|s|)|\mu|$.

3.1.3 Instationary Stokes problem

Let us recapitulate some useful well-posedness results for the instationary Stokes problem, which is formulated as follows.

Problem (A). *(The instationary Stokes problem.) Given $Re > 0$, $\eta > 0$ and a suitable force term f. Find v and P, that satisfy the equations*

$$Re \, v_t - \eta \triangle v + \nabla P = f$$

$$\text{div } v = 0$$

for almost all $t \in [0, T]$ almost everywhere in Ω, the boundary condition $v = 0$ on $\partial\Omega$ and and the initial condition

$$v(0) = v_0.$$

Assuming that $v \in L^2(\Omega)^d$, we decompose the Hilbert space in the subspace of divergence-free (solenoidal) functions denoted by $H = L^2_\sigma$ and its orthogonal complement $G = H^\perp$. G can be characterized as

$$G = \{f \in L^2(\Omega)^d : \exists P \in L^2_{loc} \text{ with } f = \nabla P\},$$

see [69], [24]. This is called the *Helmholtz-Weil decomposition*. Let us denote the orthogonal projector $L^2(\Omega)^d \to H$ by P_{HW} and define the Stokes operator

$$\mathcal{L} := -P_{HW} \triangle.$$

The operator $\mathcal{L}$ is linear and maps $D(\mathcal{L}) = V \cap H^2$ to H. It induces the graph norm in $V \cap H^2$, defined by $\|v\|_{D(\mathcal{L})} = \|\mathcal{L}v\|_2$. This norm is equivalent to the natural H^2 norm (see [24], [29]). Problem A is reformulated as

Problem (1). *(Instationary Stokes problem, pressure free formulation.) Find $v(t, \cdot)$ with $v(t, \cdot) \in H$ for almost all $t \in (0, T)$ solving the following equation in H:*

$$Re \, v_t + \eta \mathcal{L}v = f \tag{3.7}$$
$$v(0) = v_0. \tag{3.8}$$

The following result is standard, see e.g. [69], [76].

Lemma 3.1. *Let $\partial\Omega \in C^2$, $v_0 \in V$ and $f \in L^2(\Omega \times [0, T])$. If $\eta > 0$, then Problem 1 admits a unique solution $v \in L^2(0, T; D(\mathcal{L})) \cap C([0, T]; V)$ such that $v_t \in L^2(\Omega \times [0, T])$ and the associated pressure $P \in L^2(0, T; H^1(\Omega))$. Furthermore, there exists a constant $C_1(Re, \eta, \Omega)$ such that*

$$\|v\|^2_{L^2(0,T;D(\mathcal{L})) \cap L^\infty(0,T;V)} + \|v_t\|^2_2 + \|P\|^2_{H^1,2;T} \leq C_1(\|v_0\|^2_2 + \|f\|^2_2).$$

The existence and uniqueness of the solution is proved in [76], and the estimate is given in [29]. The estimate involves a norm of intersection of two Banach spaces. There are several equivalent norms that make the intersection a Banach space, for instance, the sum norm $\|\cdot\|_{X \cap Y} = \|\cdot\|_X + \|\cdot\|_Y$ or the Hilbertian norm $(\|\cdot\|^2_X + \|\cdot\|^2_Y)^{1/2}$. Throughout this chapter we equip the intersection of two Banach spaces with the sum norm.

Provided that the domain and the data are more regular, one can prove a higher regularity of the solution.

Lemma 3.2. *Assume that $\partial\Omega \in C^3$, $F_t \in L^2(0, T, H^{-1})$, $v_0 \in D(\mathcal{L})$. If $\eta > 0$, then the unique solution of Problem 1 satisfies*

$$v \in L^2(0, T; H^3) \cap C([0, T]; D(\mathcal{L})),$$
$$v_t \in L^2(0, T; V) \cap C([0, T]; H),$$
$$P \in L^2(0, T; H^2),$$

and there exists a constant $C^* = C^*(Re, \eta, \Omega)$ *such that*

$$\|v\|^2_{L^2(0,T;H^3)\cap L^\infty([0,T];D(\mathcal{L}))} + \|v_t\|^2_{L^2(0,T;V)\cap L^\infty([0,T];H)} + \|P\|^2_{L^2(0,T;H^2)}$$
$$\leq C^* \left\{ \|\mathcal{L}v_0\|^2_2 + \|f\|^2_{L^1(0,T;(H^1)^d)} + \|f_t\|^2_{L^1(0,T;(H^{-1})^d)} + \|f(0)\|^2_2 \right\}.$$

This lemma is adopted from [29].

3.1.4 Linearized transport problem

Let us introduce the bilinear mapping

$$B(v, s) := v \cdot \nabla s.$$

Provided that $\mathrm{div}\, v = 0$, any vector field of arbitrary dimension $s \in H^1(\Omega)^{d_1}$ satisfies the identity

$$\langle B(v,s); s \rangle_{L^2} = \frac{1}{2} \int_\Omega v \cdot \nabla(s^2) \mathrm{d}x = 0. \tag{3.9}$$

From Prop. 3.1 and Hölder's inequality we obtain

Proposition 3.3. *Let* $\Omega \subset \mathbb{R}^d$, $d \leq 4$, *be a bounded Lipschitz domain; then:*

1. *the trilinear form* $b_1(u,v,w) := \int_\Omega uvw \mathrm{d}x$ *is well defined and continuous on* $[H^1(\Omega)]^2 \times L^2(\Omega)$, *and* $\exists c > 0$ *s.t.*

$$|b_1(u,v,w)| \leq c\|u\|_{H^1}\|v\|_{H^1}\|w\|_{L^2}.$$

2. *(see [76], pp. 169-172) the trilinear form* $b_2(u,v,w) := \int_\Omega u\partial_i v w \mathrm{d}x$ *is well defined and continuous on* $[H^1(\Omega)]^3$ *and there exists a constant* c *such that for all* u, v, w

$$|b_2(u,v,w)| \leq c\|u\|_{H^1}\|v\|_{H^1}\|w\|_{H^1}.$$

3. *moreover, the space* $H^2(\Omega)$ *is an algebra, i.e., whenever* $u, v \in H^2$, *then the product* $uv \in H^2$ *and there exists* $c > 0$ *such that* $\forall u, v \in H^2$ $\|uv\|_{H^2} \leq c\|u\|_{H^2}\|v\|_{H^2}$.

Linearization. Let us concentrate on the dependence of the source term on s only, i.e., let $\mathcal{F}(s) : \mathbb{R}^{d_2} \to \mathbb{R}^{d_2}$ be a vector-function with components polynomial in components of s. By a linearization of $\mathcal{F}$ we understand an expression $\mathcal{F}(s) = l(s) \cdot s + g$, where $l : \mathbb{R}^d_2 \to \mathbb{R}^{d_2^2}$ is a matrix with polynomial entries, and $g = \mathcal{F}(0)$ does not depend on s. If $d_2 > 1$ and $\mathcal{F}$ contains a mixed product, e.g., $s_i s_j$ for $i \neq j$, then the linearization is not unique.

As an example we consider the source term in (3.5). It is a symmetric tensor valued function with components polynomial in s. A suitable symmetry preserving linearization in the tensor notation is

$$l(\bar{s}) \cdot s + g = (Ws - sW) - \lambda \left[2(s:D)(\bar{s} + \tfrac{1}{d}I) - Ds - sD - \tfrac{2}{d}D \right]$$
$$- U_0|D| \left[\tfrac{1}{2}(s\bar{s} + \bar{s}s^\top) + \omega s - (s:\bar{s})(\bar{s} + \tfrac{1}{d}I) \right],$$

where $g = \frac{2\lambda}{d}D$.

After the linearization with respect to s we consider the dependence of $\mathcal{F}$ on the velocity field variables such as the gradient κ and for the 3-beads model the curvature μ. Here we observe that the source terms either depend on κ and μ linearly or at least have a linear growth with respect to these variables. To prove the existence result for the coupled system, we need the assumption that the H^2 norms of the parts, which are not linear with respect to κ, can be estimated from above by the H^1 norm of v, hence the existence is only proved for a regularized version of the fibre orientation models, where the velocity curvature μ and the nonlinear parts such as $\dot{\gamma}_\epsilon$ are mollified in an appropriate way. For these reasons, we introduce an additional variable ξ with d_3 components.

Denote $B_{r_1, r_2} = \{(x, y) \in \mathbb{R}^{d_2} \times \mathbb{R}^{d^2 + d_3} : |x| \leq r_1, |y| \leq r_2\}$.

We consider a transport problem under the following assumptions.

Problem (2). *(Linearized transport problem). Given $\bar{v} \in L^\infty(0, T; H^1(\Omega)^d)$, $\bar{s} \in L^\infty(0, T; L^2(\Omega)^{d_2})$ and a functional $\bar{\xi} = \xi(\bar{v})$, such that there exists $c > 0$, for which the estimate $\|\bar{\xi}\|_{H^2(\Omega)} \leq c\|\bar{v}\|_{H^1(\Omega)}$ holds. Find $s(\cdot, t) \in L^2(\Omega)^{d_2}$, which satisfies a.e. in $(0, T)$*

$$s_t + B(\bar{v}, s) + l(\bar{s}, \nabla\bar{v}, \bar{\xi}) \cdot s + g(\nabla\bar{v}, \bar{\xi}) = 0,$$
$$s(0) = s_0. \tag{3.10}$$

Here $l \in \left[C^2(\mathbb{R}^{d_2 + d^2 + d_3})\right]^{d_2 \times d_2}$ and $g \in \left[C^2(\mathbb{R}^{d^2 + d_3})\right]^{d_2}$, where $d_2 > 0$, $d_3 \geq 0$ are integers, are given functions satisfying $\|l\|_{C^2(B_{r_1, r_2})} \leq \mathcal{P}(r_1)(1 + r_2)$ and $\|g\|_{C^2(B_r)} \leq cr$ for a polynomial $\mathcal{P}$. Furthermore, l and g at most linear in the components of (κ, ξ) in the sense that the second order derivatives with respect to any pair of the components of (κ, ξ) vanish.

Let us estabilish some continuity properties of l and g.

Lemma 3.3. *Let l and g satisfy the assumptions of Problem 2. Further, let the components of $\bar{s}$, κ and ξ be of class $H^2(\Omega)$. Then $l(\bar{s}, \kappa, \bar{\xi})$ and $g(\kappa, \bar{\xi})$ are in $H^2(\Omega)$. Moreover, there exists a polynomial $\mathcal{P}_0$ with nonnegative coefficients s.t.*

$$\|l\|_{H^2} \leq \mathcal{P}_0(\|\bar{s}\|_{H^2})(\|\kappa\|_{H^2} + \|\xi\|_{H^2} + 1), \tag{3.11}$$
$$\|g\|_{H^2} \leq c(\|\kappa\|_{H^2} + \|\xi\|_{H^2}). \tag{3.12}$$

Proof. We demonstrate the estimate (3.11). By the chain rule,

$$\frac{\partial l}{\partial x_i} = \frac{\partial l}{\partial \bar{s}} \cdot \bar{s}_{,i} + \frac{\partial l}{\partial \kappa} : \kappa_{,i} + \frac{\partial l}{\partial \xi} \cdot \xi_{,i},$$

and

$$\frac{\partial^2 l}{\partial x_i \partial x_j} = \left(\frac{\partial^2 l}{\partial \bar{s}^2}\bar{s}_{,j} + \frac{\partial^2 l}{\partial \bar{s}\partial \kappa}\kappa_{,j} + \frac{\partial^2 l}{\partial \bar{s}\partial \xi}\xi_{,j}\right)\bar{s}_{,i} + \frac{\partial l}{\partial \bar{s}}\bar{s}_{,ij} +$$
$$\left(\frac{\partial^2 l}{\partial \bar{s}\partial \kappa}\bar{s}_{,j} + \frac{\partial^2 l}{\partial \kappa^2}\kappa_{,j} + \frac{\partial^2 l}{\partial \kappa\partial \xi}\xi_{,j}\right)\kappa_{,i} + \frac{\partial l}{\partial \kappa}\kappa_{,ij} + \tag{3.13}$$
$$\left(\frac{\partial^2 l}{\partial \bar{s}\partial \xi}\bar{s}_{,j} + \frac{\partial^2 l}{\partial \kappa\partial \xi}\kappa_{,j} + \frac{\partial^2 l}{\partial \xi^2}\xi_{,j}\right)\xi_{,i} + \frac{\partial l}{\partial \xi}\xi_{,ij}.$$

Using the assumption about the C^2 norm of l and the linearity with respect to κ and ξ, we obtain the following inequalities, which hold pointwise in Ω:

$$
\begin{aligned}
|l| &\le (|\kappa| + |\bar\xi| + 1)\mathcal{P}(|\bar{s}|), \\
|\partial_{\bar{s}_i} l| &\le (|\kappa| + |\bar\xi| + 1)\mathcal{P}(|\bar{s}|), \\
|\partial_{\kappa_i} l| &\le \mathcal{P}(|\bar{s}|), \\
|\partial_{\xi_i} l| &\le \mathcal{P}(|\bar{s}|), \\
|\partial_{\kappa_i \kappa_j} l| &= |\partial_{\xi_i \xi_j} F| = |\partial_{\xi_i \kappa_j} F| = |\partial_{\xi_i \xi_j} F| = 0, \\
|\partial_{\bar{s}_i \bar{A}_j} l| &\le (|\kappa| + |\bar\xi| + 1)\mathcal{P}(|\bar{s}|), \\
|\partial_{\bar{s}_i \kappa_j} l| &\le \mathcal{P}(|\bar{s}|).
\end{aligned}
\tag{3.14}
$$

By the first part of Prop. 3.1, the pointwise values of $\bar{s}$, κ and ξ are essentially bounded by the $H^2(\Omega)$ norms. By the second part of Prop. 3.1, the right-hand side of (3.13) is square integrable. This together with (3.13-3.14) implies (3.11).

The estimate (3.12) follows by the same lines, by using $\partial_{\bar{s}_i} g = 0$ and the fact that $g(0,0) = 0$. $\square$

Now we are prepared to prove the following result for Problem 2.

Lemma 3.4. *Let $\partial\Omega$ be of class C^1, $\bar{v} \in L^2(0,T;H^3) \cap L^\infty(0,T;D(\mathcal{L}))$, $\bar{s} \in L^\infty(0,T,H^2)$ and $s_0 \in H^2$ be given, satisfying the following estimates:*

$$
\|\bar{v}\|_{L^2(0,T;H^3)} + \|\bar{v}\|_{L^\infty(0,T;D(\mathcal{L}))} \le B_1,
$$
$$
\|\bar{s}\|_{L^\infty(0,T;H^2)} \le B_2,
$$

where the constant B_2 is taken sufficiently large so that

$$
B_2 \ge 2(B_1 + \|s_0\|_{H^2}). \tag{3.15}
$$

Let $\|\bar\xi\|_{L^\infty(0,T;C^2)} \le cB_1$.

Then there exists a constant T^* depending on the domain, B_1, B_2 and the material constants such that for any $\hat{T} \le \min\{T, T^*\}$ Problem 2 admits a unique solution s in the time interval $(0,\hat{T})$ in the function class

$$
s \in L^\infty(0,\hat{T};H^2), \ s_t \in L^\infty(0,\hat{T};H^1).
$$

Furthermore, it holds

$$
\|s\|_{L^\infty(0,\hat{T};H^2)} \le B_2, \tag{3.16}
$$
$$
\|s_t\|_{L^\infty(0,\hat{T};H^1)} \le B_3, \tag{3.17}
$$

where B_3 is $(B_1 + B_2)\mathcal{P}^*(B_2)$ and $\mathcal{P}^*$ is a polynomial, depending only on the functions l and g.

Proof. The scheme of proof is similar to the proof of Lemma 2.3 in [29] and Lemma 3 in [25]. We first derive apriori estimates for the H^2 norm of a solution, from these a suitable value for T^* satisfying the estimates (3.16) and (3.17) is found. Then the construction of a solution in the space $L^2(0,T^\star;H^2)$ is sketched. The proof is completed by demonstrating the uniqueness of solution in this space.

A-priori estimates. Let $s : t \mapsto s(\cdot, t) \in H^2(\Omega)^{d_2}$ be a solution of (3.10). The rate of change of the H^2 norm of $s(\cdot, t)$ can be estimated by using (3.10). First compute the L^2 inner product of both sides of (3.10) with s. Next, for $i \in \overline{1, d}$ differentiate both sides of (3.10) with the operator ∂_i and form the inner product with $\partial_i s$. Finally, differentiate (3.10) with the operator ∂_{ij} and form the inner product with $\partial_{ij} s$. The sum of thus obtained $(1 + d + d^2)$ equations gives an equation for $\frac{d}{dt} \|s(t)\|_{H^2}^2$. Using the orthogonality property (3.9), this equation is

$$
\begin{aligned}
\tfrac{1}{2} \tfrac{d}{dt} \|s\|_{H^2}^2 &= -\langle B(\bar{v}, s); s \rangle_{H^2} - \langle l \cdot s + g; s \rangle_{H^2} \\
&= -\int_\Omega \left[\bar{v}_{i,j} \left(s_{,i} s_{,j} + 2 s_{,ik} s_{,jk} \right) + \bar{v}_{i,jk} s_{,i} s_{,jk} \right] \mathrm{d}x \qquad (3.18) \\
&\quad - \langle l \cdot s + g; s \rangle_{H^2}.
\end{aligned}
$$

(Throughout this proof, c will stand for a positive constant, which depends on the domain and probably on material constants, but never on the unknowns).

The terms of (3.18) are estimated as follows. Since $\bar{v}_{i,j} \in H^2$, the inequality (3.1) applies:

$$
\left| \int_\Omega \bar{v}_{i,j} \left(s_{,i} s_{,j} + 2 s_{,ik} s_{,jk} \right) \mathrm{d}x \right| \leq c \|\bar{v}\|_{H^3} \|s\|_{H^2}^2.
$$

Further, $v_{i,jk}$ and $s_{,i}$ are in H^1, therefore by second part of Prop. 3.3

$$
\left| \int_\Omega \bar{v}_{i,jk} s_{,i} s_{,jk} \mathrm{d}x \right| \leq c \|\bar{v}\|_{H^3} \|s\|_{H^2}^2.
$$

By triangle inequality, Cauchy-Schwarz inequality and third part of Prop. 3.3,

$$
\langle l \cdot s + g, s \rangle_{H^2} \leq c(\|l\|_{H^2} \|s\|_{H^2} + \|g\|_{H^2}) \|s\|_{H^2}.
$$

By Lemma 3.3, and the assumptions $|\bar{s}| \leq B_2$, $|\xi| \leq c B_1$,

$$
\langle l \cdot s + g, s \rangle_{H^2} \leq c \|s\|_{H^2} (\|\bar{v}\|_{H^3} + B_1 + 1) \left[1 + \|s\|_{H^2} \mathcal{P}(B_2) \right].
$$

Thus, (3.18) implies the following inequality in differential form:

$$
\frac{d}{dt} \|s\|_{H^2}^2 \leq c \|s\|_{H^2} (\|\bar{v}\|_{H^3} + B_1 + 1) \left[1 + \|s\|_{H^2} \mathcal{P}^*(\|\bar{s}\|_{H^2}) \right],
$$

where $\mathcal{P}^*$ is a polynomial with non-negative coefficients, majorizing all the $\mathcal{P}$ which appear in the estimates. Let us denote $y(t) := \|s\|_{H^2}^2$, $g(t) := \|\bar{v}\|_{H^3}$ and $\hat{B} := \mathcal{P}^*(B_2)$. Using the assumption about the norm of $\bar{s}$, we get

$$
y' \leq c \sqrt{y} (1 + \hat{B} \sqrt{y})(g + B_1 + 1).
$$

Using the inequality of arithmetic and geometric means $g c \sqrt{y} \leq \tfrac{1}{2}(g^2 + c^2 y)$ and $(B_1 + 1) c y \leq \tfrac{1}{2}((B_1 + 1)^2 + c^2 y)$, we obtain

$$
y' \leq \left(c^2 + \hat{B} c (g + B_1 + 1) \right) y + \frac{1}{2} \left(g^2 + (B_1 + 1)^2 \right).
$$

We seek the upper "barrier" of the solution in the form

$$y(t) = k(t) \exp\left[\left(c^2 + \hat{B}c(B_1 + 1)\right)t + \hat{B}c\int_0^t g(\tau)\mathrm{d}\tau\right].$$

The unknown function $k(t)$ is found by substitution:

$$k(t) = c_1 + \frac{1}{2}\int_0^t \left[g(t_1)^2 + (B_1 + 1)^2\right] \times$$
$$\exp\left\{-\left[c^2 + \hat{B}c(B_1 + 1)\right]t_1 - \hat{B}c\int_0^{t_1} g(\tau)\mathrm{d}\tau\right\}\mathrm{d}t_1,$$

and the integration constant $c_1 = y_0 = \|s_0\|_{H^2}^2$ comes just from the initial data. The negative power of e can be estimated from above by 1, giving

$$k(t) \le y_0 + \frac{1}{2}\left(B_1^2 + (B_1 + 1)^2 t\right) \le \frac{3}{8}B_2^2 + (B_1 + 1)^2\frac{t}{2};$$

the latter estimate is obtained from (3.15). We complete the estimation by using the Cauchy-Schwarz inequality:

$$\int_0^t g(\tau)\mathrm{d}\tau \le \sqrt{t}\left[\int_0^t g(\tau)^2\mathrm{d}\tau\right]^{1/2} \le B_1\sqrt{t},$$

to arrive at

$$y(t) \le k(t) \exp\left[\left(c^2 + \hat{B}c(B_1 + 1)\right)t + \hat{B}B_1 c\sqrt{t}\right].$$

In light of the continuity of y and the fact that $y(0) \le \frac{3}{8}B_2^2$, it is obvious that for a sufficiently small time interval $t \in (0, T^*)$ we have $y(t) \le B_2^2$. Notice that T^* depends on B_1 and B_2, but *not* on the particular choices of $\bar{s}$ and $\bar{v}$. This proves (3.16).

The estimate (3.17) is proven by computing the H^1 norm of the first row of (3.10); since $\bar{v} \in H^3$, one immediately has

$$\|B(\bar{v}, s)\|_{H^1} \le c\|\bar{v}\|_{H^3}\|s\|_{H^2}.$$

By assumption, setting $F := l \cdot s + g$, $\|F\|_{L^2} \to 0$ as $\|s\|_{H^2} + \|\kappa\|_{H^2} \to 0$.

Using the chain rule and estimates as in proof of Lemma 3.3, we obtain a similar estimate for the semi-norm $|F|_{H^1}$. Combining these inequalities, we obtain

$$\|F\|_{H^1} \le (B_1 + B_2)\mathcal{P}^*(B_2),$$

which is exactly (3.17).

Existence. A solution can be constructed by using the method of characteristics. In [25] Galdi suggests a way how to construct a solution $s \in L^2(0, T^\star; H^2)$ with the help of a Galerkin method.

Uniqueness. Let $s^{(1)}$ and $s^{(2)}$ be two solutions corresponding to the same data, and set $s := s^{(1)} - s^{(2)}$, we have $s(0) = 0$ almost everywhere. Further, set $l_0 := l(\bar{s}, \nabla\bar{v}, \bar{\xi})$. s satisfies the following equation:

$$s' + B(\bar{v}, s) + l_0 \cdot s = 0.$$

We compute the L^2 scalar product with s. Due to (3.9), B part vanishes, and by Lemma 3.3,

$$|\langle l_0 \cdot s; s \rangle_{L^2}| \leq c(\|\bar{v}\|_{H^3} + 1)\|s\|_{L^2}^2,$$

with $c = \mathcal{P}_1(B_2)$. It follows that

$$\frac{1}{2}\frac{d}{dt}\|s\|_{L^2}^2 - c(\|\bar{v}\|_{H^3} + 1)\|s\|_{L^2}^2 \leq 0.$$

Since the norm of s is square time-integrable, we can apply Grönwall's lemma ([87], p. 82) to deduce that $\|s\|_{L^2}^2 = 0$ almost everywhere in time, which leads to $s^{(1)} = s^{(2)}$ almost everywhere in space and time. This implies the uniqueness of the solution. $\square$

3.2 Local existence of solutions

In this section we study a coupled problem consisting of the incompressible Navier-Stokes equations with a non-Newtonian constitutive law, which depends on a multidimensional quantity s in a rather general way and a transport equation for the quantity s. The assumptions about the form of the constitutive relation and the source term of the transport equation are summarized in the formulation of the problem.

Problem $\mathscr{P}$. *Find*

$$v(\cdot, t) \in V \quad \text{and} \quad s(\cdot, t) \in (H^2(\Omega))^{d_2},$$

such that for almost all $t \in (0, T)$ the following equations are satisfied

$$Re[v_t + (v \cdot \nabla)v] + \eta \mathcal{L}v - \text{div} T = b,$$

$$T = \mathcal{T}(s, \nabla v),$$

$$s_t + (v \cdot \nabla)s = \mathcal{F}(s, \nabla v, \xi(v)),$$

and the given initial conditions $v(\cdot, 0) = v_0$ and $s(\cdot, 0) = s_0$ hold.

Here $\mathcal{T}$, $\mathcal{F}$ and ξ are given and satisfy the following assumptions.

$\mathcal{T} \in \left[C^2(\mathbb{R}^{d_2 + d^2})\right]^{d^2}$, the function $\mathcal{T}(s, \kappa)$ is linear in κ, and together with its first and second order derivatives has a polynomial growth with respect to $|s|$. Furthermore, whenever $|s| = 0$ or $|\kappa| = 0$, the gradient $\nabla_{(s,\kappa)}\mathcal{T} = 0$.

$\mathcal{F} \in \left[C^2(\mathbb{R}^{d_2 + d^2 + d_3})\right]^{d_2}$, the function $\mathcal{F}(s, \kappa, \xi)$ is linear in (κ, ξ), and together with its first and second order derivatives has a polynomial growth with respect to $|s|$. Moreover, $\mathcal{F}(0, 0, 0) = 0$.

$\xi : H^3(\Omega)^d \to C^2(\Omega)^{d_3}$ is a continuous functional with a linear growth: $\|\xi(v)\| \leq c\|v\|$.

The solution should be equal to a time-continuous function $v \in C([0, T]; V)$ and $s \in C([0, T]; H^1(\Omega)^{d_2})$ almost everywhere. We define the solution space

$$X_T := C([0, T]; V) \times C([0, T]; H^1(\Omega)^{d_2})$$

and a subset of X_T:

$$R_T := \{(v,s) : v \in C([0,T]; D(\mathcal{L})) \cap L^2([0,T]; H^3),$$
$$v' \in C([0,T]; H) \cap L^2([0,T]; V),$$
$$s \in L^\infty([0,T]; (H^2)^{d_2}), \ s' \in L^\infty([0,T]; (H^1)^{d_2}),$$
$$v(0) = v_0, \ s(0) = s_0,$$
$$\|v\|^2_{L^\infty(0,T;D(\mathcal{L})) \cap L^2(0,T;H^3)} + \|v'\|^2_{L^\infty(0,T;H) \cap L^2(0,T;V)} \le B_1^2,$$
$$\|s\|_{L^\infty(0,T;(H^2)^{d_2})} \le B_2, \|s'\|_{L^\infty(0,T;(H^1)^{d_2})} \le B_3\},$$

where B_1 is a constant, B_2 satisfies the condition (3.15) and B_3 is computed from B_1 and B_2 as in Lemma 3.3. By Arzela-Ascoli Theorem (see e.g., [87], p. 772), R_T is compact in X_T.

As in [29] and [52], we find a value of $B_1 > 0$, for which $R_T \ne \emptyset$. Consider the instationary Stokes problem

$$Rev^{*'} + \eta\mathcal{L}v^* = 0,$$

where $v^*(\cdot,t) \in V$ and $v^*(\cdot,0) = v_0$. By Lemma 3.2, this problem has a unique solution for every time interval $[0,T]$, and there exists a constant $C^*(Re, \eta, \Omega)$ such that

$$\|v^*\|^2_{L^\infty(0,T;D(\mathcal{L})) \cap L^2(0,T;H^3)} + \|v^{*'}\|^2_{L^\infty(0,T;H) \cap L^2(0,T;V)} \le C^*\|\mathcal{L}v_0\|^2_{L^2}.$$

If B_1 satisfies

$$B_1^2 \ge 2\left[C^*\|\mathcal{L}v_0\|^2_{L^2} + \|s_0\|^2_{H^2}\right] =: c_1^2, \tag{3.19}$$

then the pair $(v^*, s_0) \in R_T$ for $\forall T > 0$, and thus $R_T \ne \emptyset$. From now on, we assume that B_1 satisfies (3.19). Thus, R_T is a nonempty compact convex subset of X_T.

Suppose that $(\bar{v}, \bar{s}) \in R_T$ is given. By linearizing $\mathcal{F}$, we obtain an instance of Problem 2, and by setting

$$f = -\text{Re}B(\bar{v}, \bar{v}) + P_{HW}b + P_{HW}\text{div}\mathcal{T}(\bar{v}, \bar{s}), \tag{3.20}$$

we obtain an instance of Problem 1. By Lemmata 3.2 and 3.4, these auxiliary problems admit unique solutions (v,s).

This defines a mapping $\Phi : (\bar{v}, \bar{s}) \to (v,s)$. We want to show that for sufficiently small T and suitable choice of B_1 Φ maps R_T into itself.

In order to estimate the norm of force term $\|f\|_{H^1}$, we need to consider the H^1 norm of

$$\text{div}\mathcal{T}_j = \partial_i \mathcal{T}_{ij} = \frac{\partial \mathcal{T}_{ij}}{\partial s} \cdot s_{,i} + \frac{\partial \mathcal{T}_{ij}}{\partial \kappa} : \kappa_{,i}.$$

We use an ambigious notation $\mathcal{P}$ and $\mathcal{Q}$ for some polynomials with nonnegative coefficients, meaning that "there exists a polynomial such that..." The notation $\mathcal{Q}$ is used to signify that the polynomial satisfies $\mathcal{Q}(0) = 0$.

$$
\begin{aligned}
\|\text{div}\mathcal{T}_j\|_{L^2} &\le \left\|\frac{\partial \mathcal{T}_{ij}}{\partial s}\right\|_{L^\infty}\left\|\frac{\partial s}{\partial x_i}\right\|_{L^2} + \left\|\frac{\partial \mathcal{T}_{ij}}{\partial \kappa}\right\|_{L^\infty}\left\|\frac{\partial \kappa}{\partial x_i}\right\|_{L^2} \\
&\le \mathcal{P}(\|s\|_{H^2})\|v\|_{H^3}\|s\|_{H^1} + \mathcal{Q}(\|s\|_{H^2}) \cdot 1 \cdot \|v\|_{H^2} \\
&\le \mathcal{Q}(\|s\|_{H^2})\|v\|_{H^3}.
\end{aligned}
$$

By using chain rule, Proposition 3.1 and integrating over time, we find

$$\|\text{div}\mathcal{T}\|_{L^2(0,T;H^1)} \leq \mathcal{Q}_1(B_2)B_1.$$

The initial value of the stress term depends on initial conditions:

$$\|\text{div}\mathcal{T}(0)\|_{L^2} \leq \mathcal{Q}_2(\|s_0\|_{H^2})\|v_0\|_{H^2},$$

$$\begin{aligned}
\|\text{div}\mathcal{T}'\|_{L^2(0,T;H^{-1})} &= \|\tfrac{\partial \mathcal{T}}{\partial s}s' + \tfrac{\partial \mathcal{T}}{\partial \kappa}\kappa'\|_{L^2(0,T;H^{-1})} \\
&\leq c(1 + \mathcal{Q}_{31}(B_2))B_1B_3 + \mathcal{Q}_{32}(B_2)\|v'\|_{L^2(0,T;H^1)} \\
&\leq (cB_3 + \mathcal{Q}_3(B_2))B_1.
\end{aligned}$$

Employing these estimates and using the continuity of B in (3.20), we derive

$$\|f\|_{L^2(0,T;H^1)} \leq k_1(\mathcal{Q}_1(B_2) + B_1)B_1 + \|b\|_{L^2(0,T;H^1)} =: F_1B_1 + c_2;$$

$$\|f(0)\|_{L^2} \leq k_1[\mathcal{Q}_2(\|s_0\|_{H^2})\|v_0\|_{H^2} + \|v_0\|_{H^2}^2] + \|b(0)\|_{L^2} =: c_3;$$

$$\|f'\|_{L^2(0,T;H^{-1})} \leq k_1[cB_3 + \mathcal{Q}_3(B_2) + B_1]B_1 + \|b'\|_{L^2(0,T;H^{-1})} =: F_2B_1 + c_4.$$

Here the constants c_i depend only on the input data, and $F_i \to 0$ as $|B_1| + |B_2| \to 0$. Let us choose

$$B_1 = c_1 + 4\sqrt{C^*}(c_2 + c_3 + c_4);$$

then (3.19) is satisfied automatically, and we get

$$\begin{aligned}
C^* &\left[\|\mathcal{L}v_0\|_{L^2}^2 + \|f\|_{L^2(0,T;H^1)}^2 + \|f(0)\|_{L^2}^2 + \|f'\|_{L^2(0,T;H^{-1})}^2\right] \\
&\leq C^*\|\mathcal{L}v_0\|_{L^2}^2 + C^*\left[\|f\|_{L^2(0,T;H^1)} + \|f(0)\|_{L^2} + \|f'\|_{L^2(0,T;H^{-1})}\right]^2 \\
&\leq \tfrac{1}{2}B_1^2 + C^*[(F_1 + F_2)B_1 + (c_2 + c_3 + c_4)]^2 \\
&\leq \tfrac{1}{2}B_1^2 + \left[(F_1 + F_2)B_1\sqrt{C^*} + \tfrac{B_1}{4}\right]^2.
\end{aligned}$$

Next, we may choose

$$B_2 = 4B_1;$$

this satisfies the condition (3.15) because of (3.19). Now it is obvious that F_1 and F_2 tend to zero if $B_1 \to 0$. However, for sufficiently small data, (3.19) allow arbitrary small positive values of B_1. Let $B_1 > 0$ be so small that

$$(F_1 + F_2)\sqrt{C^*} \leq 1/4,$$

then Lemma 3.2 guarantees that the solution v of the auxiliary Problem 1 with the force term (3.20) is unique and satisfies $\|v\|^2 + \|v_t\|^2 \leq B_1^2$. This together with Lemma 3.4 proves that Φ maps R_{T^*} into itself (where T^* is given by Lemma 3.4, and depends on B_1 and B_2). A direct application of the Schauder fixed point theorem ([87], p. 57) yields the following result.

Theorem 1. *Let Ω have C^3 boundary, $b \in L^2_{\text{loc}}(\mathbb{R}^+; H^1)$, $b' \in L^2_{\text{loc}}(\mathbb{R}^+; H^{-1})$, $v_0 \in D(\mathcal{L})$ and $s_0 \in H^2(\Omega)^{d_2}$. Then there exist positive constants K and T such that whenever*

$$\|b'\|_{L^2(0,T;H^1) \cap L^2(0,T;H^{-1})} + \|v_0\|_{D(\mathcal{L})} + \|s_0\|_{H^2} \leq K,$$

then Problem $\mathscr{P}$ admits at least one solution (v, P, s) in $\Omega \times (0, T)$ in the spaces

$$\begin{aligned} v &\in L^2(0,T;H^3), \quad v' \in L^2(0,T;V), \quad P \in L^2(0,T;H^2), \\ s &\in L^\infty(0,T;H^2), \quad s' \in L^\infty(0,T;H^1). \end{aligned}$$

The constant K depends only on the domain Ω and on the material constants, while T also depends on the data. Finally, such solutions satisfy the estimate

$$\begin{aligned} &\|v\|_{L^2(0,T;H^3) \cap L^\infty(0,T;D(\mathcal{L}))} + \|v'\|_{L^2(0,T;V) \cap L^\infty(0,T;H)} \\ &+ \|P\|_{L^2(0,T;H^2)} + \|s\|_{L^\infty(0,T;H^2)} + \|s'\|_{L^\infty(0,T;H^1)} \leq k, \end{aligned}$$

where k depends on the data in such a way that

$$k \to 0 \quad \text{as} \quad \|b\|_{L^2(0,T;H^1)} + \|b'\|_{L^2(0,T;H^{-1})} + \|v_0\|_{H^2} + \|s_0\|_{H^2} \to 0.$$

3.3   Uniqueness of solution

Now we demonstrate that, for sufficiently small data, the solution given by Theorem 1 is unique. Let (v_1, P_1, s_1) and (v_2, P_2, s_2) be two solutions corresponding to the same data. By Theorem 1, for every $\delta > 0$ we can restrict the norms of initial data so that

$$\|s_1\|_{L^\infty(0,T;H^2)} + \|s_2\|_{L^\infty(0,T;H^2)} \leq \delta.$$

Let us define $v = v_1 - v_2$, $P = P_1 - P_2$, $s = s_1 - s_2$, $\tau_1 = \mathcal{T}(s_1, \nabla v_1)$, $\tau_2 = \mathcal{T}(s_2, \nabla v_2)$, $\phi_1 = \mathcal{F}(s_1, \nabla v_1, \xi_1)$, $\phi_2 = \mathcal{F}(s_2, \nabla v_2, \xi_2)$. These can be verified to satisfy the following equations.

$$\text{Re}[v' - B(v,v) + B(v_1,v) + B(v,v_1)] + \mathcal{L}v = P_{HW}\text{div}(\tau_1 - \tau_2),$$

$$s' - B(v,s) + B(v_1,s) + B(v,s_1) = \phi_1 - \phi_2.$$

Multiplying the first equation with v and the second with s and integrating over Ω, we get

$$\text{Re}\left[\frac{1}{2}\frac{d}{dt}\|v\|_{L^2}^2 + \langle B(v,v_1); v\rangle\right] + |v|_{H^1}^2 = \langle \tau_1 - \tau_2; D\rangle,$$

$$\frac{1}{2}\frac{d}{dt}\|s\|_{L^2}^2 + \langle B(v,s_1); s\rangle = \langle \phi_1 - \phi_2; s\rangle,$$

where $D = \frac{1}{2}(\nabla + \nabla^\top)v$, $\langle \cdot; \cdot \rangle$ is the L^2 inner product and $|\cdot|_{H^1}$ is the familiar Sobolev seminorm. Using Prop. 3.1,

$$|\langle B(v,v_1); v\rangle| \leq c\|v_1\|_{H^3}\|v\|_{L^2}^2,$$

$$|\langle B(v, s_1); s\rangle| \le c\|s_1\|_{H^2}\|v\|_{H^1}\|s\|_{L^2} \le c\delta\|v\|_{H^1}\|s\|_{L^2}.$$

Plugging in this and using Cauchy-Schwarz inequality yields

$$\mathrm{Re}\frac{1}{2}\frac{d}{dt}\|v\|_{L^2}^2 + |v|_{H^1}^2 \le c\mathrm{Re}\|v_1\|_{H^3}\|v\|_{L^2}^2 + \|\tau_1 - \tau_2\|_{L^2}\|v\|_{H^1}, \tag{3.21}$$

$$\frac{1}{2}\frac{d}{dt}\|s\|_{L^2}^2 \le c\delta\|v\|_{H^1}\|s\|_{L^2} + \|\phi_1 - \phi_2\|_{L^2}\|s\|_{L^2}. \tag{3.22}$$

Next, we use the linearity of $\mathcal{T}$ in κ and the estimate $|\mathcal{T}(s, \kappa)| \le \mathcal{Q}_1(|s|)|\kappa|$

$$\begin{aligned}|\tau_1 - \tau_2| &= |\mathcal{T}(s_1, \kappa_1) - \mathcal{T}(s_2, \kappa_2)|\\ &\le |\mathcal{T}(s_1, \kappa_1) - \mathcal{T}(s_2, \kappa_1)| + |\mathcal{T}(s_2, \kappa_1) - \mathcal{T}(s_2, \kappa_2)|\\ &\le |\mathcal{Q}_1(|s_1|) - \mathcal{Q}_1(|s_2|)| \cdot \|v_1\|_{H^1} + \mathcal{Q}_1(|s_2|)\|v\|_{H^1},\end{aligned}$$

where $\mathcal{Q}_1$ is a polynomial with nonnegative coefficients and $\mathcal{Q}_1(0) = 0$. Moreover, since $|s|$ is bounded by δ, $\mathcal{Q}_1$ is Lipschitz continuous with Lipschitz constant $q(\delta)$, i.e., $|\mathcal{Q}_1(|s_1|) - \mathcal{Q}_1(|s_2|)| \le q(\delta)\,||s_1| - |s_2|| \le q(\delta)|s_1 - s_2|$, where q is continuous. Let us denote $V := \|v_1\|_{H^3} + \|v_2\|_{H^3}$; then

$$\|\tau_1 - \tau_2\|_{L^2} \le q(\delta)V\|s\|_{L^2} + \mathcal{Q}_1(\delta)\|v\|_{H^1}.$$

By the Poincare-Friedrichs inequality, there exists a constant $c_* = c_*(\Omega) > 0$ such that $\forall v \in H_0^1(\Omega)$ it holds $|v|_{H^1}^2 \ge c_*\|v\|_{L^2}^2$, thus $|v|_{H^1}^2 \ge \frac{c_*}{1+c_*}\|v\|_{H^1}^2$. Let $\alpha > 0$ be a fixed constant satisfying $\frac{1}{2\alpha^2} < \frac{c_*}{1+c_*}$. By the inequality of algebraic and geometrical mean values (for real a and b, $2ab \le a^2 + b^2$),

$$q(\delta)V\|s\|_{L^2}\|v\|_{H^1} \le \frac{\alpha^2}{2}q(\delta)^2V^2\|s\|_{L^2}^2 + \frac{\|v\|_{H^1}^2}{2\alpha^2}.$$

With this, (3.21) transforms to

$$\mathrm{Re}\frac{1}{2}\frac{d}{dt}\|v\|_{L^2}^2 + |v|_{H^1}^2 \le \left[\mathcal{Q}_1(\delta) + \frac{1}{2\alpha^2}\right]\|v\|_{H^1}^2 + \frac{\alpha^2q(\delta)^2}{2}V^2\|s\|_{L^2}^2 + c\mathrm{Re}V\|v\|_{L^2}^2.$$

Using Poincare-Friedrichs inequality, we get

$$\mathrm{Re}\frac{1}{2}\frac{d}{dt}\|v\|_{L^2}^2 \le \left[\mathcal{Q}_1(\delta) + \frac{1}{2\alpha^2} - \frac{c_*}{1+c_*}\right]\|v\|_{H^1}^2 + \frac{\alpha^2q(\delta)^2}{2}V^2\|s\|_{L^2}^2 + c\mathrm{Re}V\|v\|_{L^2}^2. \tag{3.23}$$

Since $\mathcal{Q}_1(0) = 0$, we can choose $\delta_0 > 0$ so small that $\forall\delta \in (0, \delta_0)$

$$\eta := \frac{c_*}{1+c_*} - \frac{1}{2\alpha^2} - \mathcal{Q}_1(\delta) > 0.$$

By suitably increasing the right-hand side of (3.23), we conclude that there exists a constant c with

$$\frac{d}{dt}\|v\|_{L^2}^2 \le c(V^2\|s\|_{L^2}^2 + V\|v\|_{L^2}^2) - \frac{2\eta}{\mathrm{Re}}\|v\|_{H^1}^2. \tag{3.24}$$

64

Next we estimate the right-hand side of (3.22):

$$|\phi_1 - \phi_2| = |\mathcal{F}(s_1, \kappa_1, \xi_1) - \mathcal{F}(s_2, \kappa_2, \xi_2)|$$
$$\leq |\mathcal{F}(s_1, \kappa_1, \xi_1) - \mathcal{F}(s_2, \kappa_1, \xi_1)| + |\mathcal{F}(s_2, \kappa_1, \xi_1) - \mathcal{F}(s_2, \kappa_2, \xi_2)|.$$

Using the continuity properties of $\mathcal{F}$ in a similar way as for $\mathcal{T}$, we can show that there exists a constant C depending on δ with

$$\|\phi_1 - \phi_2\|_{L^2} \leq C(V\|s\|_{L^2} + \|v\|_{H^1}).$$

Plugging this into (3.22) and using inequality of algebraic and geometric means, we find a constant c with

$$\frac{d}{dt}\|s\|_{L^2}^2 \leq c\left[\|v\|_{H^1}^2 + (V+1)\|s\|_{L^2}^2\right]. \tag{3.25}$$

Now we make a linear combination of the equations (3.24) and (3.25) so that the terms proportional to $\|v\|_{H^1}^2$ cancel out. Finally, we can suitably increase the right-hand side so that there exists a $c > 0$ with

$$\frac{dE}{dt} \leq c(V^2 + V + 1)E,$$

where we have denoted $E = \|v\|_{L^2}^2 + \gamma^2\|s\|_{L^2}^2$. By assumption, $E(0) = 0$. Finally, we apply Grönwall's lemma to show that

$$E(t) = 0 \text{ almost everywhere in } [0, T].$$

This proves that the solution given by Theorem 1 is unique. More precisely, we have shown the following.

Theorem 2. *There exists a positive constant K such that if*

$$\|b'\|_{L^2(0,T;H^1) \cap L^2(0,T;H^{-1})} + \|v_0\|_{D(\mathcal{L})} + \|s_0\|_{H^2} \leq K,$$

then Problem $\mathscr{P}$ admits at most one solution in the class of solutions (v, P, s) in the spaces

$$v \in L^2(0, T; H^3), \quad v' \in L^2(0, T; V), \quad \nabla P \in L^2(0, T; H^1),$$
$$s \in L^\infty(0, T; H^2), \quad s' \in L^\infty(0, T; H^1).$$

With this, we have shown the well-posedness of the systems arising from our models for sufficiently small data.

Chapter 4

Computational experiments

This Chapter is concerned with various aspects of numerics for mesoscale fibre suspension models. The semiflexible fibre suspension model is considered in the first section. Here the performance of two closures (polynomial closure and hybrid closure) is compared by studying the behaviour of numerical solutions of the equations for a representative choice of prescribed time-independent planar flow fields. The polynomial closure is found to be more robust. In the rest of this Chapter we are dealing with coupling the fibre orientation equations to the non-Newtonian flow equations for the case of concentrated short fibre suspensions. The numerics and implementation are briefly reviewed in Section 4.2. Numerical solutions for selected domains in two and three dimensions with different parameter values are presented in the third section along with a discussion of the results.

4.1 A study of closure approximations

In this section we study the influence of closure approximations on the solution behaviour of the equations (2.22-2.24) for given local values of the spatial derivatives of the suspension velocity field κ and μ. In the Eulerian coordinates the model consists of a system of transport equations of the form $\frac{\partial s}{\partial t} + v \cdot \nabla s = \mathcal{F}(s, v)$, where $\mathcal{F}$ is the model dependent source term. For stationary flow fields, the characteristics of this hyperbolic system are the streamlines of the velocity field $v(x)$.

Thus application of the method of characteristics to the transport equation is equivalent to reformulation of the model in Lagrangian coordinates, where one follows a volume element of the suspension travelling along a streamline, and computes the fibre orientation evolution for this specific volume element. This reduces the transport equation to a system of ordinary differential equations for each point of the suspension:

$$s' = \mathcal{F}(s, \kappa, \mu). \tag{4.1}$$

For an implementation of the 3-beads model coupled to suspension flow equations it is important to have a robust closure approximation in the sense that for physically meaningful data the solutions are physically meaningful. The invariance of the physically admissible subset of the phase space is a major aspect of the robustness. We

start with a description of the admissible subset. Next we select a set of relevant flow fields. For this, we perform a simple classification of locally incompressible two dimensional flow fields and choose a few representative examples for the tests. Finally, we solve the moment equations numerically for the selected flow fields, and observe the dependence of solution behaviour on the closure relation. Some representative results are presented and conclusions are made.

4.1.1 Phase space

The following algebraic conditions for the components of the moments can be derived from the definition of the mixed moments:

$$\text{Tr}(a^{(2,0)}) = \int\int \text{Tr}(p \otimes p)\psi(p,q)\mathrm{d}\sigma(p)\mathrm{d}\sigma(q) = 1, \tag{4.2}$$

$$\langle w, a^{(2,0)}w \rangle \geq 0 \quad \forall w \in \mathbb{R}^d, \tag{4.3}$$

$$|\langle w, a^{(1,1)}w \rangle| \leq \int\int |w \cdot p||w \cdot q|\psi(p,q)\mathrm{d}\sigma(p)\mathrm{d}\sigma(q)$$

$$\leq \int\int \frac{1}{2}((w \cdot p)^2 + (w \cdot q)^2)\psi(p,q)\mathrm{d}\sigma(p)\mathrm{d}\sigma(q)$$

$$= \langle w, a^{(2,0)}w \rangle \quad \forall w \in \mathbb{R}^d, \tag{4.4}$$

$$|a^{(1,0)}| \leq 1. \tag{4.5}$$

The symmetric tensors a, b and the vector c have an interpretation as moments of a probability distribution ψ only if the relations (4.2-4.5) hold. We define the space

$$\mathcal{M}_d := \left\{ (a,b,c) : a \in \mathbb{R}^{d \times d}_{\text{sym}}, b \in \mathbb{R}^{d \times d}_{\text{sym}}, c \in \mathbb{R}^d \text{ satisfying } (*) \right\},$$

where a triple (a,b,c) is said to satisfy the relation $(*)$ if and only if all of the following conditions hold: $a = a^{(2,0)}$ satisfies (4.2-4.3), a and $b = a^{(1,1)}$ together satisfy (4.4) and $c = a^{(1,0)}$ satisfies (4.5).

Due to the symmetry of $a^{(2,0)}$ and $a^{(1,1)}$ and the constraint (4.2), the phase space $\mathcal{M}_3$ is a 14-dimensional manifold, and $\mathcal{M}_2$ is a 7-dimensional manifold. The triples satisfying the equality in some of the inequalities (4.3-4.5) define the borders of the admissible phase space manifolds.

The exact values of moments are in $\mathcal{M}_d$ by definition, however, the solutions of the equations (2.22-2.24) with a closure approximation may show different behaviour. Clearly, it is desired that the closure approximations are such that the phase space manifolds $\mathcal{M}_d$ are stable with respect to the closed equations (2.22-2.24). In other words, whenever the initial condition is in $\mathcal{M}_d$, the trajectory of the solution never leaves $\mathcal{M}_d$. When the solutions are sought numerically, the stability of $\mathcal{M}_d$ with respect to discretization and round-off errors is another concern. We are focusing on the impact of closure relations in this section, however, we note that additional care must be taken to ensure the stability of the hyperplane defined by (4.2) with respect to small perturbations, which can be achieved, e.g., by a technique of dynamic trace stabilization, see [73].

4.1.2 Space of local velocity fields

As an input for the 3-beads model, a local velocity field is specified by the point values of the velocity gradient κ and curvature μ. Thus, for the purposes of this section, local velocity fields are uniquely determined by pairs (κ, μ), with $\kappa \in \mathbb{R}^{d \times d}$ satisfying the incompressibility condition $\mathrm{Tr}(\kappa) = 0$ and $\mu \in \mathbb{R}^{d \times d \times d}$ satisfying $\mu_{ik}^i = \frac{\partial^2 v_i}{\partial x_i \partial x_k} = 0$ for $k = 1, \ldots, d$ (incompressibility) and $\mu_{jk}^i = \mu_{kj}^i$ (symmetry).

We restrict our attention to the two-dimensional case $d = 2$; the case $d = 3$ can be analyzed in a similar pattern. The equations exhibit rotational invariance, namely, let R be a rotation matrix, then after the transformations $p_i \to R_{ii'} p_{i'}$, $\kappa_{ij} \to R_{ii'} R_{jj'} \kappa_{i'j'}$ and $\mu_{jk}^i \to R_{ii'} R_{jj'} R_{kk'} \mu_{j'k'}^{i'}$ an equation is obtained, whose solutions are the corresponding rotations of the solutions of the original equation. Due to this rotational invariance, the coordinate system can be chosen such that κ is in Jordan normal form. By scaling the time variable, we find that there are three non-trivial cases:

1. Shear flow: $\kappa = \dot{\gamma} \begin{pmatrix} 0 & 1 \\ 0 & 0 \end{pmatrix}$

2. Elongational flow: $\kappa = \frac{\dot{\gamma}}{\sqrt{2}} \begin{pmatrix} 1 & 0 \\ 0 & -1 \end{pmatrix}$

3. Circulating flow: $\kappa = \frac{\dot{\gamma}}{\sqrt{2}} \begin{pmatrix} 0 & 1 \\ -1 & 0 \end{pmatrix}$

and the trivial case $\kappa = 0$. This finishes the classification of the linear parts of the velocity fields. The linear parts are superposed by an arbitrary velocity curvature tensor μ, which has four independent components: $\mu^x = \begin{pmatrix} m_1 & -m_3 \\ -m_3 & m_2 \end{pmatrix}$, and $\mu^y = \begin{pmatrix} m_4 & -m_1 \\ -m_1 & m_3 \end{pmatrix}$, where $m_i \in \mathbb{R}$. Thus the space of local velocity fields can be described as a disjoint union of four instances of $\mathbb{R}^4$.

4.1.3 Results

In order to compare the performance of homogeneous polynomial closure and hybrid closure, we compare the behaviour of numerical solutions for a representative choice of velocity gradient κ (characterizing shear flows, extensional flows and circulating flows). We consider the velocity curvature μ as a perturbation of the linear part κ. The study presented below does not aim at a full cartography of all possible classes of the pairs (κ, μ). Instead, we have numerically solved the equations with several choices of μ. The results show similar patterns for all choices of reasonably small μ (in the sense that the fibre bending stiffness is large enough to prevent the fibres from "clipping"). For the sake of illustration, we present only the results for a single typical value of μ, given by

$$m_1 = 1, \; m_2 = -1, \; m_3 = -2, \; m_4 = 1. \tag{4.6}$$

Shear flow. Let $\kappa = 10 \cdot \begin{pmatrix} 0 & 1 \\ 0 & 0 \end{pmatrix}$; some streamlines of this flow field are shown in Figure 4.1.
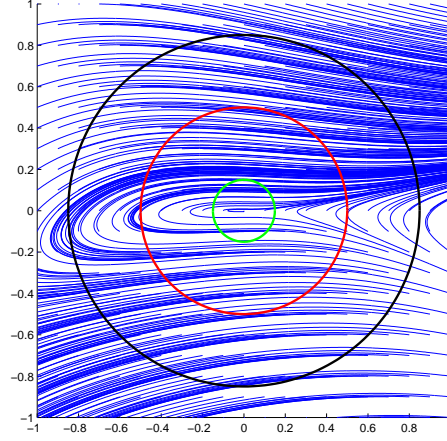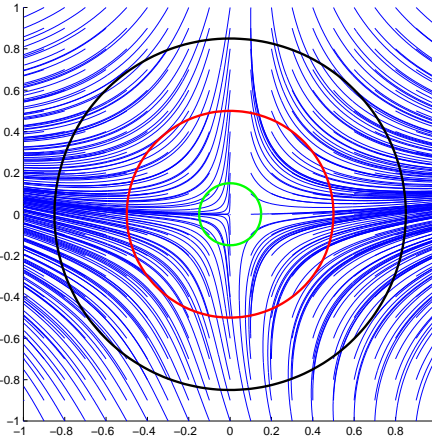

Figure 4.1: Streamlines of a perturbed shear flow. The diameters of the circles correspond to the length of fibres: green $l_B = 0.3$, red: $l_B = 1$, black: $l_B = 1.7$

We use the fibre bending rigidity constant $k = 3$ and consider the initial conditions

$$a_0 = \begin{pmatrix} 0.5 & 0.5 \\ 0.5 & 0.5 \end{pmatrix}, \; b_0 = -a_0, \; c_0 = 0, \tag{4.7}$$

corresponding to a uniaxial distribution of straight fibres (this initial condition is on the border of $\mathcal{M}_2$). The *left* part of Figure 4.2 shows the time-dependent functions $\mathrm{Tr}(b)$ (showing the bending degree of the fibres; upper plot), a_{11} (middle plot) and c_1 (lower plot), all for the *polynomial* closure. Observe that a steady state is reached.

The corresponding results for the *hybrid* closure are demonstrated in the right side of Figure 4.2. Observe that here for a sufficiently small fibre length l_B the solution is periodic.

Elongation flow. Let $\kappa = 5 \cdot \begin{pmatrix} 1 & 0 \\ 0 & -1 \end{pmatrix}$ and μ be given by (4.6). Some streamlines of this velocity field are shown in Figure 4.3.

Again we solve the equations with polynomial and hybrid closures for the initial condition (4.7) lying on the border of $\mathcal{M}_2$. The results are shown in Figure 4.4; left side: polynomial closure, right side: hybrid closure. As we see, both solutions show a similar behaviour, reaching a steady orientation state, which characterizes slightly bent fibres aligned in the direction of flow elongation.

Circulating flow. A fibre initially aligned in the plane of a circulating planar flow never reaches a steady state. Thus, effects that remain small due to the short transient phase from the initial state to a flow-aligned fibre orientation state, which is characteristic for shear and elongational flows, are expected to become evident in this case. Indeed, here the greatest variety of solution behaviour can be observed.
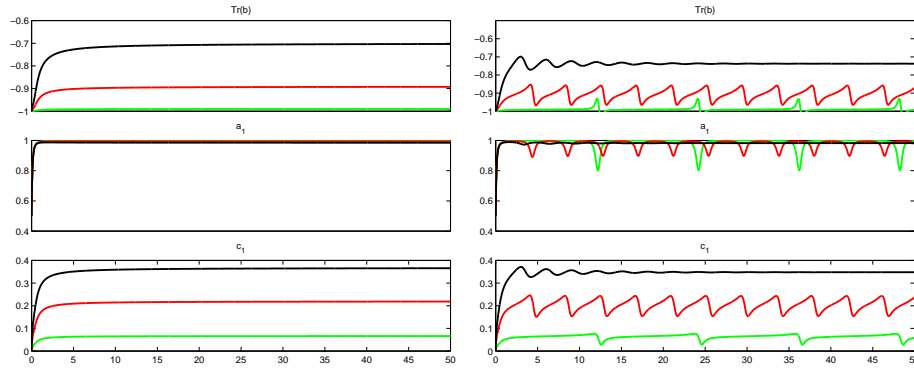
Figure 4.2: Numerical solutions of the 3-beads model with polynomial closure (left) and hybrid closure (right) in a shear flow. Components: $\text{Tr}(b)$ (top), a_{11} (middle), c_1 (bottom). Green curves: $l_B = 0.3$, red: $l_B = 0.5$, black: $l_B = 1.7$

Figure 4.3: Streamlines of a perturbed elongational flow. The diameters of the circles correspond to the length of fibres: green $l_B = 0.3$, red: $l_B = 1$, black: $l_B = 1.7$
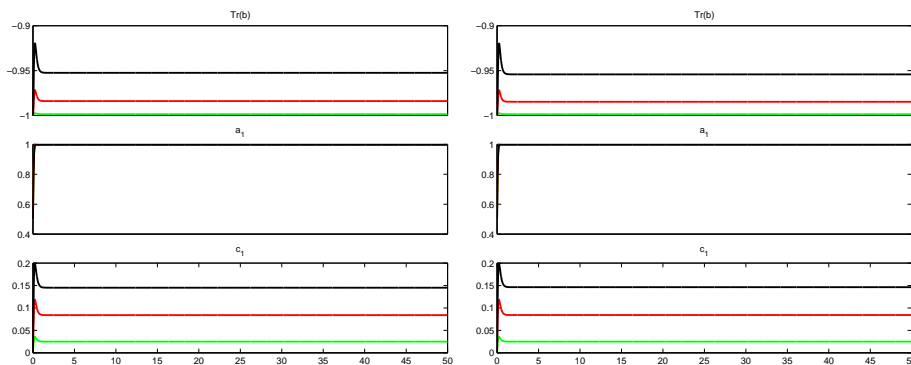
Figure 4.4: Numerical solutions of the 3-beads model with polynomial closure (left) and hybrid closure (right) in an elongation flow. Components: $\text{Tr}(b)$ (top), a_{11} (middle), c_1 (bottom). Green curves: $l_B = 0.3$, red: $l_B = 0.5$, black: $l_B = 1.7$

71

Let $\kappa = \dot{\gamma} \begin{pmatrix} 0 & 1 \\ -1 & 0 \end{pmatrix}$, and let μ be defined by (4.6). Some streamlines of the flow field corresponding to $\dot{\gamma} = 3$ can be viewed in Figure 4.5.
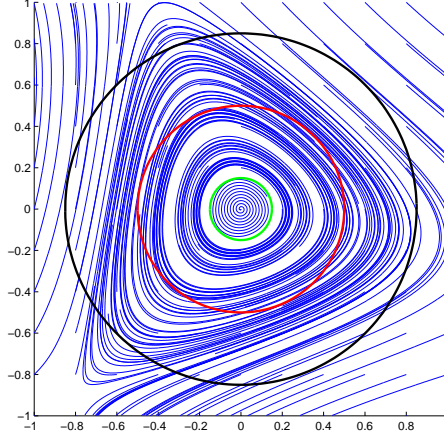
Figure 4.5: Streamlines of a perturbed circulating flow. The diameters of the circles correspond to the length of fibres: green $l_B = 0.3$, red: $l_B = 1$, black: $l_B = 1.7$

We use the initial condition (4.7) in all computations. The a_{11} component of the numerical solutions with $\dot{\gamma} = 3$ is shown in Figure 4.6. The value of bending constant is $k = 3$ for the plots in left side and $k = 0.3$ for the plots in right side. The upper plots are for polynomial closure and the lower plots - for hybrid closure.
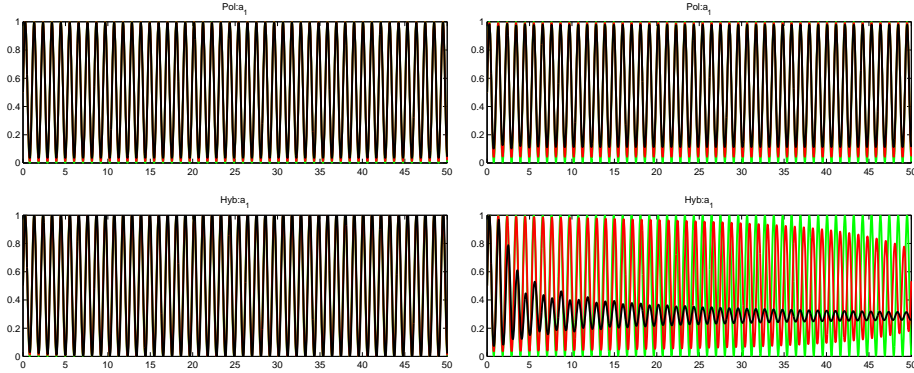
Figure 4.6: Circulating flow, $\dot{\gamma} = 3$. Left: $k = 3$, right: $k = 0.3$. Upper plots: a_{11} for polynomial closure, lower plots: a_{11} for hybrid closure. Colours: green: $l_B = 0.3$, red: $l_B = 0.5$, black: $l_B = 1.7$

We observe that at sufficiently high bending stiffness k both closures yield similar results. The decrease in amplitude of a_{11} is caused by the fibre bending. At lower values of k the two closures yield different results. The hybrid closure causes a "smear-out" of the fibre orientation distribution that is characteristic of type 1 linear closure.

An even more prominent difference is observed with a stronger flow perturbation, with $\dot{\gamma} = 1$ and unchanged μ. We have chosen the bending stiffness $k = 1$. In the left plot of Figure 4.7 we show the a_{11} for $l_B = 0.5$ (green), $l_B = 1.5$ (red) and $l_B = 1.7$ (black line); again the polynomial closure is in the upper plot and the hybrid closure is in the lower plot.
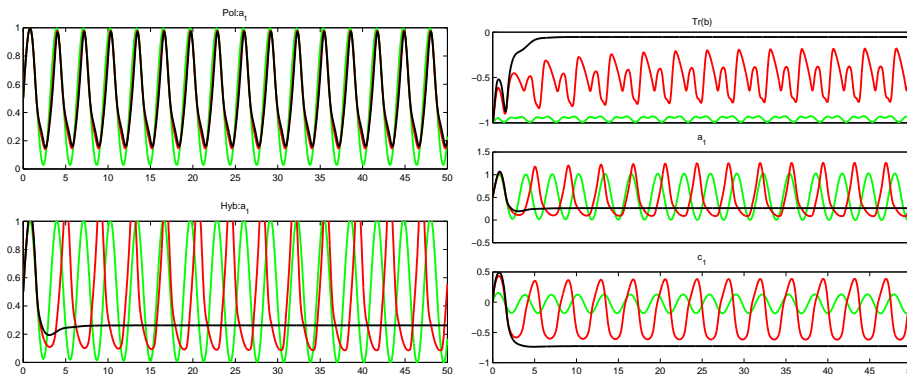
Figure 4.7: Circulating flow, $\dot{\gamma} = 1$, $k = 1$. Left: a_{11} versus time for polynomial closure (upper plot) and for hybrid closure (lower plot). Colours: green: $l_B = 0.5$, red: $l_B = 1.5$, black: $l_B = 1.7$. Right: Hybrid closure, $\mathrm{Tr}(b)$ (upper plot), a_{11} (middle plot), c_1 (lower plot)

Here we observe that the polynomial closure yields results with constant periods and amplitude while for the hybrid closure, at a critical value of fibre length l_B, the fibre rotation periods increase until the oscillations die out and a steady solution is reached.

Summary. We have seen that the solutions of (2.22-2.24) with polynomial closure reproduce the dynamics of a single fibre for all types of planar velocity fields and for a wide range of parameter values. Both the type of the orbits (periodic or stationary) and the period of the orbits are reproduced with good accuracy. In contrary, the equations with hybrid closure are more sensitive with respect to parameters like bending stiffness k. The solutions exhibit such (unphysical) phenomena as oscillations in a shear flow and steady-state solutions from uniaxial initial conditions for certain circulating flows. This can be explained by the isotropic relaxation from a bent fibre orientation state characteristic for the type 1 linear closure.

The phase space $\mathcal{M}_2$ is remarkably stable with respect to the equations with both closure relations. However, a dynamical trace stabilization for a as in computations with the Folgar-Tucker model (see [73]) is recommended in order to make the linear manifold defined by (4.2) stable. We remark that the equations with linear closure approximations violate the condition of positive semidefiniteness (4.3).

We recommend to use the polynomial closure approximation for implementations of the 3-beads fibre orientation dynamics model due to the higher robustness and lower computation costs for computing the source terms.

4.2   Algorithm

Numerical methods of various types have been proposed for solving the coupled system, using finite element methods (see e.g. [63], [64]), finite difference method, finite volume method, boundary element method, spectral methods (see [35] and references therein). In the framework of this thesis the fibre orientation models are implemented in the CoRheoS (complex rheology solver) software platform, developed at the Department *Flow and Material Simulations* of Fraunhofer ITWM. The solver is based on a *finite volume* based spatial discretization using a collocated grid. The numerics implemented for simulations of viscoelastic flows have been discussed in [54]. Let us briefly review the parts of the algorithm that are relevant for fibre suspension flows, and present the methods used for numerically solving the fibre orientation dynamics equations.

The momentum conservation equation can be rewritten in the form

$$\rho\frac{\partial v}{\partial t} + \rho(v \cdot \nabla)v = \rho b - \nabla P + 2\eta\nabla \cdot D + \nabla \cdot \mathcal{T}, \tag{4.8}$$

where $\mathcal{T} = \mathcal{T}(\nabla v, s)$, and the continuity equation is $\nabla \cdot v = 0$. The coupled system of transport equations for the components of s can be written as

$$\frac{\partial s_i}{\partial t} + (v \cdot \nabla)s_i = s_i\mathcal{F}_{L,i} + \mathcal{F}_{N,i}, \tag{4.9}$$

where the source term $\mathcal{F}$, which is polynomial in s_i, is seperated in a part depending on s_i written as $s_i\mathcal{F}_{L,i}$ and the rest $\mathcal{F}_{N,i}$, which does not depend on the component s_i.

4.2.1   Time discretization

Equations (4.8) and (4.9) are strongly coupled through the deviatoric stress term $\mathcal{T} = \eta(D : a^{(2)})a^{(2)}$. In the implementation used in this thesis the momentum equation is decoupled from the fibre orientation equation by computing $\mathcal{T}$ using s from the previous time step.

Let the time variable be discretized with a fixed time-step τ: $t_n = t_0 + n\tau$, and let the (approximated) values of variables at the time step t_n be denoted by a superscript n, e.g., $v^n \approx v(t_n)$. Suppose that the continuity, momentum and fibre orientation equations are discretized in space. Let B be the discretization of the divergence operator, $B^\top$ - the discretization of the gradient operator (using a discretization, where the divergence and gradient operators are adjoint), let C_v be a discretization of the convection operator, D_v a discretization of the viscous term $2\nabla \cdot (\eta D)$ and Σ the discretization of the deviatoric stress term. For the convection term we use the Oseen linearization

$$((v \cdot \nabla)v)^{n+1} \approx (v^n \cdot \nabla)v^{n+1},$$

therefore C_v is computed by using the values of v^n. This motivates the time-dependent notation C_v^n. Similarly, we use the values of s^n to compute Σ, this motivates the time-dependent notation Σ^n.

The discretized continuity and momentum equations are

$$Bv^{n+1} = 0, \tag{4.10}$$

$$\rho \frac{v^{n+1} - v^n}{\tau} = D_v v^{n+1} - C_v^n v^{n+1} - B^\top P^{n+1} + B\Sigma^n v^{n+1}. \tag{4.11}$$

After these linear equations are solved for v^{n+1}, we plug in these values into the discretized FO equation using either an implicit method:

$$\frac{s_i^{n+1} - s_i^n}{\tau} + C_v^{n+1} s_i^{n+1} = s_i^{n+1} \mathcal{F}_L(s^n, v^{n+1}) + \mathcal{F}_N(s^n, v^{n+1}). \tag{4.12}$$

or an explicit method:

$$\frac{s_i^{n+1} - s_i^n}{\tau} + C_v^{n+1} s_i^n = s_i^n \mathcal{F}_L(s^n, v^{n+1}) + \mathcal{F}_N(s^n, v^{n+1}).$$

Solving these equations for s^{n+1} finishes the time step.

Next we discuss the solution methods for the linear algebraic system (4.10-4.11).

4.2.2   Projection methods

The structure of the linear system is

$$\begin{pmatrix} A & B^\top \\ B & 0 \end{pmatrix} \begin{pmatrix} v \\ P \end{pmatrix} = \begin{pmatrix} f \\ 0 \end{pmatrix}.$$

The projection type methods, alternatively known as pressure correction methods and fractional time schemes, use the following approach. First, in the prediction step, the momentum equation is solved using the pressure from the previous time step. In the correction step, the velocity obtained in the first step is projected on the divergence-free subspace by finding a pressure correction. For an overview see e.g. [79], [21].

Solving the equations for pressure gives

$$BA^{-1}B^\top P = BA^{-1}f.$$

A preconditioned Richardson iteration can be used to solve the pressure equation, leading to

$$P^{i+1} = P^i + M^{-1}BA^{-1}(f - B^\top P^i),$$

where M is an easily invertible matrix, spectrally close to $BA^{-1}B^\top$. Typically, one chooses $M = BH^{-1}B^\top$, where H is a diagonal matrix, e.g., the Jacobi type preconditioner $H = \text{diag}(A)$. This choice leads to the well-known SIMPLE algorithm. The pressure corection $\delta P^i := P^{i+1} - P^i$ can be expressed in the form

$$M\delta P^i = B(A^{-1}f - A^{-1}B^\top P^i) = Bv^i,$$

where v^i is the solution of the discretized momentum equation $Av^i + B^\top P^i = f$. Now one completes the iteration step by the velocity correction

$$v^{i+1} = v^i - H^{-1}B^\top \delta P^i.$$

This leads to the following time-stepping algorihm (adapted from [54]).

1. Define $v^0 = v^n$, $P^0 = P^n$ and set $k = 0$.

2. Compute v_*^{k+1} from $Av_*^{k+1} = f - B^\top P^k$, using biconjugate gradient stabilized algorithm (BiCGStab, [67]).

3. Solve the pressure correction equation $MP' = Bv_*^{k+1}$.

4. Calculate the velocity correction $v' = -H^{-1}B^\top P'$.

5. Correct the velocities $v^{k+1} = v_*^{k+1} + v'$ and pressure $P^{k+1} = P^k + P'$.

6. If convergence reached, then set $v^{n+1} = v^{k+1}$ and $P^{n+1} = P^{k+1}$, otherwise set $k \mapsto k + 1$ and return to 2.

4.2.3 Finite volume spatial discretization

We present the discretization for the two-dimensional case; the extension to three dimensions is straight-forward. The momentum equation (4.8) in divergence form componentwise is

$$\frac{\partial(\rho v_i)}{\partial t} + \frac{\partial}{\partial x_j}(\rho v_j^* v_i) - \frac{\partial}{\partial x_j}\left(\eta\left(\frac{\partial v_i}{\partial x_j} + \frac{\partial v_j}{\partial x_i}\right)\right) = -\frac{\partial P}{\partial x_i} + f_i \qquad (4.13)$$

for $i = 1, 2$. Here $f_i = \frac{\partial}{\partial x_j}S_{ij} + b_i$, and we use the convention to sum over repeating indices. We think of v^* as an approximation to v satisfying incompressibility condition $\nabla \cdot (\rho v^*) = 0$, thus $\frac{\partial}{\partial x_j}(\rho v_j^* v_i) = (\rho v^* \cdot \nabla)v_i$.

Although in our model the effective dimensionless viscosity η is assumed to be constant, yielding the simplification $\frac{\partial}{\partial x_j}\left(\eta\left(\frac{\partial v_i}{\partial x_j} + \frac{\partial v_j}{\partial x_i}\right)\right) = \eta\triangle v_j$, we allow the more general case of variable viscosity η in (4.8) since the components of the momentum equation are coupled through the mixed derivatives anyway because of the form of the extra stress term.

Let us assume that the domain Ω is subdivided in rectangular control volumes (CV). Let the axes of the coordinate system be parallel to the edges of the elements, then we define East (x_1^+), West (x_1^-), South (x_2^-) and North (x_2^+) directions.

We use a collocated grid, i.e., the degrees of freedom for v_i, P and s_i are defined in the center-points of the CVs. The discretization variables relative to a fixed CV are indexed as follows.

Let an arbitrary CV be given. The center point of the CV is denoted by C. The center points of the edges (also called *walls* of the CV) are denoted by the lower-case letters e, w, s and n depending on the direction from the central point C. The

center points of the neighbouring CVs that share a common edge with our CV are denoted by the capital letters E, W, N and S. The neighbouring CVs that share a single common point with our CV have center points denoted by NE, NW, SW, SE. Finally, the center of the northern edge of the western neighbouring CV is denoted by nW and so on. See Figure 4.8 for an illustration.
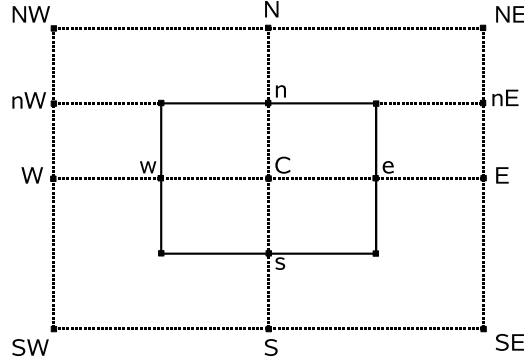

Figure 4.8: A representative control volume with the center point C, center points of the neighbouring CVs (N, E, S, W and NE, SE, SW, NW), center points of the faces (n, e, s, w) and the center points of the faces of neighbouring CVs (nE, nW etc.)

The area of the CV is denoted by S_V, the equal length of the south and north walls is denoted by h_x, and the length of the east and west walls - by h_y.

We integrate the equation (4.13) over a CV, use the Gauss divergence theorem transforming the volume integrals of a divergence to surface integrals. Further, we apply the midpoint integration rule. This yields a spatial "semi"-discretization of the momentum equation:

$$\left(\frac{\partial(\rho v_1)}{\partial t}\right)_C S_V + h_y \left\{\rho_e v_{1,e}^* v_{1,e} - \rho_w v_{1,w}^* v_{1,w} - 2\left[\eta_e \left(\frac{\partial v_1}{\partial x}\right)_e - \eta_w \left(\frac{\partial v_1}{\partial x}\right)_w\right]\right\} +$$
$$h_x \left\{\rho_n v_{2,n}^* v_{1,n} - \rho_s v_{2,s}^* v_{1,s} - \left[\eta_n \left(\frac{\partial v_1}{\partial y} + \frac{\partial v_2}{\partial x}\right)_n - \eta_s \left(\frac{\partial v_1}{\partial y} + \frac{\partial v_2}{\partial x}\right)_s\right]\right\} \qquad (4.14)$$
$$= S_V \left[\rho b_1 - \left(\frac{\partial P}{\partial x}\right)_C\right] + h_x(S_{11,e} - S_{11,w}) + h_y(S_{12,n} - S_{12,s})$$

and a similar equation for the second component of (4.13).

Next we approximate (4.14) by a linear system for the values of v_i at the centers of the central and neighbouring CVs. The values of the variables at the walls are approximated using the linear interpolation of the node values, e.g.,

$$v_e = (1 - f)v_C + f v_E, \quad f = \frac{x_e - x_C}{x_E - x_C}.$$

Of course, boundary conditions are applied whenever the wall is on the boundary. If a Dirichlet condition is prescribed, then the value of v_e is readily available. For Neumann condition additional variable at the center of the wall is introduced.

The convective part is discretized by an upwind difference scheme, for instance, the following first-order scheme can be used to compute the term $(\rho h_y v_{1,e}^*)v_{1,e}$ depending on the direction of the convection velocity:

$$v_{1,e} = \begin{cases} v_{1,C} & \text{if } v_{1,e}^* > 0, \\ v_{1,E} & \text{if } v_{1,e}^* < 0. \end{cases}$$

Should the eastern wall be a part of the Dirichlet boundary, the prescribed value of $v_{1,e}$ is used.

The diffusive (viscous) terms are approximated by a central second-order difference scheme, e.g.,

$$\left(\frac{\partial v_1}{\partial x}\right)_e \approx \frac{v_{1,E} - v_{1,C}}{x_e - x_C},$$

with the obvious modifications for a boundary wall.

Finally, the mixed derivatives of the type $\left(\frac{\partial v_2}{\partial x}\right)_n$ are discretized by using the symmetric scheme (see also [82]). For an internal wall it is

$$\left(\frac{\partial v_2}{\partial x}\right)_n \approx \frac{1}{2}\left(\frac{v_{2,NE} - v_{2,NW}}{x_{NE} - x_{NW}} + \frac{v_{2,E} - v_{2,W}}{x_E - x_W}\right).$$

For a boundary wall we use an implicit discretization due to stability considerations (see [54] and references therein):

$$\left(\frac{\partial v_2}{\partial x}\right)_n \approx \frac{1}{2}\left(\frac{v_{2,nE} - v_{2,nW}}{x_{NE} - x_{NW}} + \frac{v_{2,E} - v_{2,W}}{x_E - x_W}\right).$$

The value of S_{ij} is computed using the orientation tensor from the previous time step. Similarly, for v^* in the convective part we use the velocity from the previous time step. Thus, an implicit in time spatial discretization of the momentum equation is obtained in the form of a linear system with dN_{CV} unknowns, where d is the dimension of the domain and N_{CV} is the number of CVs.

FO equations. The equations can be written in the form

$$\frac{\partial s_i}{\partial t} + (v \cdot \nabla)s_i = s_i \mathcal{F}_{L,i} + \mathcal{F}_{N,i}, \tag{4.15}$$

where in two dimensions for rigid fibre models $i = 1, 2, 3$, the unknowns being $s_1 = a_{11}^{(2)}$, $s_2 = a_{22}^{(2)}$, $s_3 = a_{12}^{(2)} = a_{21}^{(2)}$. The coefficients for the first component are given by

$$\begin{aligned} \mathcal{F}_{L,1} &= 2\left[D_{11}(1 - s_1) - D_{22}s_2 - 2D_{12}s_3\right] - 2\dot{\gamma}C_i + \\ &\quad U_0\dot{\gamma}(s_1 - (s_1^2 + s_2^2 + 2s_3^2)), \\ \mathcal{F}_{N,1} &= 2\kappa_{21}s_3 + \dot{\gamma}C_i + \dot{\gamma}U_0 s_3^2. \end{aligned}$$

After integrating (4.15) over a CV and using Gauss divergence theorem and center point integration rule, we obtain

$$\begin{aligned} &\left(\frac{\partial s_i}{\partial t}\right)_C + h_y\left[s_{i,e}v_{1,e} - s_{i,w}v_{1,w}\right] + h_x\left[s_{i,n}v_{2,n} - s_{i,s}v_{2,s}\right] \\ &= S_V\left(s_i\mathcal{F}_{L,i} + \mathcal{F}_{N,i}\right)_C. \end{aligned}$$

By using the values of s_i from the previous time step to compute the terms $\mathcal{F}$ and an upwind approach to compute the convective terms, we arrive at an implicit discretization in the form of a linear system with $3N_{CV}$ unknowns. The generalization to three dimensions is straight-forward.

4.3 Short fibre suspension flows: computations on 2D and 3D domains

The fibre suspension is modelled as an incompressible fluid, governed by the incompressibility condition $\nabla \cdot v = 0$, the conservation of momentum equation (4.8), the constitutive relations (3.3-3.4) and the fibre orientation dynamics equation for concentrated short fibre suspensions (2.3) with the quadratic closure relation $a^{(4)} \approx a^{(2)} \otimes a^{(2)}$.

In all computations presented in this Section we use the effective suspension viscosity $\eta = 1000 Pa \cdot s$ and suspension density $\rho = 800 kg/m^3$.

The equation (2.3) depends on two parameters - the orientation diffusion constant C_i and the Maier-Saupe constant U_0. A qualitative understanding of the effects that these constants have on the solution can be achieved by computing the stationary solutions of (2.3) in stationary flow fields. We present a graph of the eigenvalues of the stationary solution, which do not depend on the shear rate or directional information, but only on the Jordan normal form of the gradient κ. For a two-dimensional shear flow, Figure 4.9 shows the largest eigenvalue of the stationary solution versus the variable U_0 while C_i is kept constant at the value of $C_i = 0.01$ for the black curve, $C_i = 0.05$ for the red curve and $C_i = 0.1$ for the green curve.
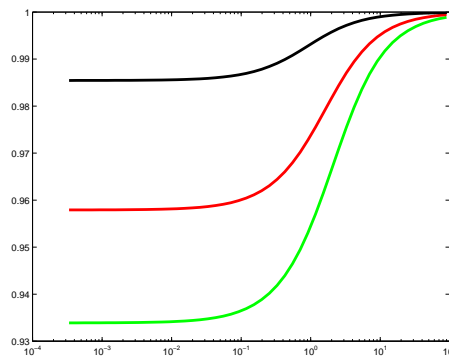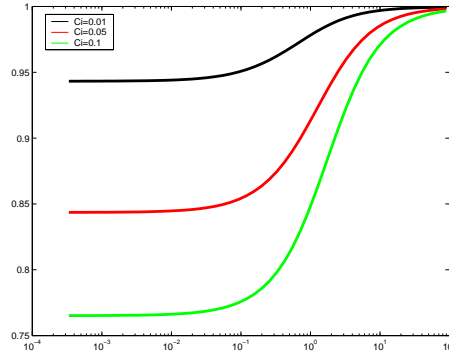

Figure 4.9: Maximal eigenvalue of the stationary solution versus U_0 for $C_i = 0.01$ (black curve), $C_i = 0.05$ (red curve) and $C_i = 0.1$ (green curve) for a simple planar shear flow

The classification of velocity gradients κ for incompressible three-dimensional flows leads to more qualitatively different cases than for planar flows, see [73]. A general tendency can nevertheless be observed: for fixed values of (C_i, U_0), the maximal eigenvalues of the stationary solution for three-dimensional case tend to be smaller than for the two-dimensional case because of the additional dimension of fibre orientation

diffusion. Figure 4.10 illustrates this tendency for a simultaneous shear flow in planes y-z and x-z with $\kappa = \begin{pmatrix} 0 & 0 & 1 \\ 0 & 0 & 1 \\ 0 & 0 & 0 \end{pmatrix}$.

Figure 4.10: Maximal eigenvalue of the stationary solution versus U_0 for $C_i = 0.01$ (black curve), $C_i = 0.05$ (red curve) and $C_i = 0.1$ (green curve) for a 3D shear flow simulatanelusly in x-z and y-z directions

For the purposes of this thesis we find it sufficient to study the dependence on U_0 since the dependence on C_i has been well understood in the context of Folgar-Tucker model. Therefore we fix a typical value $C_i = 0.05$ (the red curve in Figures 4.9 and 4.10), which are used for all the simulations presented in this Section.

The extra stress term given by (3.4) also contains two constants - the particle number N_p and the shear number N_s. These constants origin from a theory by Dinh and Armstrong [15]. The particle number represents the property of a suspended fibre to resist stretching along its axis; the contribution of a single fibre to the stress tensor is proportional to $p_i p_j p_k p_l D_{kl}$. Here $p_k p_l D_{kl}$ is interpreted as the elongation rate parallel to the fibre axis ([78]). The shear number represents the orientation dependent contribution to stress of a fibre in shear flows, namely, that the fibres aligned in flow direction create more resistance to the shear flow than fibres aligned in the vorticity direction.

The particle number increases with increasing concentration and aspect ratio. However, as the aspect ratio increases, N_p grows much faster as N_s, so that for aspect ratios greater than 10 we may assume $N_s \ll N_p$ (see e.g. [78]). Basing on these considerations, we set $N_s = 0$ and vary the parameter N_p as a measure of "non-Newtonicity" of the fluid. Since $N_p = 0$ gives a Newtonian fluid, where the momentum and continuity equations are decoupled from the fibre orientation equations, we start with this case to isolate the effects of the constant U_0 on the values of $a^{(2)}$. After that we observe the back-coupling effects of U_0 to the flow field.

We make the following choice of computation domains. In two dimensions: a channel domain, where the flow gradient is mainly shear-like, and a 4:1 contraction domain, featuring regions with shear flow, contraction/elongation flow and recirculating flow in the corner vortices. In three dimensions: a pipe with square and

rectangular cross section and a square-to-square contraction domain.

For the boundary conditions:

- at *inflow*: Dirichlet condition for velocity (with a Poiseuille profile), and Dirichlet condition for $a^{(2)}$, more specifically, the isotropic condition $a^{(2)}_{\text{inflow}} = \frac{1}{d}I$.

- at *outflow*: homogeneous Dirichlet condition for pressure

- at *walls*: no-slip condition for velocity, homogeneous Neumann for $a^{(2)}$.

4.3.1 Planar channel flow

As the first example we consider a fibre suspension flow through a planar channel geometry, corresponding to a laminar flow between parallel plates.

The computation domain is a rectangle $\Omega = \{(x, y) \in \mathbb{R}^2 : 0 < x < L_c, 0 < y < d_c\}$ with the length $L_c = 10m$ and the width $d_c = 4m$. The boundaries are described as follows. The boundary at $x = 0$ is inflow; here a Dirichlet condition is prescribed for velocity with a parabolic velocity profile: $v(0, y) = 4v_{max}y(d_c - y)e_x$, where the maximal inflow velocity $v_{max} = 0.1m/s$ (e_x is the unit vector pointing in the x-direction). The corresponding Reynolds number is $Re = \frac{\rho v_{max} d_c}{\eta} = 0.024$. The fibre orientation at the inflow is assumed to be isotropic: $a^{(2)} = \frac{1}{2}I$. The opposite boundary at $x = L_c$ is an outflow boundary, and the other parts at $y = 0$ and $y = d_c$ are walls.

The domain is discretized using a regular mesh consisting of quadratic volume elements with edge length $h = 0.1m$ (the mesh contains 4000 elements).

We start with the **Newtonian fluid** case, $N_p = 0$. In this case the momentum equations are decoupled from the fibre orientation equations, and the velocity field can be computed analytically:

$$v(x, y) = 4v_{max}\frac{y(d_c - y)}{d_c^2}e_x.$$

The streamlines are parallel to the walls, hence this is a pure shear flow except on the center-line $x = 2$, where the velocity gradient vanishes. Since the velocity gradient is constant along a streamline, each infinitesimal fluid element experiences a constant shear flow, thus far enough downstream the maximal eigenvalue of $a^{(2)}$ reaches the value predicted by the red curve in Figure 4.9.

The tensor field $a^{(2)}$ in a volume element is visualized by an ellipsoid. The main axes of the ellipsoid correspond to the eigenvectors of the matrix $a^{(2)}$, but the aspect ration equals the ratio of the matrix eigenvalues. The orientation field for $U_0 = 0$ (here the model is equivalent with the Folgar-Tucker model) is visualized in Figure 4.11. The background colour signifies the value of the maximal eigenvalue and the blue ellipses represent the fibre orientation.

Following the streamlines from the inflow (left) to the outflow (right), we observe that the fibres gradually reach a nearly uniaxial orientation state. Near the inflow

the fibres form a characteristic "fishbone" like pattern, but the angle that the fibres form with the flow direction decreases until the fibres align in flow direction. A qualitative understanding of the fibre orientation state over the domain is given by the dimensionless quantity $t\dot\gamma$, where t is the time that a fibre spends in the shear flow. At the point (x, y) we have $t\dot\gamma \propto \frac{x|d_c - 2y|}{y(d_c - y)}$. For fixed $x > 0$ the quantity $t\dot\gamma$ as a function of y is maximal at the walls and minimal on the center line, explaining the computed pattern of orientational degree.
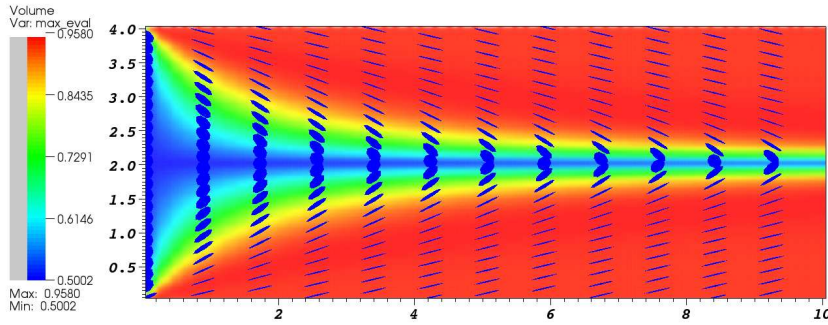
Figure 4.11: Fibre orientation tensor field in a channel domain; Newtonian fluid with Folgar-Tucker model ($N_p = 0$, $U_0 = 0$). Colour code: maximal eigenvalue of $a^{(2)}$. The orientation ellipsoids (blue) represent the eigenvectors (pointing along the main axes of the ellipsoids). The aspect ratio of the ellipsoids represents the ratio of the corresponding eigenvalues.

An increase in U_0 does not affect the velocity v, we only observe quantitative changes in fibre orientation tensor field. For the value $U_0 = 1$ the field is visualized in Figure 4.12, and for the large value $U_0 = 100$ the field is illustrated in Figure 4.13. Due to the large ratio between the bigger and smaller eigenvalue of $a^{(2)}$, the aspect ratio of the orientation ellipsoids is scaled to $(9\lambda_{max} + 1)/(9\lambda_{min} + 1)$ in both pictures. Note that the increase in maximal eigenvalue for larger values of U_0 as well as the shorter transition from the fishbone orientation pattern to a flow-aligned state.

Non-Newtonian case. For positive values of N_p the suspension is a non-Newtonian fluid because of the coupling of the momentum equation to the fibre orientation field through the stress term. However, the extra stress term S (see (3.4)) vanishes if $a^{(2)} : D = 0$. For the isotropic fibre orientation state $a^{(2)} = \frac{1}{d}I$ the incompressibility condition implies $S = 0$.

This observation is important for constructing consistent boundary conditions at the inflow. If isotropic fibre orientation state is prescribed at the inflow, then the inlet velocity should be prescribed as for a Newtonian fluid. For the channel geometry this means a parabolic inlet velocity profile. Due to non-Newtonian nature of the flow, the velocity profile is expected to change in other cross-sections of the channel.

Experiments and simulations ([62], [64]) suggest that the velocity profile tends to "flatten out". If a parabolic velocity profile is prescribed at the inlet, then a
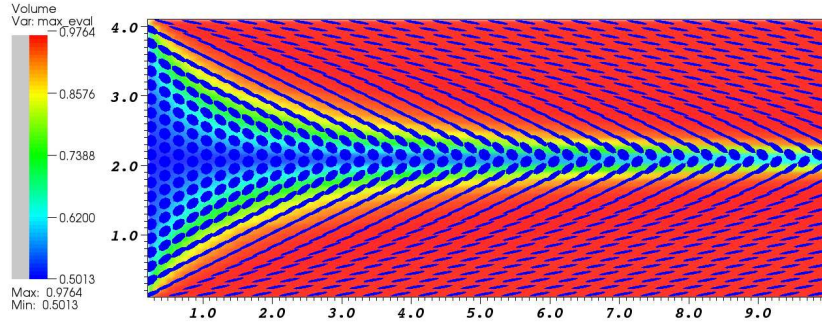
Figure 4.12: Fibre orientation tensor field in a channel domain. $N_p = 0$, $U_0 = 1$. Color codes the maximal eigenvalue. The aspect ratio of orientation ellipsoids is scaled to $(9\lambda_{max} + 1)/(9\lambda_{min} + 1)$ for better visualization.
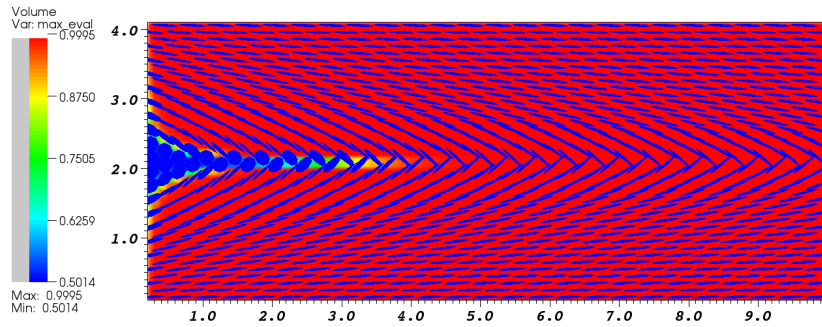

Figure 4.13: Fibre orientation tensor field in a channel domain. $N_p = 0$, $U_0 = 100$. Color codes the maximal eigenvalue. The aspect ratio of orientation ellipsoids is scaled to $(9\lambda_{max} + 1)/(9\lambda_{min} + 1)$.

divergence of the streamlines from the central parts to the lateral parts of the channel can be observed in regions where the velocity profile is changing. The divergence of streamlines is illustrated by Figure 4.14. Here the parameters are $N_p = 50$, $U_0 = 1$.
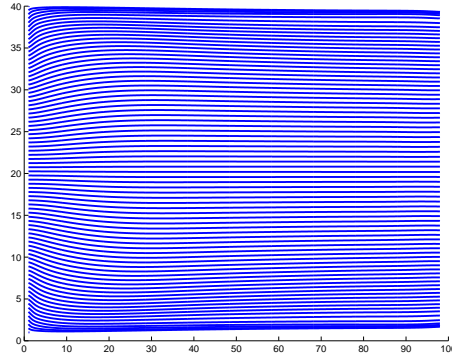
Figure 4.14: Diverging streamlines in a channel domain; $N_p = 50$, $U_0 = 1$. The flow is from the left to the right

The dependence of the velocity profile at the outlet $x = 10$ on the particle number N_p is demonstrated in Figure 4.15. The red curve shows the well-known parabolic velocity profile for the Newtonian case $N_p = 0$. The green curve is the velocity profile computed with $N_p = 5$, the black curve with $N_p = 20$ and the blue curve with $N_p = 100$. We observe the progressive flattening of the velocity profile with growing N_p. The results are in good agreement with the ones reported in [64].
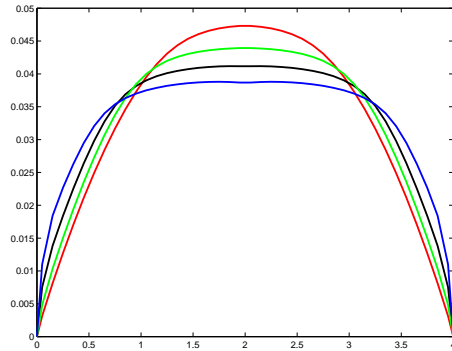
Figure 4.15: The profile of the flow velocity component v_1 at the outlet. $N_p = 0$ (red), $N_p = 5$ (green), $N_p = 20$ (black) and $N_p = 100$ (blue). $U_0 = 0$.

In Figure 4.14 we observe a central region near the inlet, where the streamlines diverge (i.e., the distance between two neighbouring streamlines increases). In such regions the flow is expanding (extension in the y-direction), thus the fibres tend to align in perpendicular direction to the flow.

This phenomenon is illustrated in Figure 4.16, where the parameters are $N_p = 50$, $U_0 = 1$. The background color visualizes $a_{1,1}^{(2)}$, which is the averaged squared cosine of the angle that the fibres form with the flow direction. Observe the central core

region, where the fibres show a prefered alignment direction perpendicular to the flow direction. For Newtonian flow $N_p = 0$, the minimal value of $a_{1,1}^{(2)}$ for the stationary solution in the channel domain is 0.5. For $N_p = 5$ the minimum is 0.4311, while for $N_p = 50$ the minimum is 0.2807, cf. Figure 4.16.

Due to the flat velocity profile, the shear rate $\dot{\gamma}$ decreases in the central region of the channel. Hence, the transient effects such as the fishbone orientation pattern are preserved for longer distances from the inlet.
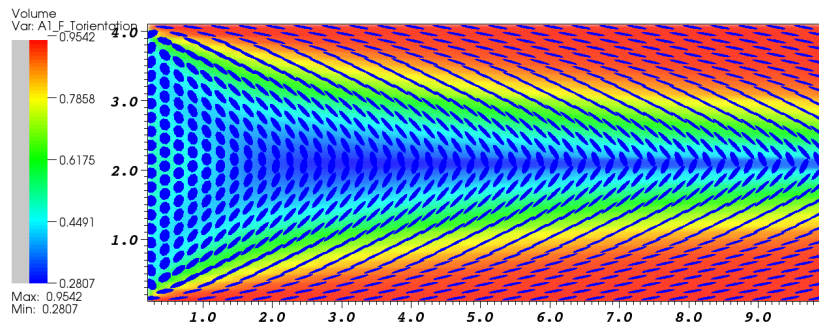
Figure 4.16: $N_p = 50$, $U_0 = 1$. Colour: $a_{11}^{(2)}$.

4.3.2   Planar contraction flow

Experimental and numerical studies of suspension flows through channel geometries with abrupt contraction or expansion have been published in scientific literature, see e.g. [48], [64] (contraction domains), [9], [86] (expansion domains). The contraction and expansion domains are examples of relatively simple geometries featuring different flow types such as shear, contraction, expansion and recirculating flows in a single domain, hence such domains are important benchmark cases.

The computational domain is sketched in Figure 4.17. It is a union of two rectangular domains $\Omega = \Omega_1 \cup \Omega_2$, where $\Omega_1 = \{(x, y) \in \mathbb{R}^2 : \ x \in (0, 5), y \in (0, 4)\}$ and $\Omega_2 = \{(x, y) \in \mathbb{R}^2 : \ x \in [5, 10], y \in (1.5, 2.5)\}$. The boundary at $x = 0$ is inlet, and at the oposite end $x = 10$ we define the outlet. The remaining boundaries are treated as walls. The discretization is similar as for the planar channel flow, the volume elements are squares with side length $h = 0.1$ (coarse mesh) and $h = \frac{1}{30}$ (fine mesh).

Newtonian case. First we present the results with $N_p = 0$. The Reynolds number calculated for the narrower part of the contraction domain satisfies $Re < 1$, therefore the flow is laminar. Some streamlines are visualized in Figure 4.18. Observe the regions with recirculating flow near the corners at $x = 5$. These regions are sometimes called *corner vortices*.

The fibre orientation field for $U_0 = 0$ is visualized in Figure 4.19. Since the velocity field is decoupled from the fibre orientation, a variation of the value of U_0 influences
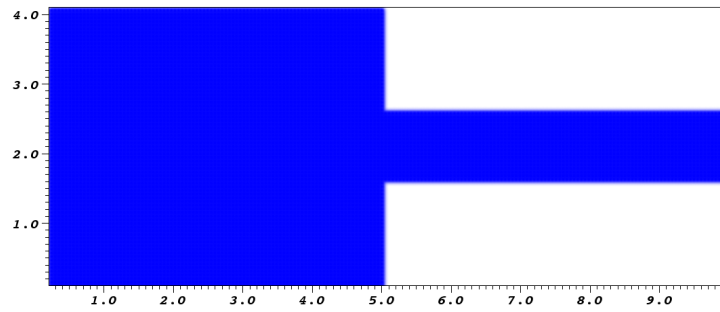
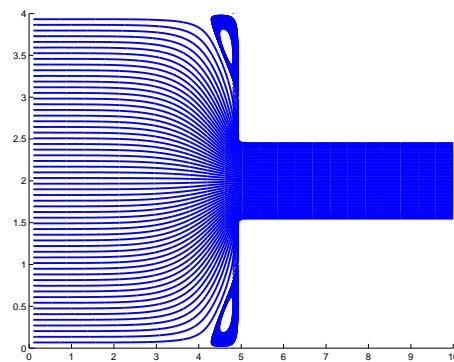Figure 4.17: Planar contraction domain. Left boundary: inlet, right: outlet.

Figure 4.18: Streamlines for a Newtonian fluid in contraction domain. $N_p = 0$

only the fibre orientation state, namely, the aspect ratio of the orientation ellipsoids increases with increasing U_0.
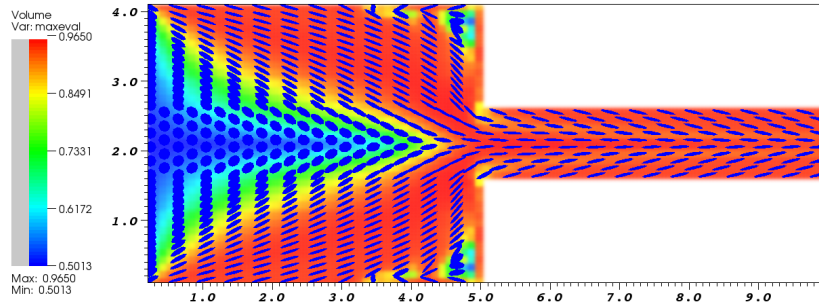

Figure 4.19: Fibre orientation in contraction domain. $N_p = 0$, $U_0 = 0$

The fibre orientation field near a corner vortex is visualized in Figure 4.20 ($U_0 = 1$). Note that the fibres show a preferred orientation parallel to the flow, hence we conclude that the flow in a vertex is locally shear-like and that the velocity is small enough so that the fibres can align with the flow.
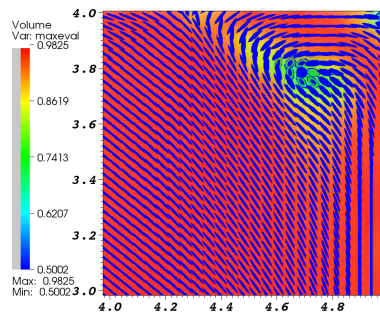
Figure 4.20: A close-up view on the fibre orientation in a corner vortex for a contraction domain, $N_p = 0$, $U_0 = 1$

Non-Newtonian case. Experimental evidence (see [48]) shows that the corner vortex size increases with the fibre concentration (i.e., with the particle number N_p) and that the size of the vortex is independent on the flow rate as long as the Reynolds number remains small. We can confirm these results. For the particle number $N_p = 5$ some streamlines are visualized in Figure 4.21. The data for the left picture were computed using $U_0 = 1$ and for the right picture using $U_0 = 100$. Note the growth of the corner vortices compared to Figure 4.18, and also that no visible difference between the flows with different values of U_0 can be observed.

Comparing the experimental results from [48] with the simulations shows a good agreement. Figure 4.22 shows the comparison for the Newtonian case (left: ex-
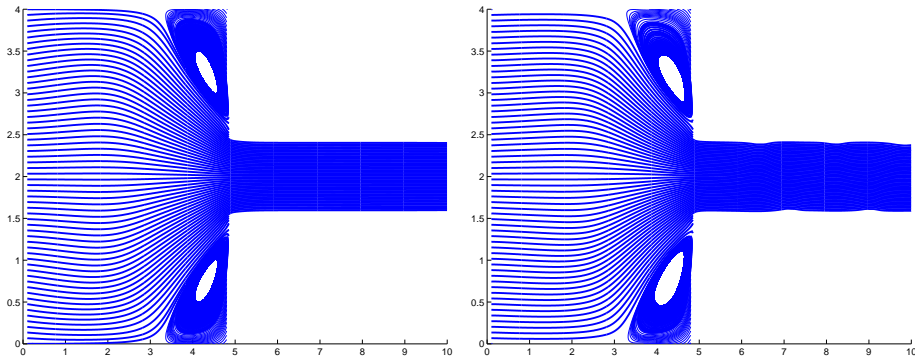
Figure 4.21: Streamlines, $N_p = 5$. Left: $U_0 = 1$, right: $U_0 = 100$

perimental, right: simulation), and Figure 4.23 shows the comparison for the non-Newtonian case.
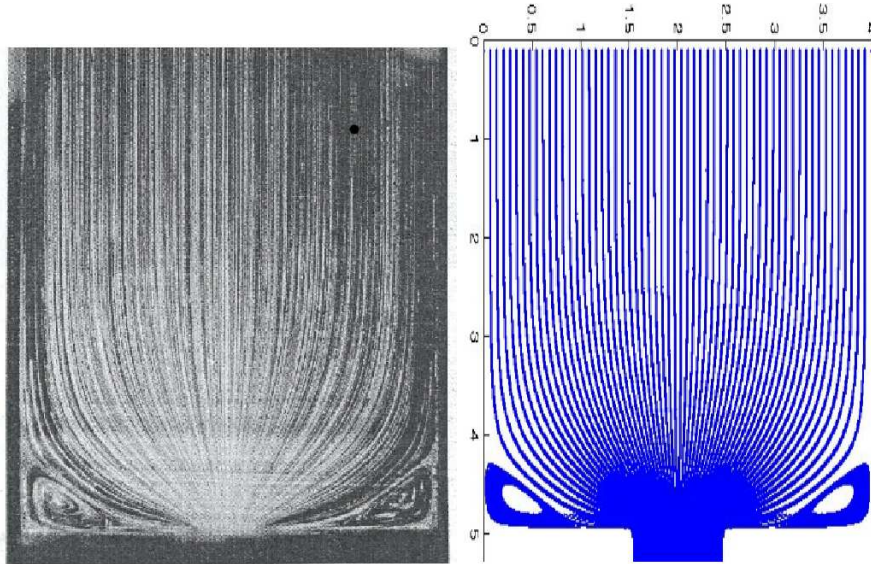

Figure 4.22: Comparison of the streamlines for a fibre suspension flow: experimental results from [48] in the Newtonian flow regime (left) and simulation with $N_p = 0$, $U_0 = 0$ (right)

Increasing the particle number leads to a further growth of the corner vortices. Some streamlines computed for $N_p = 50$ are visualized in Figure 4.24.

For moderate values of U_0 the orientation fields show a similar pattern as seen in Figure 4.19, with the corner regions associated with the vortices growing with N_p. The magnitude of U_0 influences the fibre orientation state, in particular, the extreme values of aspect ratio of orientation ellipsoids. For higher values of U_0 nearly uniaxial fibre orientation state is reached closer to the inflow. An extreme case with $U_0 = 100$ ($N_p = 5$) is presented in Figure 4.25. Observe the prominent core region near the inflow, where the fibre orientation direction is perpendicular to the flow direction.
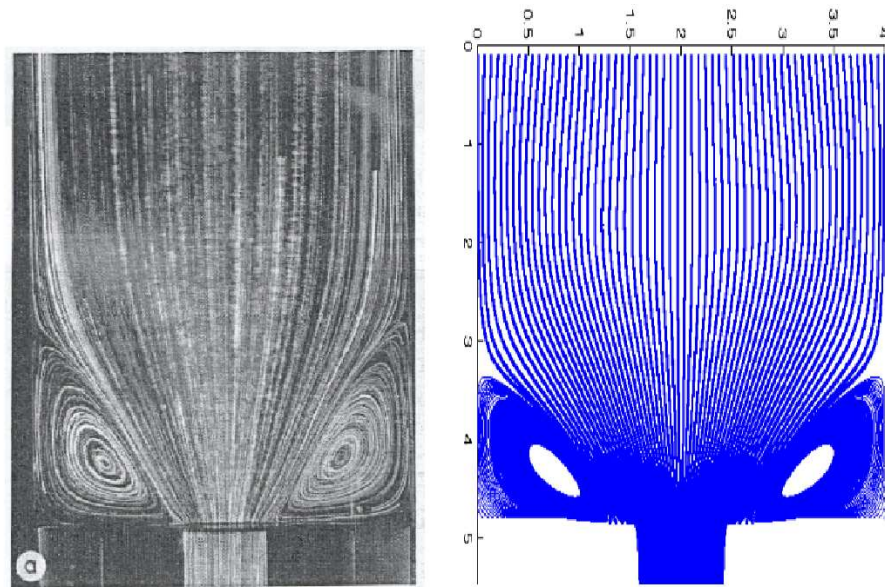
Figure 4.23: Comparison of the streamlines for a fibre suspension flow: experimental results from [48] in the non-Newtonian flow regime (left) and simulation with $N_p = 5$, $U_0 = 1$ (right)
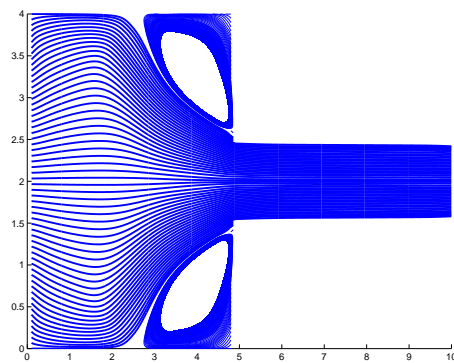

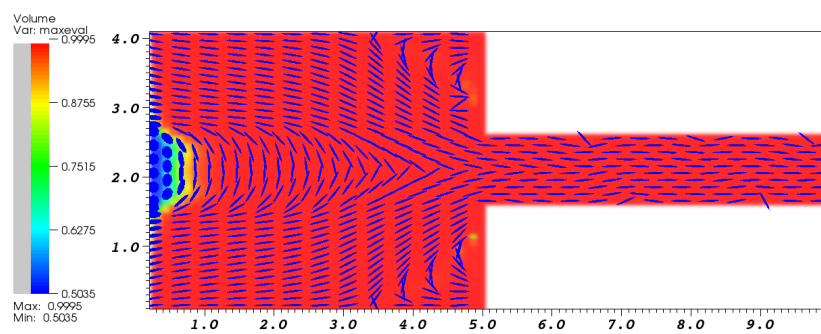Figure 4.24: Streamlines. $N_p = 50$, $U_0 = 1$

Figure 4.25: Orientation field. $N_p = 5$, $U_0 = 100$

89

4.3.3 Flow in a pipe with square cross section

As a first example of a three-dimensional domain we choose a pipe with square cross section. The computational domain is a rectangular box defined by $0 < x < 10$, $0 < y, z < 4$. The domain is discretized in cubic elements with edge length $h = 0.1$. The inlet is positioned at $x = 0$, the outlet is at $x = 10$. At the inlet we prescribe Dirichlet boundary conditions for the velocity

$$v_x(0, y, z) = 16 v_{max} \frac{y(d_y - y)}{d_y^2} \frac{z(d_z - z)}{d_z^2}, \ v_y = v_z = 0, \ \text{for } x = 0,$$

where $d_y = d_z = 4$, $v_{max} = 0.05$ and for orientation distribution $a^{(2)} = \frac{1}{3}I$ (isotropic distribution).

At the given inlet velocities, the flow Reynolds number is low (less than 1), therefore the flow is laminar. The velocity profile depends on the concentration. For $N_p = 0$ we observe a Poiseuille velocity profile in all cross-sections perpendicular to the flow direction. With increasing values of N_p the velocity profile changes from Poiseuille at the inlet to a flatter velocity profile at the outlet.

In Figure 4.26 we visualize the velocity profile, i.e., the magnitude of the x-component of the velocity v_x as a function of y and z at the outlet $x = 10$ for different values of N_p. The left picture shows the profile for the Newtonian flow $N_p = 0$, the middle one is the computed velocity profile for $N_p = 5$ and the right one for $N_p = 50$. The colour code is the same for all pictures. Observe the transition from a Poiseuille like flow to a plug like flow.
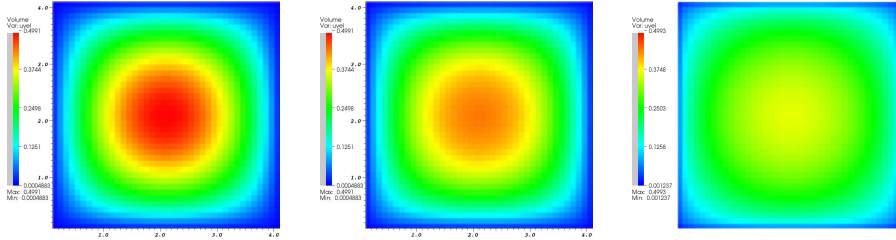

Figure 4.26: Velocity profiles at the outlet for $N_p = 0$ (left), $N_p = 5$ (middle) and $N_p = 50$ (right)

Next we present results for the orientation field. The orientation in cross-sections perpendicular to the flow field at different distances from the inlet ($x = \text{const}$) are visualized in Figure 4.27 for the case $N_p = 5$, $U_0 = 0$. The results are consistent with the two-dimensional case, e.g., one can observe that the size of the core region, where the fibres exhibit low orientation alignment in the flow direction, is decreasing. The magnitude of the maximal eigenvalue of $a^{(2)}$ as a function of U_0 can be estimated from the graph in Figure 4.10.

Fibre orientation in cross sections $y = \text{const}$ is demonstrated in Figure 4.28. The upper picture is a cross-section through the centerline of the domain and shows a
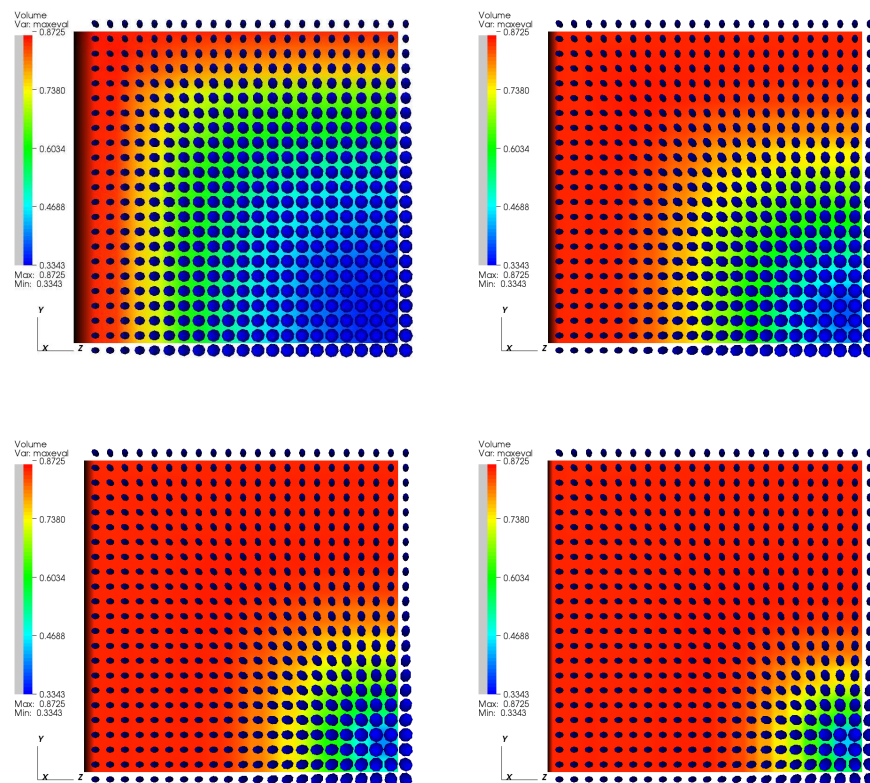
Figure 4.27: Fibre orientation in a square pipe domain. Cross-sections at $x = 1$ (upper left), $x = 3$ (upper right), $x = 6$ (lower left) and $x = 9$ (lower right). $N_p = 5$, $U_0 = 0$.

similar orientation pattern as in the two dimensional simulations. The lower picture shows a cross-section near the boundary. Here the fibre orientation is highly aligned in the flow direction, as expected due to the higher shear rate.
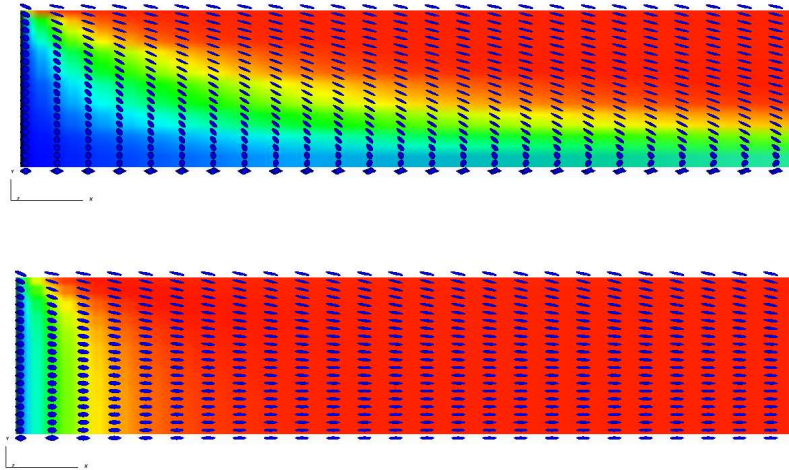

Figure 4.28: Fibre orientation in a square pipe domain. Cross sections at $y = 2$ (upper) and $y = 0.5$ (lower picture). The flow is from left to right; the upper boundary is the wall $z = 0$ and the lower line is the center-line $z = 2$.

For a higher fibre concentration $N_p = 50$ the orientation is visualized in Figure 4.29. Observe that the core region where the fibres are *not* completely flow aligned is preserved longer due to lower shear rate associated with the flatter velocity profile in the core region.

4.3.4 Flow in a pipe with rectangular cross section

We consider the rectangular computational domain defined by $0 < x < 10$, $0 < y < 4$, $0 < z < 1$, i.e., a pipe with rectangular cross-section with the relative dimensions 4×1. Again, the domain is discretized in cubic volume elements with edge length $h = 0.1$, the inlet is positoned at $x = 0$ and the outlet at $x = 10$. At the inlet we prescribe isotropic orientation distribution and a quadratic inlet velocity profile similar as for the previous geometry.

The fibre orientation field for $N_p = 5$ and $U_0 = 10$ is shown in Figure 4.30. Again we observe a non-Newtonian flow and the formation of a core region near the inlet, where the fibres tend to turn away from the flow direction. Note however, that in the core region the fibres tend to orient in the direction of the maximal shear (z-direction) rather than the vorticity direction (y-direction), what has been observed in suspensions with a non-Newtonian matrix, see e.g. [20].
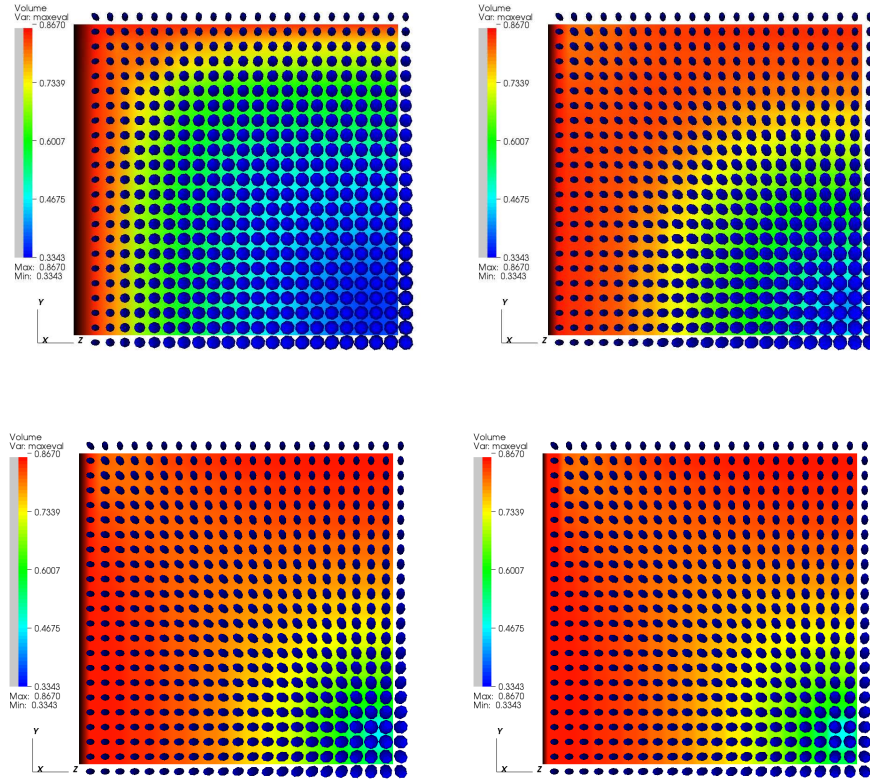
Figure 4.29: Fibre orientation in a square pipe domain. Cross-sections at $x = 1$ (upper left), $x = 3$ (upper right), $x = 6$ (lower left) and $x = 9$ (lower right). $N_p = 50$, $U_0 = 0$.
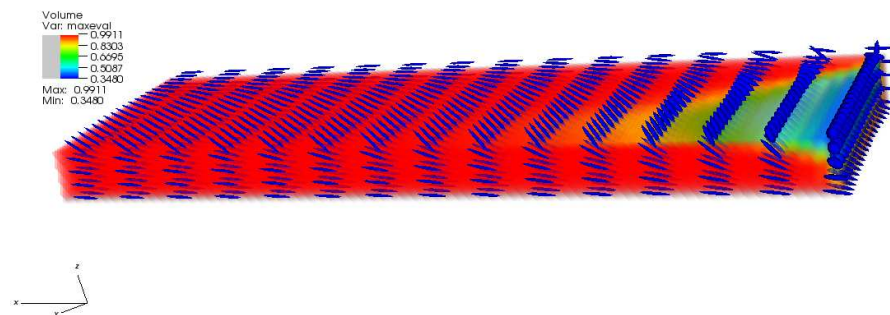

Figure 4.30: Fibre orientation in a pipe of rectangular cross-section. We see a cut-out for $0 \leq y \leq 2$ and $0 \leq z \leq 0.5$. The flow is from right to left.

Flow in a square-to-square contraction domain

The domain is union of two rectangular domains Ω_1 defined by $0 < x < 0.5$, $0 < y, z < 0.64$ and Ω_2, defined by $0.5 \leq x < 1$, $0.24 < y, z < 0.4$, see Figure 4.31. The inflow is at $x = 0$, the outflow is at $x = 1$. At the inlet we prescribe isotropic Dirichlet condition for $a^{(2)}$ and a Dirichlet velocity condition with parabolic v_x profile.

The streamlines for $N_p = 0$ and $N_p = 5$ are demonstrated in Figure 4.32. As in the two-dimensional case, we observe growing corner vortices. The fibre orientation in central ($z = 0.32$) and lateral ($z = 0.08$) cross sections is illustrated in Figure 4.33.
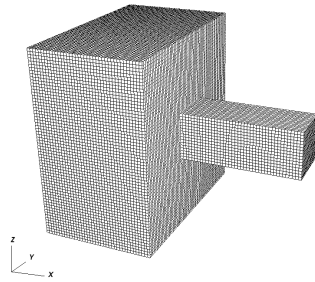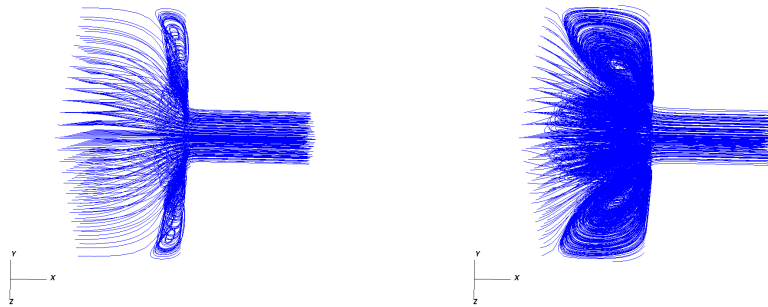

Figure 4.31: Contraction domain.

Figure 4.32: Streamlines. $N_p = 0$ (left one), $N_p = 5$ (right one)

4.3.5   Concluding remarks

On modelling. The presented numerical results with various parameter values allow to assess the influence of the excluded volume effect on the behaviour of solutions. We have observed that the computed orientation state depends on the value U_0; for sufficiently small values $U_0 \leq 1$ the change is only of qualitative nature. For sufficiently small values of N_p and U_0 the flow velocity field is observed to be much more sensitive with respect to N_p than to U_0. However, if both N_p and U_0 are of the
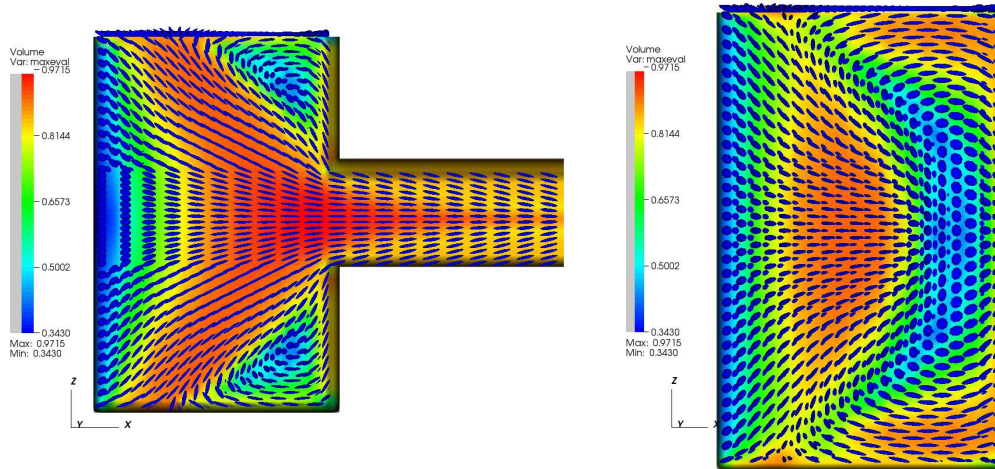
Figure 4.33: Fibre orientation at the centerline $z = 0.32$ (left) and near the wall $z = 0.08$ (right)

order of magnitude 10 or larger, instabilities in the velocity field appear, see e.g. the streamlines near the wall in the outlet pipe in the right picture of Figure 4.21.

On validation. For the Folgar-Tucker limit, the simulation results have been validated against the simulation results published in [64] and experimental results from [48]. For the concentrated fibre suspension model only a qualitative validation in terms of the ratio between maximal and minimal eigenvalue of the orientation tensor can be performed due to lack of experimental data.

On numerics. The finite volume method used in this work has been tested for several domains in two and three dimensions. A rigorous study of convergence of the algorithms with respect to the mesh size is beyond the scope of this thesis, however, the comparison of the results computed with different mesh sizes (refinement from h to $h/3$) shows that the sensitivity of numerical solutions with respect to the mesh size is low.

Chapter 5

Conclusions

This thesis is devoted to studies of mesoscale based fibre suspension flow models. The modelling of fibre suspension flow was extended to two industrially important classes of fibre suspensions, namely, the concentrated regime for short fibre suspensions and dilute regime for long semi-flexible fibre supensions. The contribution to the modelling of short fibre suspension flows is the model (2.3) describing the fibre orientation dynamics in the concentrated regime, which extends the Folgar-Tucker model by improving the treatment of the fibre-fibre interaction. The proposed model accounts for the excluded volume effect, using a phenomenological Maier-Saupe potential with the strength U_0.

A novel way of description of the fibre orientation state in semi-flexible fibre suspensions has been proposed, based on low order statistical moments of a probability distribution function defined on the Cartesian product of two unit spheres. A model for the evolution of these orientation state variables has been proposed, accounting for the fibre bending in velocity fields, where the macroscopic velocity gradient changes considerably along the fibre. Furthermore, several closure approximations have been proposed in Section 2.4 and analyzed in the Section 4.1, where the homogeneous polynomial closure was found to be sufficiently robust and reliable to be used in implementations.

The modelling techniques developed in Chapter 2 can be extended further to derive mesoscale models based on different physical assumptions about flow driven fibre orientation dynamics and fibre-fibre interactions. Moment based mesoscale models share a common mathematical structure, namely, the fibre orientation equations form a hyperbolic system of linear first order partial differential equations and depend on algebraic closure relations.

The common structure allows a unified mathematical analysis of well-posedness of the system describing fibre suspension flows, which was performed in Chapter 3. The existence of a unique solution in a Sobolev space for a sufficiently small time interval and for sufficiently small input data (initial conditions and external forces) was demonstrated. The meaning of "sufficiently small" depends on the source terms in the fibre orientation model and the constitutive relations as well as on the domain. If the source terms of the fibre orientation equations are non-linear in the

velocity gradient or depend on higher spatial derivatives of the fluid velocity field, then the model must be regularized in order to apply the well-posedness results. Since the averaging process is at the very core of mesoscale models, such regularization is consistent with the modelling.

The implementation of the models was performed in the framework of *CoRheoS*, which is a complex rheology solver developed at the department *Flow and Material Simulation* (SMS) of the Fraunhofer ITWM. The contribution of this thesis is the implementation of the hyperbolic system for the fibre orientation state variables and the constitutive relation for calculating the extra stress term. Numerical experiments on two and three dimensional domains show that the decoupling approach presented in Section 4.2 provides a good enough approximation, however, the time step should be chosen small enough. Convergence with respect to time step τ and mesh size h was observed in two dimensional case. The code is robust in the parameter range $N_p < 100$, $U_0 < 10$. The simulation results were validated for the Folgar-Tucker limit $U_0 = 0$ against experimental data and simulation results published in literature.

Due to the common mathematical structure of the mathematical models, a unified structure for description of mesoscale based suspension flow models can be envisioned, ranging from the modelling steps to the implemention and mathematical analysis.

Appendix A

List of notation

Vector and tensor operations

A d-dimensional tensor of rank n is defined by its components $a_{i_1,\ldots,i_n}$ for all possible combinations of indices $i_j \in \{1,\ldots,d\}$. If the indices represent the coordinates in the physical space, then we sometimes identify the coordinates $(1,2,3)$ with (x,y,z). We use the summation convention over repeating indices and use coordinate free notation where possible, for example, the definition of the dot-product of two vectors can be written as $a \cdot b = a_i b_i = \sum_i a_i b_i$ and the contraction of two second rank tensors $a : b = a_{ij} b_{ij} = \sum_{ij} a_{ij} b_{ij}$. The trace of a second order tensor is defined as $\mathrm{Tr}(a) := a_{ii}$. Tensor product is denoted by $\otimes$.

Domains and spaces

$\Omega \subset \mathbb{R}^d$ - the domain of the flow with the dimension d
$\partial\Omega$ - boundary of Ω
$x \in \Omega$ - position vector
$B_r(x) = \{y : |x-y| \leq r\}$ - closed ball with center x and radius r
$S^{d-1} = \{x \in \mathbb{R}^d : |x| = 1\}$ - unit sphere
$p, q \in S^{d-1}$ - unit vectors

Operators

$\nabla = \nabla_x$ - gradient with respect to the variable x
$\frac{\partial u}{\partial x_i} = \partial_{x_i} u = u_{,i}$ - partial derivative of u
P_{HW} - Helmholtz-Weyl projection operator
$\dot{a}$ - time derivative of a
$\mathcal{L} = -P_{HW} \nabla \cdot \nabla$ - Stokes operator
$\frac{D}{Dt} = \frac{\partial}{\partial t} + v \cdot \nabla$ - material derivative

∇_p - gradient on the unit sphere with respect to the variable p

$\mathscr{R}_p = p \times \nabla_p$ - a differential operator on S^{d-1}

I - unit operator, unit matrix

Functions

v, P - fluid velocity field and pressure field

$\kappa_{ij} = \frac{\partial v_i}{\partial x_j}$, $\mu_{jk}^i = \frac{\partial^2 v_i}{\partial x_j \partial x_k}$ - velocity gradient and velocity curvature

$D = \frac{1}{2}(\kappa + \kappa^\top)$, $W = \frac{1}{2}(\kappa - \kappa^\top)$ - rate of deformation tensor and vorticity tensor

$\dot{\gamma}, \dot{\gamma}_\epsilon$ - velocity shear rate and its regularization

M - effective velocity gradient in Jeffery's equation

ψ - probability distribution function

$a^{(n)}, a^{(n,m)}$ - moments of ψ

$s : \Omega \to \mathbb{R}^{d_2}$ - function characterizing fibre orientation field

$\xi : \Omega \to \mathbb{R}^{d_3}$ - regularized part of the fibre orientation models

T - stress tensor

$S = \mathcal{T}$ - additional stress due to presence of fibres

$\mathcal{F}$ - source term in fibre orientation equations

$\bar{v}, \bar{s}$ - given velocity and fibre orientation fields

Parameters

η - dynamic viscosity

N_p, N_s - particle number and shear number

Re - Reynolds number

$C_i, D_r, U_0,$ - Folgar-Tucker constant, orientation diffusivity and Maier-Saupe constant

l_f, d_f, r_a - fibre length, diameter and aspect ratio

l_B, χ - connector length of a semiflexible fibre and flexibility coefficient

n_f, ϕ_f - fibre number density and volume fraction

ζ - Stokes drag coefficient

Discrete operators

$B, B^\top$ - discrete divergence and gradient operators

C_v - discrete convection operator

D_v - discretization operator for the viscous term

Σ - discretization operator for the extra stress term

τ, h - time step and edge length of a volume element

Bibliography

[1] S.G. Advani, C.L. Tucker III, *The use of tensors to describe and predict fiber orientation in short fiber composites*, J. Rheol. 31:751-784, 1987

[2] S.G. Advani, C.L. Tucker, *Closure approximations for three-dimensional structure tensors,* J. Rheol. 34:367-386, 1990

[3] S.G. Advani (Ed.), *Flow and Rheology in polymer composites manufacturing*, Composite Mater. Series Vol. 10, Elsevier, Amsterdam, 1994

[4] J.W. Barrett, C. Schwab, E. Süli, *Existence of global weak solutions for some polymeric flow models,* Math. Mod. Meth. Appl. Sci. 6:939-983, 2005

[5] G.K. Batchelor, *The stress generated in non-dilute suspension of elongated particles by pure straining motion*, J. Fluid Mech. 46:813-829, 1971

[6] A. Bonito, P. Clement, M. Picasso, *Mathematical and numerical analysis of a simplified time-dependent viscoelastic flow*, Numer. Math. 107:213-255, 2007

[7] F.P. Bretherton, *The motion of rigid particles in a shear flow at low Reynolds number*, J. Fluid Mech. 14:284-304, 1962

[8] A.P. Calderón, *Lebesgue spaces of differentiable functions and distributions,* Proc. Sympos. Pure Math. Vol. IV, AMS; Providence, RI, pp. 33-49, 1961

[9] K. Chiba, K. Nakamura, *Numerical solution of fiber suspension flow through a complex channel,* J. Non-Newt. Fluid Mech. 78:167-185, 1998

[10] H.T. Chung, S.H. Kang, W.R. Hwang, *Numerical simulations of elliptic particle suspensions in sliding bi-periodic frames*, Korea-Australia Rheol. J. 17:171-180, 2005

[11] D.H. Chung, T.H. Kwon, *Applications of recently proposed closure approximations to injection molding filling simulation of short-fiber reinforced plastics*, Korea-Austr. Rheol. J. 12:125-133, 2000

[12] D.H. Chung, T.H. Kwon, *Invariant based optimal fitting closure approximation for the numerical prediction of flow-induced fiber orientation,* J. Rheol. 46:169-194, 2002

[13] J.S. Cintra, C.L. Tucker, *Orthotropic closure approximations for flow-induced fiber orientation,* J. Rheol. 39:1095-1122, 1995

[14] J.K.G. Dhont, *Rotational Brownian Motion of Colloidal Rods*, in J.K.G. Dhont, G. Gompper, D. Richter, *Soft matter: complex materials on mesoscopic scale*, Forschungszentrum Jülich, 2002

[15] S.H. Dinh, R.C. Armstrong, *A rheological equation of state for semiconcentrated fibre suspensions*, J. Rheol. 28:207-227, 1984

[16] M. Doi, N.Y. Kuzuu, *Nonlinear Elasticity of Rodlike Macromolecules in Condensed State*, J. Polymer Sci: Polymer Phys. Ed. 18:409-419, 1980

[17] M. Doi, S.F. Edwards, *The theory of polymer dynamics.* Clarendon Press, Oxford, 1986

[18] P. Dumont, J.P. Vassal, L. Oregas, V. Michaud, D. Favier, J.A.E. Manson, *Processing, characterisation and rheology of transparent concentrated fibre-bundle suspenions*, Rheol. Acta 46:639-651, 2007

[19] F. Dupret, V. Verleye, *Modelling the flow of fiber suspensions in narrow gaps. Advances in the flow and rheology of Non-Newtonian fluids,* Elsevier, Amsterdam, 1999

[20] X. Fan, *Numerical study on some rheological problems of fibre suspensions*, PhD Thesis, The Univ. of Sydney, 2006

[21] J.H. Ferziger, M. Peric, *Computational methods for fluid dynamics*, Springer-Verlag, 1999

[22] F. Folgar, C.L. Tucker III, *Orientation behavior of fibers in concentrated suspensions.* J. Reinf. Plast. Comp. 3:98-119, 1984

[23] O.L. Forgacs, S.G. Mason, *Particle motions in sheared suspensions: X. Orbits of flexible threadlike particles*, J. Colloid Interf. Sci., 14:473-491, 1959

[24] G.P. Galdi, *An Introduction to the Mathematical Theory of the Navier-Stokes Equations* Vol. 1, Springer Tracts in Natural Philosophy, New York, 1994

[25] G.P. Galdi, D.B. Reddy, *Well-posedness of the problem of fiber suspension flows.* J. Non-Newt. Fluid Mech. 83:205-230, 1999

[26] G.W. Gardiner, *Handbook of Stochastic Methods for Physics, Chemistry and the Natural Sciences,* 2nd Ed., Springer-Verlag, 1990

[27] C.G. Gray, K.E. Gubbins, *Theory of Molecular Fluids Vol. 1: Fundamentals*, Oxford University Press, 1984

[28] M. Grosso, P.L. Maffettone, F. Dupret, *A closure approximation for nematic liquid crystals based on the canonical distribution subspace theory,* Rheol. Acta, 39:301-310, 2000

[29] C. Guillope, J.C. Saut, *Existence results for the flow of viscoelastic fluids with a differential constitutive law,* Nonlinear Analysis, Theory, Methods Appl., 15:849-869, 1990

[30] G.L. Hand, *A theory of anisotropic fluids,* J. Fluid Mech. 13:33-62, 1962

[31] C. Helzel, F. Otto, *Multiscale simulations for suspensions of rod-like molecules,* J. Comp. Phys. 216:52-75, 2006

[32] E.J. Hinch, *The distortion of a flexible inextensible thread in a shearing flow,* J. Fluid Mech. 74:317-333, 1976

[33] E.J. Hinch, L.G. Leal, *The effect of Brownian motion on the rheological properties of a suspension of non-spherical particles,* J. Fluid Mech., 52:683-712, 1971

[34] E.J. Hinch, L.G. Leal, *Constitutive equations in suspension mechanics. Part 2. Approximate forms for a suspension of rigid particles affected by Brownian rotations,* J. Fluid Mech., 76:187-208, 1976

[35] R.R. Huilgol, N. Phan-Tien, *Fluid Mechanics of Viscoelasticity,* Elsevier, 1997

[36] Y. Iso, D.L. Koch, C. Cohen, *Orientaion in simple shear flow of semi-dilute fiber suspensions. 1. Weakly elastic fluids,* J. Non-Newt. Fluid Mech. 62:115-134, 1996

[37] D. Jack, D. Smith, *An invariant based fitted closure of the sixth-order orientation tensor for modelling short fiber suspensions,* J. Rheol 49:1091-1115, 2005

[38] G.B. Jeffery, *The motion of ellipsoidal particles immersed in a viscous fluid,* Proc. R. Soc. A102:161-179, 1922

[39] C.G. Joung, N. Phan-Thien, X.J. Fan, *Direct simulation of flexible fibers,* J. Non-Newt. Fluid Mech. 99:1-36, 2001

[40] B. Jourdain, T. Lelievre, C. Le Bris, *Existence of solution for a micro-macro model of polymeric fluid: the FENE model,* J. Funct. Anal. 209:162-193, 2004

[41] M. Junk, R. Illner, *A new derivation of Jeffery's equation,* J. math. fluid mech. 8:1-34, 2006

[42] M. Kröger, *Simple models for complex nonequilibrium fluids,* Phys. Reports 390:453-551, 2004

[43] S. Le Corre, D. Caillerie, L. Oregas, D. Favier, *Behavior of a net of fibers linked by viscous interactions: theory and mechanical properties,* J. Mech. Phys. Sol. 52:395-421, 2004

[44] S. Le Corre, P. Dumont, L. Oregas, D. Favier, *Rheology of highly concentrated planar fiber suspensions*, J. Rheol. 49:1029-1058, 2005

[45] M. Letz, A. Latz, *Fluids of hard ellipsoids: Phase diagram including a nematic instability from Percus-Yevick theory*, Phys. Rev E 60:5865-5871, 1999

[46] T. Li, P. Zhang, *Mathematical analysis of multi-scale models of complex fluids*, Commun. math. sci. 5:1-51, 2007

[47] P.L. Lions, M. Masmoudi, *Global solutions for some Oldroyd models of non-Newtonian flows*, Chin. Ann. of Math. 21B131-146, 2000

[48] D.D. Lipscomb, M.M. Denn, D.U. Hur, D.V. Boger, *The flow of fibre suspension in complex geometry,* J. Non-Newt. Fluid Mech. 26:297-325, 1988

[49] M.B. Mackalpow, E.S.G. Shahfeq, *A numerical study of the rheological properties of suspensions of rigid., non-brownian fibres*, J. Fluid Mech., 329:155-186, 1996

[50] W. Maier, A. Saupe, *Eine einfache molekular-statistische Theorie der nematischen kristallinflüssigen Phase, Teil I*, Z. Naturforsch. 14a:982-988, 1959; *Teil II*, Z. Naturforsch. 15a: 287-292, 1960

[51] A. Megally, *Etude et Modelisation de l'orientation de fibres dans des thermoplastiques reinforces*, PhD Thesis, L'Ecole Nationale Superieure des Mines de Paris, 2005

[52] J.M.W. Munganga, D.B. Reddy, *Local and global existence of solutions to the equations for fibre suspension flows*, Math. Models and Meth. in Appl. Sci., 12:1177-1203, 2002

[53] J.M.W. Munganga, D.B. Reddy, K.J. Diatezua, *Aspects of the thermodynamic stability of fibre suspension flows,* J. Non-Newt. Fluid Mech. 92:135-150, 2000

[54] D. Niedziela, *On numerical simulations of viscoelastic fluids*, Dissertation, TU Kaiserslautern, 2006

[55] L. Onsager, *The effects of shape on the interaction of colloidal particles,* Ann. N.Y. Acad. Sci. 51:627-659, 1949

[56] H.C. Öttinger, *Stochastic processes in polymeric fluids: tools and examples for developing simulation algorithms*, Springer, Berlin, 1996

[57] M.P. Petrich, D.L. Koch, C. Cohen, *An experimental determinatio of the stress-microstructure relationship in semi-concentrated fiber suspensions*, J. Non-Newt. Fluid Mech. 95:101-133, 2000

[58] C.J.S. Petrie, *The rheology of fibre suspensions*, J. Non-Newt. Fluid Mech. 87:369-402, 1999

[59] N. Phan-Thien, R. Zheng, *Macroscopic modelling of the evolution of fibre orientation during flow*, in D. Guell, T. Papathanasiou (Eds.), *Flow-Induced Alignment in Composite Materials,* pp. 77-111, Woodhead Publ., Cambridge, 1997

[60] M. Rahnama, D.L. Koch, E.S.G. Shahfeq, *The effect of hydrodynamic interactions on the orientation distribution in a fiber suspension subject to simple shear flows,* Phys. Fluids 7(3):487-506, 1995

[61] M. Rajabian, C. Dubois, M. Grmela, *Suspensions of Semiflexible Fibers in Polymeric Fluids: Rheology and Thermodynamics*, Rheol. Acta 44:521-535, 2005

[62] S. Ranganathan, S.G. Advani, *A simultaneous solution for flow and fiber orientation in axissymmetric diverging radial flow,* J. Non-Newt. Fluid Mech. 47:107-136, 1993

[63] B.D. Reddy, G.P. Mitchell, *Finite element analysis of fibre suspension flows*, Comput. Methods Appl. Mech. Engr. 190:2349-2367, 2001

[64] A. Redjeb, L. Silva, P. Laure, M. Vincent, T. Coupez, *Numerical simulation of fiber orientation in injection molding process*, Polymer Processing Society. 21st Ann. Meet. Leipzig, 2005

[65] J. Rosenberg, M.M. Denn, R. Keunings, *Simulation of non-recirculating flows of dilute fiber suspensions,* J. Non-Newt. Fluid Mech. 37:317-345, 1990

[66] R.F. Ross, D.J. Klingenberg, *Dynamic simulation of flexible fibers composed of rigid bodies*, J. Chem. Phys 106:2949-2960, 1997

[67] Y. Saad, *Iterative Methods for Sparse Linear Systems,* 2000

[68] E.S.G. Shahfeq, G.H. Fredrickson, *The hydrodynamic stress in a suspension of rods*, Phys. Fluids A2:7-24, 1990

[69] H. Sohr, *The Navier-Stokes Equations: An elementary functional analytic approach*, Birkhäuser Verlag, Berlin, 2001

[70] J.M. Stockie, S.I. Green, *Simulating the motion of flexible pulp fibres using the immersed boundary method,* J. Comp. Physiol. 147:147-165, 1998

[71] J.M. Stockie, *Analysis and Computation of Immersed Boundaries, with Appication to Pulp Fibres,* PhD thesis, Univ. of British Columbia, Vancouver, 1997

[72] U. Strautins, A. Latz, *Flow-driven orientation dynamics of semiflexible fiber systems*, Rheol. Acta 46:1057-1064, 2007

[73] U. Strautins, *Investigation of fiber orientation dynamics within the Folgar-Tucker model with hybrid closure*, Master Thesis, TU Kaiserslautern, 2004

[74] R.R. Sundararajakumar, D.L. Koch, *Structure and Properties of Sheared Fiber Suspensions with Mechanical Contacts*, J. Non-Newt. Fluid Mech. 73:205-239, 1998

[75] W. Tang, S.G. Advani, *Dynamic simulation of Long Flexible Fibers in Shear Flow*, CMES 8:156-176, 2005

[76] R. Temam, *Navier-Stokes Equations*, North Holland Publ. Comp., Amsterdam, 1979

[77] A.K. Tornberg, M.J. Shelley, *Simulating the dynamics and interactions of flexible fibers in Stokes flows*, J. Comp. Physics 196:8-40, 2004

[78] C.L. Tucker III, *Flow regimes for fibre suspensions in narrow gaps,* J. Non-Newt. Fluid Mech., 39:239-268, 1991

[79] S. Turek, *Efficient solvers for incompressible flow problems. An algorithmic approach in view of computational aspects,* Springer-Verlag, 1998/99

[80] V. Verleye, F. Dupret, *Numerical prediction of fiber orientation in complex injection molded parts,* Proc. ASME Winter Annual Mtg, p. 264-279, 1994

[81] B.E. Verweyst, *Numerical predictions of flow-induced fiber orientation in three-dimensional geometries,* PhD Thesis, Univ. of Illinois at Urbana-Champaign, 1998

[82] P. Wesseling, *Principles of computational fluid dynamics*, Springer-Verlag, 2001

[83] S. Yamamoto, T. Matsuoka, *A method for dynamic simulation of rigid and flexible fibers in a flow field*, J. Chem. Phys. 98:644-650, 1993

[84] S. Yamamoto, T. Matsuoka, *Dynamic Simulation of Microstructure and Rheology of Fiber Suspensions*, Polymer Engnr. Sci. 36:2396-2403, 1996

[85] Y. Yamane, Y. Kaneda, M. Doi, *Numerical simulations of semi-dilute suspensions of rodlike particles in shear flow*, J. Non-Newt. Fluid Mech. 54:405-421, 1994

[86] K. Yasuda, S. Henmi, N. Mori, *Effects of Abrupt Expansion Geometries on Flow-Induced Fiber Orientation and Concentration Distributions in Slit Channel Flows of Fiber Suspensions*, Polymer Comp. 26:660-670, 2005

[87] E. Zeidler, *Nonlinear functional analysis and its Applications Part I: Fixed point theorems*, corrected Ed., Springer Verlag, 1993

CURRICULUM VITAE

30.07.1980	geboren in Riga, Lettland
1987 – 1992	Besuch der 69. Mittelschule in Riga
1992 – 1996	Besuch des Imanta lettischen Gymnasiums in Riga
1996 – 1998	Besuch des 1. Gymnasiums in Riga
Sept. 1998 – Jun. 2002	Batchelor Studium an der Universität Lettland, Fachbereich für Physik und Mathematik, Abteilung Mathematik
SS 2001	Auslandsemester and der Universität Bremen
Okt. 2002 - Okt. 2004	Master Studium an der TU Kaiserslautern, im Rahmen vom Programm Mathematics International, Vertiefungsrichtung Technomathematik
Okt. 2004 - Mai 2008	Doktorand an der TU Kaiserslautern